Lukas Stranger, BSc

Can EEG oscillations reveal patterns in arithmetic problem solving processes?

MASTERARBEIT

zur Erlangung des akademischen Grades

Diplom-Ingenieur

Masterstudium Biomedical Engineering

eingereicht an der

Technischen Universität Graz

Betreuerin

Ass. Prof. Mag.rer.nat Dr.phil Selina Christin Wriessnegger

Institut für Neurotechnologie

Dipl.-Ing. Dr.techn. Clemens Brunner
Institut für Psychologie, Universität Graz

Graz, Jänner 2020

EIDESSTATTLICHE ERKLÄRUNG

AFFIDAVIT

Ich erkläre an Eides statt, dass ich die vorliegende Arbeit selbstständig verfasst, andere als die angegebenen Quellen/Hilfsmittel nicht benutzt, und die den benutzten Quellen wörtlich und inhaltlich entnommenen Stellen als solche kenntlich gemacht habe. Das in TUGRAZonline hochgeladene Textdokument ist mit der vorliegenden Masterarbeit identisch.

I declare that I have authored this thesis independently, that I have not used other than the declared sources/resources, and that I have explicitly indicated all material which has been quoted either literally or by content from the sources used. The text document uploaded to TUGRAZonline is identical to the present master‘s thesis.

Datum / Date

Unterschrift / Signature

1 Acknowledgment

First, I would like to thank my supervisor Dipl.-Ing. Clemens Brunner for his support. He gave me important and inspiring feedback and shared his experience throughout the whole analysis with me.
Further, I want to thank Ass.Prof.Mag.rer.nat Dr.phil. Selina Christin Wriessnegger for her support.
Finally, I want to say thanks to my family. They gave me the opportunity to study and supported me over all the years.

2

Symbols, Abbreviations

MRI magnetic resonance imaging

fMRI functional magnetic resonance imaging,

EEG electroencephalography

MEG magnetoencephalography

NIRS near-infrared spectroscropy

fNIRS functional near-infrared spectroscropy

ERP evoked related potentials

ERD/S event-related (de)synchronizations

SNR signal-to-noise ratio

RANSAC random sample consensus

IC independent component]

IC Independent Component

BSS Blind source separation

ERSPs event related spectral perturbations

PCA principal component analysis

ROI region of interest

AG angular gyrus

STS superior temporal sulcus

FG fusiform gyrus

IPS intraparietal sulcus

FEF frontal eye field

DLPFC dorsolateral prefrontal cortex

SMA supplementary motor area

PMC premotor cortex

BG basal ganglia

AI anterior insula

VLPFC ventrolateral prefrontal cortex

MTL medial temporal lobe

V1 visual cortex

FFA fusiform face area

FG fusiform gyrus

SPL superior parietal lobule

IPS intraparietal sulcus

ITC ITC

AG angular gyrus

PPC PPC

PFC prefrontal cortex

DPFC dorsolateral prefrontal cortex

WM working memory

LTM long-term memory

RT response time

AF anteriofrontal

F frontal

FC frontocentral

C central

CP centroparietal

P parietal

PO parietooccipital

T temporal

3 Zusammenfassung

Das Electroencephalogramm (EEG) erlaubt die Analyse kognitiver Prozesse im Allgemeinen [1]–[3] und arithmetischer Probleme im Speziellen [4], [5]. Obwohl vom Einfluss der Problemgröße und der selbstberichteten Lösungsstrategie auf die Bandleistung von EEG-Oszillationen wiederholt berichtet wird, bestehen nach wie vor Unklarheiten über die Ursache dieses Effekts [6]. Deshalb wird in dieser Arbeit der Einfluss von Problemgrößen und selbstberichteten Lösungsstrategien einstelliger Rechenaufgaben auf EEG-Korrelate des Rechenprozesses untersucht.
Die statistische Dekomposition von Sensorwerten in unabhängige Prozesse erlaubt die Identifikation von Signalquellen, welche mit herkömmlichen Methoden auf Sensor-Ebene nicht möglich wäre. Zunächst werden die Ergebnisse der Sensor- und Quellraumanalyse verglichen. Darüber hinaus stellen wir die Behauptung von [6], [7], dass winzige Additionsprobleme durch unterbewusste, hochautomatisierte Zählprozesse gelöst werden in Frage, indem wir EEG-Schwingungen winziger und kleiner Additions- und Multiplikationsaufgaben analysieren und vergleichen. In unserer Analyse können wir den Effekt der Problemgröße und die Unterschiede der Strategien zwischen kleinsten, kleinen und großen Problemen erkennen. Dies deckt sich mit den Ergebnissen vorhandener Literatur [4], [5]. Außerdem zeigen die Ergebnisse kürzere Reaktionszeiten, höhere Theta-ERS und niedrigere Alpha-ERD Werte für kleinste und kleine im Vergleich zu großen Problemen im Sensor und im Quellraum. Darüber hinaus wurden stärkere Deaktivierungen im Alpha-, sowie höhere ERS-Werte im Theta-Band für die selbst berichteten prozeduralen Strategien im Sensorraum gefunden die sich in den Regionen Parieto-Occipital/Occipital für alpha und Frontal für Theta, befinden. Der qualitative Vergleich der beiden Analysetypen zeigt jedoch keine wesentlichen Vorzüge, die es rechtfertigen würden Prozesse in den Quellraum zu transferieren. Abschließend, können wir zeigen, dass winzige und kleine Probleme auf ähnliche Weise gelöst werden, da sie bei den EEG-Schwingungen keine signifikanten Unterschiede aufweisen.

4

Abstract

Electroencephalography (EEG) is used to analyze neural processes in general [1]–[3] and those related to arithmetics in particular [4], [5]. Over the course of the last years researchers have found converging evidence that oscillations in the EEG signal are influenced by the sum of the operands and the used strategies during the process of solving arithmetic problems. However, there is still no consensus about the influence of the problem size on the measurable effect in response times and EEG-oscillations [6].
Therefore, in this thesis, we analyzed the influence of problem-sizes and self-reported solution strategies of single-digit arithmetical problems on EEG-correlates of the arithmetical solving process. First, the results of the sensor- and source-space analysis are compared. Additionally, we challenge the current belief that tiny and small problems are solved through a recall from long-term memory by analyzing and comparing EEG oscillations of tiny and small addition and multiplication tasks. This follows the claim of [6], [7] that tiny addition problems are solved through procedural techniques. In our analysis we can detect the problem size effect and the differences of strategies between tiny, small vs. large problems as described in [4], [5]. The results show shorter response times, higher theta-ERS and lower alpha ERD for tiny and small compared to large problems in the sensor and in the source space. Furthermore, lower alpha-ERD and higher theta-ERS ratios are found for the self-reported procedural strategies in the sensor-space and were located in the parieto-occipital/occipital and frontal regions. However, the qualitative comparison between the two types of analysis don't indicate considerable improvements for the source space. Finally, we can demonstrate that tiny and small problems are solved in a similar way, as they show the same EEG-oscillations. Still, an important difference is found in the composition of problem types. Using a Bayesian Analysis, we can reveal that the ERD/S data is best described by the sum of the operands together with the information whether one operator equals 1.

Contents

5 Introduction

5.1 Arithmetic

Arithmetic is one of the oldest fundamental concepts of mathematics. It deals with numbers and properties of elementary operations on them. The most prominent examples are addition, multiplication, subtraction, and division. Proficiency in arithmetics allows us to identify quantities, to compare, count, and rank them. As such, arithmetic is not only essential to make a living in modern society, but also one of our most primitive higher cognitive functions. This makes it a delightful domain to study the neural processes involved in human reasoning, strategy selection, and execution.

5.1.1 Neuroscience of arithmetic calculations

In the early days of neuroscience, research was carried out almost solely by the use of lesion studies. Medical examinations of individuals with brain injuries allow scientists to identify correlations between pathologies and local brain injuries. These correlations help to assign cognitive functions to locally segregated regions (e.g., motor cortex). Emanuel Swedenborg was the first to come up with this insight in 1740. Almost a century later (1825), the first neurophysiological model was described by the German anatomist Gall. He found systematic patterns between the cerebrum and the truncus cerebrum that inspired him to create a map of functional brain regions. Amongst other regions, he described a center of calculation and assigned it to the inferior frontal lobe. Gall's model and the regions he describes are out of date, but his model is still noteworthy due to its reliance on clinical-pathological correlations [8]. In the following years, lesion studies helped to renew the model and identify additional regions related to mathematical ability. One of the most prominent examples, the left angular gyrus (AG) was mentioned together with calculations already in 1919 [9]; Years before modern imaging modal-

ities emerged. Today, lesion studies are still crucial to observe first insights, but due to small sample sizes, they provide limited insight. Small sample sizes, together with a large number of uncontrollable variables, make imaging methods preferable. Methods like functional magnetic resonance imaging (fMRI), electroencephalography (EEG), magnetoencephalography (MEG), near-infrared spectroscropy (NIRS) allow investigations in real-time and non-invasively. Further, specific task characteristics can be manipulated, and the change of their neurological correlates helps to identify causal relationships. Actual examples are fMRI studies described in [10], [11] and [12]. These compare neurological correlates of calculations to attentional, linguistic (phoneme detection), mnemonic, visuospatial (grasping, pointing, saccades) or working memory tasks.
Other parameters that are typically varied are the type of task (verification (e.g. [13]) vs production), the type of arithmetic rules (addition, multiplication, division, subtraction, integration [14]. Further, parameters include the split between proposed and correct answer, the number of operands (two or more [15]), the number of digits in the operands [16], the strategy to use [17], the difficulty [16] and the problem size. Last but not least, the age and skills of participants [18] are also important factors.
The corresponding neurological correlations are typically measured with electroencephalography (EEG), fMRI, or functional near-infrared spectroscropy (fNIRS), mainly because they do not only provide objective insights but have an excellent spatial and for temporal resolution. Additionally, measures like verbal reports may be used to gain insights into the conscious problem-solving process. However, the collection of self-reports may influence the speed, accuracy, and strategy of the solving process itself [19], [20]. Thus, their validity is controversially discussed.
After years of research in arithmetic processing, we have very profound models and theories of the underlying cognitive processes. Still, some questions remain unanswered. The selection and execution of arithmetic strategies need further investigation, and the neural bases of mental calculation are still not fully understood [21]. Another interesting question is whether the arithmetic operation modulates the recruitment of functional brain networks in the early encoding stage [22]. This question arises due to conflicting results in small addition and multiplication problems. Some findings suggest that memory retrieval is used to solve small addition and multiplication problems [23], [24]. Others find memory retrieval only for multiplications and suggest that some single-digit additions are solved by procedural strategies [7], [25], [26].

5.1.2 Arithmetic strategies

Solving mathematical problems is a systematic process. Although the world comes up with infinitely many different problems, it turns out that most of them are remarkably similar. The logic that underlies mathematics involves developing plans to solve each of them efficiently.

It is consistently found that mathematical ability depends on the individuals working memory, culture [27], and age ([28], [29] and [30] for a review). As these factors are not influecable by an individual, it is more interesting that mathematical ability also depends on the ability to control and maintain information [31] and the used strategy.

Strategies are "a procedure or a set of procedures to achieve a higher level goal or task." [32]. In order to investigate arithmetic strategies, the authors identified four aspects of strategies that influence the overall performance of the solving process [33]. These are repertoire, distribution, selection, and execution.

Strategy repertoire: The repertoire includes all known and usable strategies. It differs between verification tasks (plausibility checking: estimation and rule-rule validation; rounding: up and down) and production tasks [34]. The latter are solved through a recall from the long-term memory (retrieval) or procedural strategies. Procedural strategies include counting (+1,+2,+3,...) and more advanced decompositions [5], [35]. These are usually taught as mental models. Prominent examples for additions are compensating (e.g. $53 + 29 = 53 + 30 - 1$), splitting ($53 + 27 = (50 + 20) + (3 + 7)$), taking doubles ($20 + 17 = 2 \cdot 20 - 3$) and jumping ($394 + 148 = 394 + 100 + 40 + 8$). Strategies applied at multiplication problems often involve transformations that make use of the associative property ($125 \cdot 32 = 25 \cdot 5 \cdot 8 \cdot 4 = 25 \cdot 4 \cdot 5 \cdot 8$) like taking times 10 ($32 \cdot 5 = 32 \cdot 10/2$).
Independent of the operation, it is essential to have a rich pool of strategies. This forms the basis for selecting the most efficient procedure.

Strategy distribution: The distribution of strategies varies across operations and cultures. The authors of [27] found that Chinese origin students outperform non-Chinese origin students significantly at simple arithmetic tasks. Besides less efficient retrieval skills, a higher rate of procedural strategies was found to be the cause of the worse performance of non-Chinese origins.
This is consistent with the general knowledge that individuals prefer easier strategies when available. Thus, adults use a recall from long-term memory for simple problems, whereas children still use the more demanding counting and other-procedures. Larger problems are usually solved by procedural strategies in general.

Strategy selection: The proper selection of strategies is essential for high performance. People tend to prefer easier strategies over more general ones, and the summary in [34] suggests that problem characteristics serve as a selection criterion. Findings in simple multiplication tasks support this statement. [27] and [36] found that small multiplication problems are mostly solved by memory retrieval. These types of problems are learned by hard with multiplication tables in primary school. Therefore, most of them are easily accessible from long-term memory. As the operand size increases, more and more individuals tend to select procedural strategies [7], [35], [37], [38].
Children learn addition problems through finger-counting, number lines, or the abacus. Therefore, they learn these facts by doing rather than by hard. Here, the min procedure, where one starts at the larger operand and counts on min-operand times, replaces counting. Finally, we remember results by hard and can retrieve them directly from long-term memory [39].
Furthermore, [40] found that retrieval interference influences the selection whether to use retrieval or procedural.

Strategy execution: Memory retrieval is fast and requires fewer cognitive resources and less cognitive demand than procedural strategies. Furthermore, the performance and error rate depends on the familiarity with the numerical stimuli. Both vary with differing presentation formats (Arabic digits vs. written number words) [41]. Errors are often results of associative and semantic neighbors in the same (3x6=21) and related (3x6=9) operations [42].

5.1.3 Numerical cognition

Research came up with three main models that aim to explain the cognitive architecture of numerical cognition during the last thirty years.

Abstract-code model: The abstract-code model [43]–[45] describes number cognition as a three-step process. The so-called comprehension system translates numbers from Arabic digits and verbal numerals into abstract code. The intraparietal sulcus is thought to hold the representation of the abstract code [46]. Depending on the form of representation, different paths of translation are used. The second process is responsible for the calculation. It includes the memory of arithmetic facts, mathematical rules, and procedures to break down more complex tasks. After the actual calculation, the answer is translated back to number words and Arabic digits by the response production system. [43]. Most of the arithmetic strategy papers rely on this model.

Triple-code model: The triple-code model [47]–[49] predicts neuroanatomical correlates better than the abstract-code model. It does not require to translate external representations into an abstract internal form. Instead, Dehaene et al. assume that depending on the input, one of three codes is activated. The visual *Arabic number* form responds for digital inputs and is responsible for parity judgments and multidigit operations. The auditory-*verbal word* frame gets active for spoken and written number words. It includes arithmetic fact memory mainly as language-based representations and is responsible for simple arithmetic additions and multiplications. The *analog magnitude* representation is responsible for numerical size comparisons and approximate calculations. It is noteworthy that codes are convertible without an abstract intermediate layer. The solution of tasks is either retrieved through the direct route or processed by an indirect semantic route. The former converts operands (3x4) into the verbal code (three times four) and uses that representation to retrieve the result through the left cortico-subcortical loop. This involves the basal ganglia and thalamus [50]. The indirect route makes use of analog magnitude representations and performs semantical operations onto them. This involves the parietal cortex (angular gyrus, supramarginal gyrus) and the perisylvian network. The performance depends on the input format.

Encoding-complex model: The encoding-complex model [51] builds upon the triple-code model and describes the representation codes (visual, verbal, visuospatial, motoric) as modular too. However, these two models differ when it comes to the form of interaction between the codes. The encoding-complex model assumes that additive interactions are not realistic and describes them as more interactive. A single numeral activates several associations to comparisons, estimations, and facts. (In other words, a rich association network of task-relevant and irrelevant information.) Excitatory and inhibitory connections ensure that one comes up with the right conclusion. The performance and error rate depends on the familiarity of the numerical stimuli. Both can be very different for different presentation formats (Arabic digit vs. written number words) [41], [52]. Errors are linked to both associative and semantic neighbors in the same (3x6=21) and related (3x6=9) operations [42].

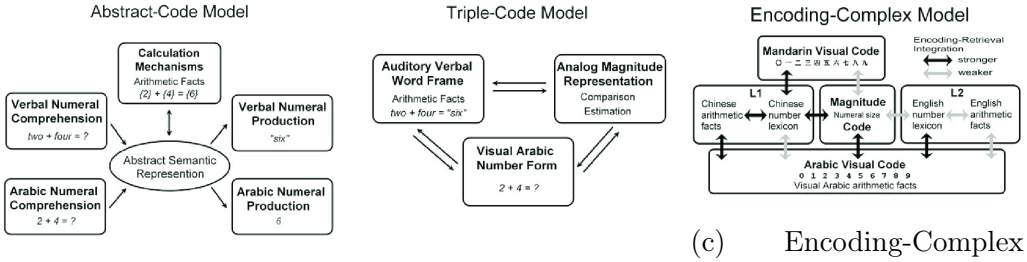

(a) Abstract-Code Model (b) Triple-Code Model (c) Encoding-Complex Model

Figure 5.1: Three architectures for numerical cognition [42]

5.2 Electroencephalogram (EEG)

The impossibility to gain external evidence about the correctness of current theories of arithmetic solving processes, makes it necessary to combine a range of research methodologies. Besides structural insights from autopsies and magnetic resonance imaging (MRI) and functional insights (lesion studies, fMRI, verbal self-reports), it is of high interest to collect information about the time course of neurological processes. Here, measuring the response time allows us to infer how long it takes an individual to solve a mathematical problem. More detailed time information about the activation of specific brain regions can be acquired with the electroencephalogram.

Its name best explains EEG (Electroencephalography). 'Electro' stands for electrical activity, 'encephalon' relates to the brain, and 'graph' refers to the time course of the recorded data. EEG is a method that registers electrical activities in the cortex and gives us insights about the inner dynamics. A beneficial characteristic of EEG is that it is non-invasive, meaning measurements without surgical interventions.

The measurable EEG signal originates in the neocortex and is modulated by several anatomical tissues before it reaches the skin. The neocortex is a part of the cerebral cortex. It is 3-14mm thick and consists of approximately 20 billion neurons [53]. Each of the neurons processes information through temporal and spatial integration of the incoming signal and spikes once a certain threshold is reached. It is known that the large pyramidal cells of the fifth (out of six) layer process incoming information and contribute most to the measurable signal. Sensors on the scalp measure the superposition of large cohorts of neurons and the signal is strongest when large cohorts of neurons are inactive. Then they are maximally synchronous, and the measurable signal lies at about 50 µV. Once brain regions are recruited, they desynchronize, and the superposition of their electrical fields decreases. The anisotropic composition of the head increases the difficulty

of localizing activated regions, because it makes the signal propagation from the neurons/source dipoles to the sensors non-ideal. The frequency range of the measured signal is within 0.1 Hz and 200 Hz.

Two main effects are found in the EEG time course: evoked related potentials (ERP) and event-related (de)synchronizations (ERD/S).
ERPs occur after an external stimulus (visual, auditory, olfactory,..) reaches the brain through afferent pathways. The analysis of such phase-locked responses allows us to infer conclusions about the time course and duration of strategy processes [54] and to distinguish different rule-violation problems [55].

Brain induced ERD/S are not phase-locked to stimuli, but occur due to the coupling and decoupling of functional brain networks. This measure is a central topic of this thesis. Therefore, oscillations are explained in the following chapter.

5.2.1 EEG oscillations

Neurons are synchronized in the idle state and desynchronize when they process information. Pfurtscheller et al. related the coupling and decoupling of functional brain nets to changes in EEG oscillations ([56], see also [2], [3], [57]). Thus, EEG oscillations provide information about the interaction of task-related networks. In order to do so, one compares the spectral band power of the task to a baseline period, either within many frequency bins (ERD/ERS or ERSP) or averaged in broader frequency bands (delta, theta, alpha, beta, gamma).

Theta-band

Power in the theta band ($4 - 7$ Hz) is related to different cognitive processes like working memory [58], [59], attention control [60]–[62], information encoding or mental manipulations.
Theta ERS is predominant while solving smaller (sum < 10) problems and self reported retrieval processes. The authors of [63] and [64] found theta ERS over the left hemisphere when they compared small and large problems. [64] found theta ERS for multiplication tasks too and [5] reported it for self-reported retrieval strategy usage. ERS is linked to memory encoding and retrieval [65]–[67] and may reflect fact retrieval [3], [4], [68], [69].
Phasic theta synchronization of different regions is thought to represent functional integration during information encoding [58], [59], [61], [70], [71]. In the frontoparietal regions, this is mainly controlled by the demand of the working memory system while manipulating information [72], [73].

Alpha-band

Power in the alpha band ($8 - 12\,\mathrm{Hz}$) is high when the default network is activated [74]. Moreover, alpha power inversely correlates with the invested cognitive resources [56] and mental activity [56]. Alpha ERD occurs when information is accessed and retrieved from the knowledge system [75], [76], which includes long-term memory, procedural, and implicit-precentral knowledge. In arithmetic, alpha power changes with the difficulty of cognitive tasks [77], [78]. Decreased alpha band power was found bilaterally for large problems [4], [63], [69], [79]–[81] and for self-reported procedural strategies [35].

Delta-band

ERS in the delta-band (0.5-4Hz) arises when the default network is inhibited. Thus, it is predominant at procedural tasks in arithmetics [82].

5.2.2 Processing EEG data

Neurons that cause the EEG are anatomically placed inside an anisotropic volume conductor that damps the measurable signal strength to values of only some µV. Therefore, small measurement noise has already a tremendous influence on the data. Artifacts can reach several orders of magnitude of the EEG signal itself and share the same frequency ranges as relevant physiological signals. Therefore, simple filtering methods are often not sufficient to increase signal-to-noise ratio (SNR). In practice, several approaches exist to clean EEG data.

Artifacts observed for EEG data have two main origns. Some are caused by biological processes, whereas the others arise through interactions with the environment (external interference fields, movement of the subject) and the measurement process (calibration error, crosstalk between sensors, and sporadic sensor artifacts). The latter ones include electrode displacement, movement artifacts, and interference from the environment and are avoidable by a carefully designed measurement setup and clear subject instructions [83]. As EEG captures the signal from outside the body, the measured signal will always contain a mixture of interfering sources. Some of them are interesting, as they represent neurological networks, while others are irritating. They have their origin in other physiological processes such as eye, heart, and muscles, to name the most prominent ones. Biological artifacts usually share frequency ranges with neurological sources. Therefore, biological artifacts are not removable by simple filter methods. However, most of them have well-described stereotypical properties in the spatial, frequency, and temporal domain. Therefore, they are identifiable and removable by blind source separation methods.

Biolgical artifacts:

A range of biological artifacts distorts the EEG-signal. The following paragraph describes their origin and typical characteristics and figure 5.1 shows typical scalp distributions as well as the time- and frequency- course of the most prominent artifacts.

Eyeblink artifacts are caused by brief dipole changes of the eye [84] and are of considerable magnitude. Therefore, they distort the measured EEG to a large extent, mainly in the frequency below 4Hz. The source dipole is located in the very front of the scalp and is oriented vertically.

Eye movement (e.g. from one side to the other) cause artifacts too. Eye movements last approximately 2s. The magnitude of the signal increases significantly and decreases again in a sinusoidal way later on. The dipole representing the source is located in the very front of the scalp and is oriented horizontally from left to right.

The heart's pacemakers causes *cardiac interference*. It shows the well-known waveform, including the P-wave caused by the pacemaker in the sinoatrial node followed by the excitation in the right atrium and the following forwarding to the AV node. The QRS-complex is has its origin at the excitation of the ventricles. The heart is evoked at frequencies of about 1-2Hz. Dipole-fitting techniques often locate the ECG dipole outside the head. The spatial pattern shows an activation at the boundary of the head.

Myogenic interference is caused by muscle cells. The time signal shows very dense oscillations of high amplitude that are known as bursts. The frequency spectrum overlaps with EEG to a high degree. It starts at approximately 20Hz and ranges to above 100Hz. The spatial patterns are very dense and not dipolar. The source is usually located on the outer side of the scalp.

Electrical interference is caused by cables that consistently induce voltage from the oscillating line frequency and occasionally when participants move their heads. The major part of the signal is found at 50Hz. The spatial pattern is usually dipolar, its distribution is supra-gaussian.

Table 5.1: Stereotypical properties of biological artifacts

eye blink	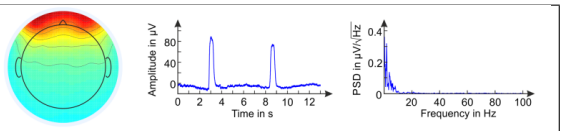
eye movement	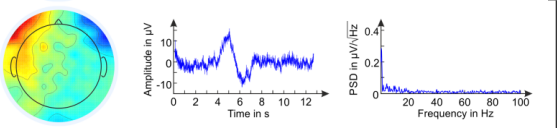
cardial interference	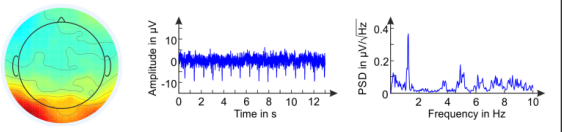
myogenic interference	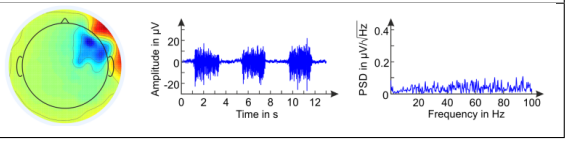

Common methods

In order to clean EEG signals, one can look at the problem from two perspectives. At first, it is possible to characterize a clean EEG and remove all information that is out of this range. The second way takes advantage of stereotypical properties of the artifacts, and aims to extract, estimate, and remove this information. This method may not identify all unwanted disturbances but is less likely to remove interesting parts of the signal mistakenly. Therefore, this approach is preferred by most scientists [85], [86].
Further, one can take advantage of the fact that neural responses to a stimulus are often phase-locked. Measuring the response multiple times and calculating the mean cancels out the non-phase-locked components. This requires the recording of multiple trials, which is not suitable in real-time applications. However, it is entirely sufficient for offline data processing as is done in this thesis.

In Table 5.2, some of the most popular methods are presented together with their main assumptions.

Table 5.2: Example methods and their assumptions

Principle	some assumptions	example
Data rejection	artifacts have abnormal statistics (magnitude,...) noisy channels are restorable by healthy surroundings channels are correlated	AutoReject [87]
Artifact-subtraction	artifacts are predictable artifacts are not correlated to the signal	Regression
Source-rejection	sources are independent artifacts have stereotypical properties requires many channels	MARA [86] ICLabel [85]
Statistical	EEG is stationary artifacts are non-stationary and additive works on single-channels	

Sensor-rejection In EEG, it is easily possible that individual sensors get loose, interfere with electrical noise, or capture other artifacts. In the later processing steps, it is common to combine the signal from a set of sensors (e.g., common average reference) or trials (e.g., signal averaging) in order to subtract a baseline or get further insight to the data. This spreads noise from single sensors over the whole dataset. Therefore, it is reasonable to exclude bad sensors immediately after the measurement. An easy way to perform this is by statistically comparing the values of sensors to typical M/EEG values and rejecting the atypical ones. The difficulty of this task lies in finding a tradeoff for the threshold values. The exclusion of noisy sensor data often contradicts the goal to keep as much of the useful signal in the data as possible. Popular methods use the statistical measures peak-to-peak value [88] and covariance matrices [89]. A limit of these methods is that the thresholds are often predefined, which is not optimal as these values depend on the recording method (wet vs. dry), the used amplifier, and the hardware filters. More modern approaches automate the manual process of trial and error by finding an optimal threshold value [87].

Artifact-subtraction methods are based on the assumption that signals that cause noise can be estimated. The estimation relies on a reference channel. A necessary assumption is that the reference channel and the cortical signal are not correlated.
A representant of this category is *regression*. It uses prior knowledge like the waveform of the net frequency or reference channels (EOG, ECG,...) to estimate their contribution to the signal of interest.
The clean signal is calculated by subtracting the estimated noise-signal from the raw EEG.

Source rejection algorithms rely on the assumption that neuronal and non-cortical signals are not only measured as summed mixture of the sources but that these sources are independent of each other. This makes it possible to separate the individual components. Measures in the time, frequency, and spatial domain allow us to compare the activation of components to stereotypical features of artifacts. Thus, it makes it possible to identify and remove Independent Component (IC)s representing artifacts.
The separation of ICs is based on BSS algorithms, as described in the next chapter.

5.2.3 Blind source separation

Blind source separation (BSS) bases on the assumption that the measured EEG signal is caused by a summed mixture of cortical and other biological sources. Further, these components are assumed to be statistically independent of each other. BSS algorithms help to identify and separate the underlying independent processes.

Principal component analysis (PCA)

A prominent example is principal component analysis (PCA), which bases on variance. It projects data to a new space whose axes are spanned orthogonally by the maximum variance. The so-called principal component analysis decomposes the (empirical) covariance matrix into its eigenvectors and eigenvalues. As the matrix is square, the left and right eigenvectors are equal and span the new space. This approach works fine to compress or whiten the data. Nevertheless, it is not sufficient to separate the sources as they are often not orthogonal and non-Gaussian (e.g., line noise).

Independent component analysis (ICA)

A more sophisticated approach to separate sources bases on information theory and the inverse central limit theorem. This theorem assumes that the superposition of infinitely many independent variables results in a single Gaussian distribution. ICA takes the inverse approach and separates sources by picking independent variables that are maximal non-Gaussian. ICA minimizes the mutual information between the sources. Unfortunately, this measure is very costly to calculate. Thus, we use measures like the negentropy (which is still costly) or non-Gaussianity.
Various implementations of ICA exist, but in a machine learning context, it is close to using a maximum likelihood approach. The realization of such an implementation requires to formulate an objective function whose extrema are then found by

an optimization algorithm.

Objective function:
A reasonable objective function is a negentropy. It measures the difference between the independent components distribution and a Gaussian distribution and hence is always positive and 0 for a Gaussian distribution. Unfortunately, the calculation requires finding all density distributions. Measures that are simpler to calculate are higher moments like the kurtosis. It is negative for sub-Gaussians and positive for super-Gaussians. Therefore, the square of the kurtosis is the correct approximation for independence (under the constraint of zero-mean and unit covariance).

Optimization algorithm:
Various optimization algorithms exist that allow us to find the mixing coefficients of ICA. The gradient descent algorithm works fine but is very time-consuming due to the zig-zagging phenomenon. Extrema are found faster by the conjugate gradient algorithm as it constrains the search direction to orthogonality. As the EEG source reconstruction is typically an underdetermined problem, Newton-methods perform much better. As the Hessian matrix is costly to calculate, especially for large data, it is useful to approximate the matrix. Quasi-Newton algorithms like the LBFG-s are typically much faster.

Localizing ICs:
Often it is useful to localize the independent processes. A dipole fit can do this. This algorithm starts by assuming approximate locations of each IC. It then solves the forward problem (which is how the signal spreads to the surface). The comparison of calculated sensor values to measured ones helps to adjust the locations of the ICs through an optimization problem.
Solving the forward model requires the knowledge of the conductive properties of the head. An MRI scan can acquire these values or based on a standard model. The former is exact, but it is expensive and consumes much time. An easier approach is the standard model, as it does not require additional imaging technologies. It may be based on already existing MRI studies or assumes that the head has isotropic properties within the most prominent layers (skin, skull, cerebrospinal fluid, cortex).
The actual fit of locations starts with a rough grid-search. A precise cost-minimization algorithm then finds final locations.

5.3 Anatomy

Mathematical cognition requires the interplay of many specialized brain regions. [90] describes one way to segregate the subfunctions (see Figure 5.2). They distinguish six subsystems that are responsible for processing visual number form, auditory number form, numerical quantity, working memory / cognitive control, for storing information in the episodic/semantic memory, and for salience/attention control. Information exchange occurs through hubs, as the integration of information is essential. This makes solving arithmetic problems possible.
The two most basic subsystems (auditory and visual number form) are responsible for recognizing the incoming information. Visual and auditory stimuli like symbols (3) and verbals (three) are decoded and connected with their underlying numerosities. The superior temporal sulcus (STS) decodes phonological numbers, and the fusiform gyrus (FG) processes written numbers. The FG is also thought to build orthographic representations of numbers and connect them to their meaning.
The intraparietal sulcus (IPS) [91] performs the integration of the auditory and visual pathway. The IPS is, together with the FG, also the main structure for dealing with and understanding numerical quantities.
Regions responsible for the working memory and cognitive control are the frontal eye field (FEF), dorsolateral prefrontal cortex (DLPFC), the supplementary motor area (SMA), the premotor cortex (PMC) and the basal ganglia (BG). They contain functions to hold variables in the working memory temporarily. The DLPFC generates strategies for solving multi-step problems.
Episodic and semantic memory systems play a crucial role in learning and solving arithmetic problems. The hippocampus in the medial temporal lobe is the major part when it comes to forming long-term memories. It stores arithmetic facts and allows individuals to generalize the solution process to unknown problems.
Finally, the anterior insula (AI) and the ventrolateral prefrontal cortex (VLPFC) connect IPS and medial temporal lobe (MTL). They integrate information coming from both and are responsible for salience, attention, and control.

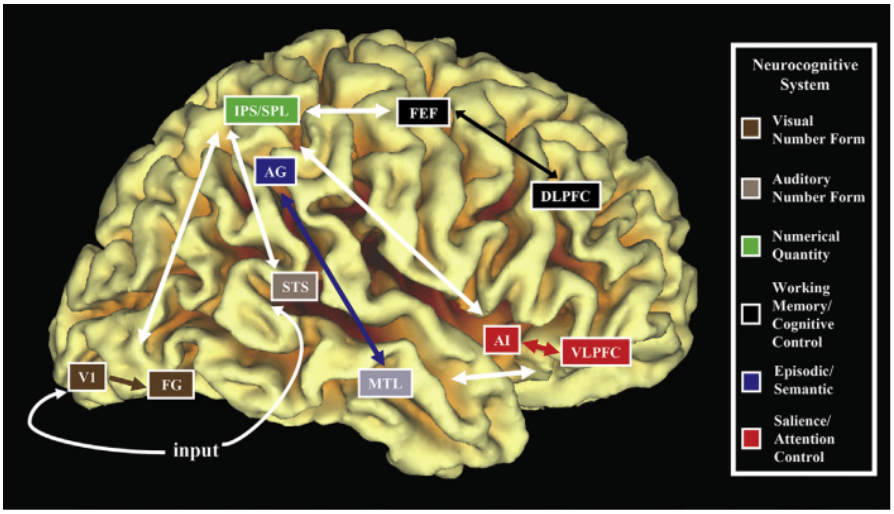

Figure 5.2: Schematic illustration of the involved brain areas in arithmetic calculation [90]

5.3.1 Visual number form

Visual stimuli are captured by photoreceptors that pass the information on to the retinal ganglion cells. From here, the lateral geniculate nucleus located in the thalamus relays the signal to the visual cortex (V1) in the occipital lobe. The V1 detects low-level features like orientation and disparity and some of its regions process color. After the low-level features are recognized, information is passed on to the extrastriate cortex. From here on, two pathways exist to resolve higher-level features. The dorsal stream recognizes 'where' something is happening, and the ventral stream identifies 'what' is going on. The ventral pathway decodes midlevel features like the shape, motion, and color in the lateral occipital cortex, the middle temporal visual area, and the CC. These midlevel features serve as input to the fusiform face area (FFA) that is mainly involved in detecting faces, the parahippocampal place area, which is responsible for recognizing places, and the extrastriate body area. The temporal cortex plays a role in visual number form.

Fusiform gyri (FG)

The fusiform gyrus (FG) plays a role in recognizing and combining visual stimuli and helps to put them into a higher context like faces, words, or equations.
It is the most prominent structure in the ventral temporal-occipital cortex and is integrated into the ventral visual stream. The mid-fusiform sulcus splits the FG into two parts; a medial and a lateral portion. The lateral FG contains the

well-known FFA that is responsible for recognizing faces. Besides face recognition in the FFA, the FG plays crucial roles in processing color information (together with other V4 areas). It is responsible for making sense of symbols and integrating these features into schemes that represent words and equations (left FG) and identifies whether face-like features are faces.
Further, the fusiform gyrus is thought to play a crucial role in encoding object properties [92], [93] and categorizing objects. It is linked to diseases like synesthesia, dyslexia, and prosopagnosia. During visual word recognition, the left FG responds to orthographic structures [94] and the authors of [95] think that the FG integrates features into elaborate schemes that represent whole words or objects. The meta-study of Arsalidou found activations of the left FG for number and calculation tasks. The right fusiform gyrus is responsible for processing global structures like faces [96] but is probably not involved in number processing.

5.3.2 Auditory number form

Superior temporal sulcus (STS)

The superior temporal sulcus decodes phonological features of heard numbers.

5.3.3 Numerical quantity

Superior parietal lobule (SPL)

The superior parietal lobule (SPL) supports numerical quantity processing and is consistently activated during number processing [15], [16], [49], [97]–[99]. Blocking its function with transcranial

Intraparietal sulcus (IPS)

The IPS plays a crucial role in quantity processing and understanding numbers.
It is a part of the parietal lobe, is included in the dorsal stream, and has five substructures. The IPS is involved in visuomotor functions and guides grasping and hand movements (anterior), reaching and pointing (ventral and medial), saccadic eye movements, and visual attention (lateral). It is further responsible for the perception of depth (caudal). Although the IPS is integrated into the dorsal stream, it dynamically interacts with ITC (ITC). This interplay between the two visual streams is thought to be necessary for deconstructing arithmetic problems. Together, the IPS and ITC are essential for representing numerical quantities and manipulating them by the use of arithmetic rules and procedures. [46] observed an activation for quantities in the left (independent of the stimulus format) and right (only for Arabic numerals) IPS.

[15] varied the number of operands and the rate of stimulus presentations and found the main effect of arithmetic difficulty in the IPS. This is consistent with the finding that a wide-spread network, including bilateral parietal regions, is activated while processing large problem sizes [100]. However, the IPS is also required for operations that are solved by the retrieval strategy [101]. Blocking the IPS with transcranial magnetic stimulation led to an increase in response times and error rates.

5.3.4 Episodic / Semantic memory

Angular gyrus (AG)

The AG is responsible for complex language functions, memory retrieval, mathematical and spatial cognition, and the awareness of the self. The language functions include understanding words by transferring visual information to Wernicke's area ([102], Textbook of medical physiology p699), and integrating information of words and locations (e.g., distinguishing left from right). Further, it can access episodic memories and content, but most importantly, it notes contradictions between expected and retrieved information. The self-monitoring process is also crucial for comparing intended and performed movements as it allows the experience of the awareness of self. Notably, the right AG is associated with orienting in 3D-space by directing the attention to salient features.
The triple-code model proposes that the AG, together with other regions of the inferior parietal cortex (supramarginal gyrus) and the left perisylvian network is an essential part of the indirect semantic route [103]. This allows the AG and supramarginal gyrus to attach meaning to words and simplify equations. Further, the AG is probably involved in controlling visuospatial attention while calculating problems [104]. The ability to retrieve information from the knowledge system allows the AG to perform exact calculations, which is in contrast to other regions of the parietal lobe that come up with approximate calculations. In particular, activations are particularly strongest in the left AG when retrieving mathematical facts [97]. The activation is even higher for mathematically, competent individuals.

Medial temporal lobe (MTL)

The MTL contains the declarative memory system, including the episodic and semantic memory system. The hippocampus stores arithmetic concepts and facts. The MTL is thought to generalize solutions to unfamiliar problems.

5.3.5 Salience / Attention control

Anterior insula (AI)

The insula is known to play roles in emotional processes [105]–[109], execution of responses [110], and error processing [111]. Together with the ventrolateral prefrontal cortex, it integrates information between the IPS and MTL.
In mathematical cognition, the AI is thought to be responsible for switching between working memory and resting states during information processing [112], and initiating motivated behaviors [113]. The anterior insula is activated bilaterally for number and calculation tasks [104].

Ventrolateral prefrontal cortex (VPFC)

The activation of the left ventrolateral prefrontal cortex depends on the domain-general task difficulty and is 'sensible to incorrect arithmetic expressions' [13].
A comparison of PPC (PPC) and prefrontal cortex (PFC) did not allow to distinguish their roles clearly yet [114], [115].

5.3.6 Working memory / Cognitive control

Dorsolateral prefrontal cortex (DPFC)

The dorsolateral prefrontal cortex (DPFC) is associated with executive functions like managing resources of working memory [116], [117], cognitive flexibility, planning, inhibition, and abstract reasoning. The functions are performed together with its connected regions. Linked to the thalamus, the dorsal caudate nucleus of the basal ganglia, the hippocampus and regions of the neocortex, the DLPFC is the endpoint of the dorsal stream.
Cognitive functions are organized hierarchically. This is true for simple number tsks too [116]. The inferior frontal gyrus (BA9) is activated for simple number tasks, and whenever more than a few items or procedural steps are required, the middle frontal gyrus (BA 46) gets involved too. The superior frontal gyrus (BA 10) is involved in solving multi-step tasks and in generating strategies.

Supplementary motor areas

Mathematical understanding evolves from counting methods like finger-counting or using the abacus. Although we do not calculate with the use of our fingers, motor areas are still involved in adults. Due to the training with the abacus, the involvement of motor areas is even stronger in Chinese individuals.

Basal ganglia

The basal ganglia is a complex of smaller structures, including the caudate, putamen, globus pallidus, substantia nigra, and thalamic nucleus. It plays a supportive role in the maintenance of information in the working memory [118] and is crucial for learning procedures and habits.

Left putamen:
The left putamen is involved in tasks like motor control (Marchland 2008, Menon 1998) and learning of stimulus-response associations [119]. It is thought to integrate information in arithmetics by pacing the coordination of top-down and bottom-up items [100] and plays a role in number tasks.

Right caudate:
The caudate is thought to play roles in higher-order motor control (Menon, 1998) as well as in learning and memory.

Cingulate gyrus

The cingulate gyrus is part of the limbic system and plays key roles in working memory [104]. The anterior part is involved in controlled value judgments and impulse control. It helps to allocate attention and select actions. Further, it is involved in reward anticipation.

Cerebellum

The cerebellum is involved in motor control, goal directed actions and visual motor sequencing. It plays parts in working memory [120] and action sequencing [121] too. The cerebellum shows activations in mathematics [10], [122], [123], but its involvement is not systematically discussed [104]. Arsalidou suggests that it is "influenced by a prescribed plan" and involved in "coordination of viusal motor sequencing particularly under conditions with time constraints, as are often required in number and calculation tasks".

Thalamus

The thalamus acts as a hub between cortical and subcortical regions (midbrain) [124], [125]. It is linked to the execution of responses [110] and executive control [126]. Higher goals can influence the function of subcortical regions. In arithmetics, it is linked to the left cortico-subcortical loop and contributes to the retrieval of arithmetic facts.

Prefrontal cortex

The prefrontal cortex is highly involved in executive functions like working memory. It plays roles in developing and executing strategies, making choices, and planning. Especially, the medial frontal gyrus is thought to generate strategies for problems that involve more than one step.

5.4 Aim of the study

Several years of research found converging evidence that EEG oscillations are modulated by the problem-size effect and by the used strategy (retrieval vs. procedural). Further, imaging studies involving fMRI identified key regions involved in number processing and arithmetic. Most prominent is the involvement of the V1 and fusiform gyrus for identifying numbers, the key role of the IPS for processing numerical quantities, and cognitive control, including working memory of the frontal regions involving the DLPFC.
A very interesting part of this master thesis is to verify whether a special linear decomposition technique (ICA) allows insights into the data that would not be possible otherwise. For this, a data set recorded on European adults challenged with single-digit addition and multiplication problems is used.
This thesis comprises three main research questions. It starts with the investigation of the problem size effect onto response times and ERD/S patterns. The problem-size effect is the consistently found effect of increasing response times, theta ERS and decreasing alpha ERD. Second, we inspected the effect of strategies (retrieval vs. procedural). Retrieved problems show higher theta ERS and lower alpha ERD than procedurally solve ones. Third, a newer behavioral study is challenged. The authors of [7] question the validity of the current state of research that small addition problems are solved through a recall from long-term memory. Instead, they suggest a new model according which small addition problems would be solved through fast, automated procedures.

For all of these questions, hypothesis are formulated for the sensor-space and investigations of the found independent processes. The main purpose of their comparison is to verify whether the inspection of independent components is worth the additional computational effort.

5.5 Research Questions and Hypothesis

5.5.1 Problem size: Are there differences between tiny, small and large addition problems?

The problem size effect occurs very consistently at solving arithmetic problems. It is known that large problems are solved slower, cause a lower left-hemispheric theta-ERS and a lower bilateral alpha-band power in the parieto-occipital regions [5].
The first question asks whether the analysis of independent processes reveals a clearer insight into differences between tiny, small, and large problems. Ten hypotheses cover the current research.
Hypothesis 1: There is a difference in response times between tiny and large problems [127], [7].
Hypothesis 2: There is a difference in response times between small and large problems [35].
Hypothesis 3: There is no difference in response times between tiny and small problems. [7]

Recent research showed that theta ERS is linked to the retrieval of semantic information from the long-term memory (LTM). It plays an important role in memory encoding [128] and is involved in the storage and recall of verbal working memory (WM) [80]. [66] observed mainly frontal theta ($7 - 8.5Hz$) ERS during a WM task that increased with the number of items remembered.
In arithmetical processing, amongst others, [5] found that small problems cause a stronger activation in (left-hemispheric) theta activity. Thus, the following hypotheses are:
Hypothesis 4: Tiny problems show a higher left-hemispheric theta ERS than small problems.
Hypothesis 5: Small problems show a higher left-hemispheric theta ERS than large problems.
Hypothesis 6: Tiny problems show a higher left-hemispheric theta ERS than large problems.
Hypothesis 7: Large problems show a lower alpha band power in the bilateral parieto-occipital regions than tiny problems [5].
Hypothesis 8: Large problems show a lower alpha band power in the bilateral parieto-occipital regions than small problems [5].
Hypothesis 9: Small problems show a lower alpha band power in the bilateral parieto-occipital regions than tiny problems.

The AG and MTL (hippocampus) are involved in the recall of arithmetical

facts from memory [97]. Taking the previous references into account, we expected to find independent neurological processes that are not observable on the sensor space. Dipoles related to these processes are located in the left-hemispheric perisylvian region and parieto-occipital. Therefore, the hyposes 10 and 11 state as follows:
Hypothesis 10: At least one IC-Cluster is found in the left-hemispheric perisylvian region that shows enhanced activity in the theta-band for small problems.
Hypothesis 11: At least one IC-Cluster is found in the parieto-occipital region that shows enhanced upper-alpha ERD for large problems.

5.5.2 Strategies: Are there differences between recalled and procedurally solved strategies at large problems?

The aim is to show that differences are found between large addition problems, which solution was recalled, and those that were solved using procedural strategies. The hypotheses for response times and sensor space EEG oscillations follow from the existing literature. Hypothesis relating the found independent processes are similar to the sensor-space.

Hypothesis 12: There is a difference in response times between recalled and procedurally solved problems.

Converging evidence shows that recalled problems cause a stronger activation in left-hemispheric regions, including the angular gyrus [97], while larger problems show stronger activation in the frontoparietal networks including the intraparietal sulcus. Thus, hypotheses are given by
Hypothesis 13: Recalled problems show a higher left-hemispheric theta ERS than procedurally solved ones [5].
Hypothesis 14: Procedurally solved problems show less low alpha band power in the bilateral parieto-occipital regions than the ones solved through retrieval [5].
Hypothesis 15: Procedurally solved problems show a lower upper alpha band power in the bilateral parieto-occipital regions than the ones solved through retrieval [5].

Hypothesis 16: At least one IC-Cluster is found in the left-hemispheric perisylvian region that shows enhanced activity in the theta-band for recalled problems than for procedurally solved problems.
Hypothesis 17: At least one IC-Cluster is found in the parieto-occipital region that shows enhanced upper-alpha ERD for procedurally solved problems (over recalled ones).

6 Methods

6.1 Data acquisition

6.1.1 Participants

This work uses a data set consisting of 40 healthy participants aged 18 to 29 (mean 21.93, SD 2.99). Gender distributed equally (20 female, 20 male), and exclusion criteria were calculation difficulties, education below high school, left-handedness, and an age above 35. The Ethics Committee of the University of Graz approved the study. They received course credits and could win one of two gift cards.

6.1.2 Materials

EEG recording

The data set consisted of single-digit production tasks (addition and multiplication). The tie problems were excluded as they are recalled very quickly from memory. Similar to [7] all other operand combinations between 1 and 9 were grouped into three problem sizes. In a newer study [7] Uittenhove et al. found a monotonic increase in response time (RT) for operand sums between 3 and 7, a rapid increase for problem sizes between 11 and 13, a constant RT above 13, and no clear trend between 7 and 9. Following this observation, they suggest that additions involving only operands below five are solved through fast reconstructive processes. This claim contradicts the common belief that we retrieve the results from LTM. Therefore, here we grouped tiny problems (operands below 5) separately from small ones ($7 \leq sum \leq 10$). The category for large problems consisted of sums greater than 10. This resulted in 16 tiny, 24 small, and 32 large problems per operation. As the main focus of the experimenter was to reproduce the results of [7], tiny problems were presented nine times each and small and large problems were shown only two times each. This resulted in 256 trials for the addi-

tion problems. Multiplication tasks consisted of the same operand combinations. Thus, tiny problems showed a product between two and 12. Small tasks led to a product of $6 \leq \Pi \leq 24$ and the product of large problems lies between 18 and 72.

Each trial started with a fixation point for two seconds. After this pause, subjects solved the presented problems as quick as possible and spoke the answer into the microphone. A microphone detected the voice onset and measured the time that passed since the problem presentation. A pause separated the trials, which lasted 1 s if the problem was answered and otherwise 5 s. The typical trial is illustrated in Figure 6.1.

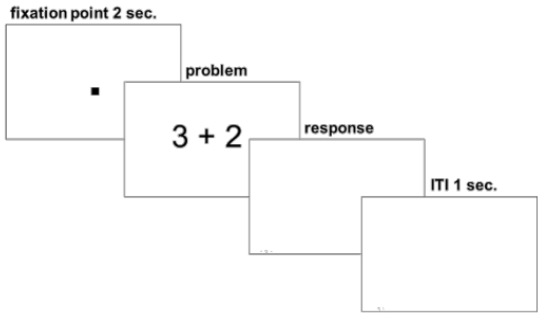

Figure 6.1: Schematic illustration of an EEG trial. [129]

Solution strategy session

Self-reported solution strategies were assessed after the EEG session as displayed in Figure 6.2. The questionaire was separated from the EEG session, otherwise it might have influenced the subjects performance of the solving process [19]. The subjects were first instructed by an information sheet that explained simple arithmetic solution strategies [27], [37]. Then, they had to solve the same problems as in the EEG session only once another time and reported their used strategies via a number pad. Possible strategies are 1 (retrieve), 2 (count), 3 (transform) and 4 (other strategy).

Data recording

A BioSemi ActiveTwo system (BioSemi, Amsterdam, Netherlands) allowed recording the EEG with 64 active electrodes. They were placed on the positions given by the extended 10–20 system.
The open-source toolbox Psychopy (http://www.psychopy.org/, [130]) was used to

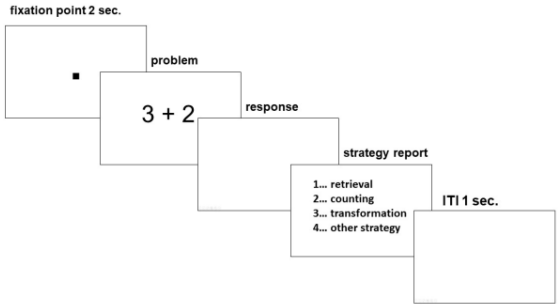

Figure 6.2: Schematic illustration of a trial for the solution strategy report.

implement the stimulus presentation. The recorded signals were low-pass filtered at 128Hz.

Procedure

All 512 trials were presented in four blocks with each block comprising 128 trials of the same operation type. The operation-homogeneity ensured that task-switching costs are minimal. However, within each block, the different operand combinations were presented in a pseudo-randomized order. Still, the order of problems was the same for all participants in one group. The two groups differed such that one started with addition problems and the other with multiplication problems.
The collection of self-reported solution strategies was done in a fifth block that consisted of all operand combinations (72 addition and 72 multiplication tasks). Trials were again pseudo-randomized within operations. The subjects started with the same operation as in the EEG paradigm. The whole procedure lasted for 2.0 to 2.5 hours.

6.2 EEG analysis

The EEG analysis was performed in three major steps. First, the data was preprocessed. This included the removal of improbable data to increase the signal quality. The data preparation was implemented in MATLAB (R2017b) with EEGLAB (v15) and the plugins ADJUST (v1.1.1), Cleanline (v1.04), ICLabel (v1.1), MARA (v1.2), PrepPipeline (v0.55.3), clean_rawdata (v1.00) and firfilt (v2.1).

Second, independent processes were identified in Python v3.7.1 with the use of numpy (v1.15.4), scipy (v1.1.0), mne (v0.17.0), pandas (v0.23.4), and a modified version of python-picard (v0.4). With this setup the processing is sped up compared to the ICA-Infomax implementation of EEGLAB.

The reimported ICs were localized by the dipfit plugin(v3.0), and clusters were found in EEGLAB.

Third, statistical tests were performed on the sensor level and on the source level. On the sensor level, the pingouin (v0.2.8) plugin for python provides an interface for repeated measures ANOVA and post-hoc tests, but misses opportunities for mixed models and a Bayesian analysis. Therefore, the data was also analyzed in R (v3.6.1). Here, the libraries data.table (1.12.2), dplyr (0.8.3) and tidyr (0.8.3) served for data handling. Moments (0.14), ez (4.4-0), afex (0.24-1), emmeans (1.3.5.1), effects (4.1-0), BayesFactor (0.9.12-4.2), and bestNormalize (1.4.0) helped to calculate statistical measures, and lattice (0.20-38) was used for plotting the results.
The same R libraries were used to perform statistical analysis on the source-space clusters. Additionally, we performed paired t-tests on individual time-frequency bins in MATLAB.

6.2.1 Preprocessing

The preprocessing pipeline was selected according the comparison found in [131]. The modified version is described here in detail.

Filtering

Electrode drifts and line noise are identifiable in the frequency domain. Thus, we applied a high-pass filter with a stop-band at 1 Hz. This fixed the electrode drifts and adjusted the data to fulfill the preconditions of the later alllied ICA. ICA assumes the data to be stationary. An FIR Hamming window with a settling time of DF=3.3 filtered out the low frequencies. The passband was set to 1.75 Hz and the cutoff frequency to 1.25 Hz.

Sensor rejection

We have used the EEGLab plugin Cleanline to reject sensors with improbable data. This plugin initially applies a high-pass filter with a cutoff frequency at 0.5 Hz to the signal. Note, that this is less stringent than the 2Hz high-pass that was applied before. The band-pass filtered signal is then thresholded at 20 times MATLAB's epsilon. The algorithm removed channels with null-segments that lasted longer than 5 seconds.
The second and third steps of cleanline are responsible for the most challenging part which is the detection of improbable data. For this, the plugin uses the *Channel-* and the *Line-Noise-Criterion*. The channel criterion determines whether the selected channel is correlated less than 0.85 to a random sample consensus (RANSAC) estimate, which is determined by the other channels. The line noise criterion determines whether the noise-to-signal ratio is higher than four times the standard deviation of the channel population mean.
Lastly, if the standard deviation to clean segments extended the defined value, the electrode was also considered as bad. Bad channels were removed and replaced by an interpolation of the surrounding clean channels.

Channel rejection

Channels with magnitudes exceeding three times the standard deviation of all other channels were considered as bad and removed. In order to be more robust against outliers, this step was applied two times.

Wavelet-thresholding

The signal was further influenced by muscular interference. These signal proportions are of high magnitude and relatively high frequency. A reducion of these components allowed a better identification of independent components. This was done similar as described in the Harvard-pipeline [131]. At first independent components were separated by an Infomax-ICA. A coiflet (level 5) served then to identify wavelet coefficients. A global threshold then identified high magnitude values which were aftwards damped by a factor of 0.75. The damped wavelet coefficients were backprojected and the sensor values were restored from the cleaned independent components.

6.2.2 Independent Component Analysis

Blind source separation

In the following, we assume that retrieval and reconstructive processes used to solve arithmetic tasks are represented in different regions of the brain and that they operate independently as proposed by . Then, Independent Component Analysis (ICA) allows to identify and separate these processes.
The Infomax-ICA implementation of EEGLAB takes more than a day of processing time on a common desktop computer for finding the mixing matrix. Therefore, a more performant ICA implementation was used. The picard algorithm solves the Infomax problem by a quasi-newton approach (LBFG-s) instead of the original stochastic descent. As this version was not available in MATLAB, the preprocessed EEG signal was exported from EEGLAB to Python, and the trained weights were then reimported to EEGLAB.
The weights were trained with epoched ($-2\,\mathrm{s}$ to $+5\,\mathrm{s}$) data that were manually inspected and from which noisy segments and wrongly answered segments were removed. Epoched data were used because the amount of data is sufficient according to the rule of thumb of Onton et al. [132]. They suggest using at least $20 \cdot n^2$ samples when n is the number of sensors. This choice is confirmed by Delorme et al.[133]. They measured the influence of training data onto the reliability of the ICA by running the algorithm multiple times on the same data set and concluded that besides the amount of data, additionally the quality plays a role.

Dipole Fit

In the next step we used a dipole-fit to find the location of the ICs. Therefore, we defined a simple model with the conductance properties of the head. It consisted of the four layers of skin, skull, cerebrospinal fluid, and the cortex itself. Then

the dipole fitting algorithm was applied. This algorithm places the n dipoles at a random position in the head, calculates the distribution of the magnetic field caused by the dipoles, and compares the superposition of the fields to the measured sensor values. The determined deviation from zero serves as the cost for the proper position of the dipoles. An optimization algorithm minimizes the cost by re-arranging the dipoles and terminates when the most optimal location is found.

Removing artifactual ICs

Further, Debener et al. suggested to remove components with a higher variance [134]. They found that sources with a low residual variance have a high reliability for different training data selections. Therefore, we removed components with a residual variance that exceeded 15 %.

Although noise that arises from other biological processes (ECG, EOG, EMG) is not completely unrelated to activations in the brain, it is commonly assumed that large proportions of noise are separable by ICA. This is often done manually by inspecting the time, frequency and spectral domains. In this thesis, however, noisy components are identified with an EEGLab plugin which has the benefit, that classification results are objective and consistent.
The preprocessing pipeline used the ADJUST plugin by Mognon et al. [135]. This uses spatial and temporal features to detect artifactual components and tendically remains more components in the signal.

6.3 Influence of problem-size

Possible differences between the three problem size categories tiny, small, and large regarding their response times and EEG oscillation activation patterns.

6.3.1 Behavioral analysis

The data subset involving response times was prepared in Python 3.6 and analyzed in R (version 3.6.1, 2019-07-05). It consisted of the subject IDs (40 levels, nominal) and problem sizes (3 levels, ordinal) of addition tasks and the dependent variable of response times. A descriptive analysis gave the first insights into the data. The actual statistical analysis was performed by a mixed model. The mixed model was chosen, because simpler methods such as ordinary least squares or between-subject ANOVA assume that the data points are i.i.d. This means that a) all observations need to be sampled from the same underlying distribution, and b) the probability of data points taking a specific value needs to be independent of the other samples.

Otherwise, the probability of Type I errors would be too high.
In the present data set, sample values depend on the individual subjects performance and the problem size. Therefore, the second condition of simple models is violated, and mixed models are needed to keep Type I errors low. They include a safe-guard mechanism against outliers due to their hierarchical structure and partial pooling.

The statistical interference is obtained by the Satterthwaite approximation. FDR-corrected post hoc tests were applied to test the stated hypothesis and find other signficant effects.

6.3.2 Sensor space EEG analysis

Three band-pass filters were applied on the preprocessed data (theta: $4 - 7\,\mathrm{Hz}$; lower alpha: $8 - 10\,\mathrm{Hz}$; upper alpha: $10 - 12\,\mathrm{Hz}$) and yielded the frequency bands of interest. From each of these bands, epochs were extracted starting 2 s before the trial onset and lasting until 125ms before the voice onset. Median values were then calculated for the activation (starting at the onset) and the baseline period ($-1750\,\mathrm{ms}$ to $-250\,\mathrm{ms}$). The ERD/ERS ratio was then calculated by the use of the formula:
ERDS = -(baseline - activity)/(baseline) $\cdot 100\,\%$ and averaged for each of the eight regions of interest (ROI). The electrodes belonging to the regions anteriofrontal (AF), frontal (F), frontocentral (FC), central (C), centroparietal (CP), parietal (P), parietooccipital (PO), and temporal (T) are listed in Table 6.1.

Table 6.1: The regions of interest (ROI) and their related electrodes in the left and right hemisphere.

region	left	right
anteriofrontal (AF)	FP1, AF7, AF3	FP2, AF4, AF8
frontal (F)	F7, F5, F3, F1	F2, F4, F6, F8
frontocentral (FC)	FC5, FC3, FC1	FC2, FC4, FC6
central (C)	C5, C3, C1	C2, C4, C6
centroparietal (CP)	CP5, CP3, CP1	CP2, CP4, CP6
parietal (P)	P7, P5, P3, P1	P2, P4, P6, P8
parietooccipital (PO)	PO7, PO3, O1	PO4, PO8, O2
temporal (T)	FT7, T7, TP7	FT8, T8, TP8

A linear mixed model with the factors operation (addition, multiplication), strategy (retrieve, procedure), size (tiny, small, large), hemisphere (hemi: left, right) and region of interst (ROI: AF, F, FC, C, CP, P, PO, T) was trained. The

right-fit of the models was verified by checking the kurtosis of their residuals. Due to non-normality, a square-root transformation was performed on the data. Thus, the resulting model is described by $(op * size * hemi * roi + (1|id))$.

An analysis of the variance revealed significant effects and interactions. For this, p-values were approximated by the Satterthwaite method on type III sum-of-squares.
Post-hoc tests performed on the estimated marginal means allowed to find significant contrasts for the effects of interest and an FDR-correction was used to correct for multiple comparisons.

ERD/S values for the combination of the ROI, hemisphere and problem size were averaged and the mean values were plotted as well as the exact values.
Additionally, a Bayesian analysis was performed to determine the influence of the problem size factor on data predictability.

6.3.3 Source-space EEG Analysis

PCA-based K-means clustering

The main goal of the K-means clustering was to group similar event related spectral perturbations (ERSPs) with a near-source location together. For this, features were derived from the frequency spectrum ($2 - 50$ Hz), from ERSPs ($2 - 50$ Hz; time: 0 to trial-length time-warped to the longest trial of all subjects; baseline: -1500 ms to -500 ms), scalp projections, dipole locations (x,y,z) as well as dipole moments (dx, dy, dz). The dimensions of all feature vectors were reduced to 10 and weighted by dipole locations ($w = 12$), scalp projections ($w = 4$), spectra ($w = 3$) and ERSPs ($w = 10$). By the use of these features, ICs were then grouped into 10 clusters plus one outlier cluster. The outlier cluster comprised all ICs that were further than 3 times the standard deviation away from the cluster mean.

Time-frequency information

For each of the IC-clusters, we calculated two time-frequency maps, ERSPs and ERD/ERS. For this, epochs were time-warped to the longest trial duration. Then, the power of each time-frequency bin was calculated over the whole epoch-length for a frequency range of $2 - 50$ Hz and corrected by a baseline from -1500 ms to -500 ms. The power spectrum was averaged over the condition (problem size: tiny vs. small vs. large) for each IC and finally over all ICs contained in one cluster.
The location of ICs was assigned to regions defined in the Desikan-Killany atlas. This, together with the ERSPs patterns helped to analyze the cluster's functional meaning.

Additionally, median ERD/ERS values were calculated for three frequency bands (theta: 4-7Hz; lower alpha: 8-10Hz; upper alpha: 10-12Hz) by the formula: ERD/S = -(baseline - activity)/(baseline) ·100 %. The activity lasts from the task onset (0 s) to the end of the epoch and the baseline from -1750ms to -250ms.

Statistics

With a mixed model we verified the significance of the effect for the within-subject factors problem size (tiny vs. small vs. large) as well as the clusters. The ERD/S values were log-transformed with the effect that the residuals of the fit models were more normally distributed. The Analysis of Variance was performed on Type III sum-of-squares. P-values were obtained by the Satterthwaite approximation which is equal to the Kenward-Roger approximation as it provides the best control of Type I errors for limited sample sizes.
Post-hoc tests were performed on the estimated marginal means. The results were FDR-corrected.

6.4 Influence of strategies

In this chapter, we examined whether differences between self-reported retrieve and procedure strategies exist regarding their response times and EEG oscillation activation patterns.

6.4.1 Behavioral analysis

Similar to the analysis in section 6.3.1 differences in response times were analyzed. The data consisted of subject IDs (40 levels, nominal) and self-reported stratregies (2 levels, ordinal). A descriptive analysis allowed first insights into the data. ANOVA tests were performed on a linear mixed model that was trained with log-transformed response times. FDR-corrected post-hoc tests were calculated on the signficiant effects in order to validate the stated hypothesis.

6.4.2 Sensor space analysis

Similar to the analysis in 6.3.2 ERD/S values were acquired for all three frequency bands of each region of interest per hemisphere. A mixed model consisting of the within-subject factors strategy (retrieval vs. procedural), region of interest (AT, F, FC, C, CP, P, PO, T) and hemisphere (left vs. right) was trained by the use of square root-transformed ERD/S values. ANOVA was used to indicate significant effects. Actual differences were evaluated by FDR-corrected post-hoc tests.

6.4.3 Source-Space analysis

Similar to the analysis in section 6.3.3 ICs were grouped into 10 clusters. ERSPs were calculated, the time-frequency bins were statistically tested with a paired t-test and corrected with FDR=0.05. Furthermore, significant differences of the frequency bands were tested similarly as in the sensor space analysis.

6.5 Interaction of problem-size and strategies

In this section, we investigate the differences between problem sizes regarding their response time and EEG oscillation patterns when the dependent values are controlled for strategy. Further, for differences between strategies regarding their response time and EEG oscillation patterns when the dependent values are controlled for problem size.

Similar to the analysis in section 6.3.2 ERD/S values were acquired for all three frequency bands of each region of interest per hemisphere. A mixed model consisting of the four within-subject factors strategy (retrieval vs. procedural), problem-size (tiny vs. small vs. large), region of interest (AT, F, FC, C, CP, P, PO, T) and hemisphere (left vs. right) was trained by the use of square root-transformed ERD/S values. An ANOVA indicated significant effects that were then analyzed in more detail by post-hoc tests. Results were FDR-corrected.

6.6 Interaction of problem-size, strategies and n+1

The fourth research question aimed to find differences between the factors problem size, strategy and add+1 for problem sizes smaller or equal than 10. This allowed to investigate the solving process of tiny problems and answer the question whether they are solved through automated processes or through memory retrieval.

Similar to the analysis in section 6.3.2 ERD/S values were acquired for all three frequency bands. A mixed model consisting of the within-subject factors problem size (3 to 10), strategy (retrieval vs. procedural), add+1 (True/False), region of interest (AT, F, FC, C, CP, P, PO, T) and hemisphere (left vs. right) was trained by the use of log-transformed ERD/S values. An ANOVA indicated significant effects that were then analyzed in more detail by post-hoc tests. Results were FDR-corrected.

7 Results

7.1 Influence of problem-size

7.1.1 Behavioral analysis

The descriptive analysis revealed that subjects required a median response time of 0.91 s to answer tiny problems, 0.93 s to answer small and 1.19 s to caclulate the solution of large problems. Figure 7.1 shows that response times of large tasks are much higher than the ones for small and tiny problems. Values between the categories tiny and small differ only slightly. It is also worth mentioning that one extreme outlier occurs at small and large problems.

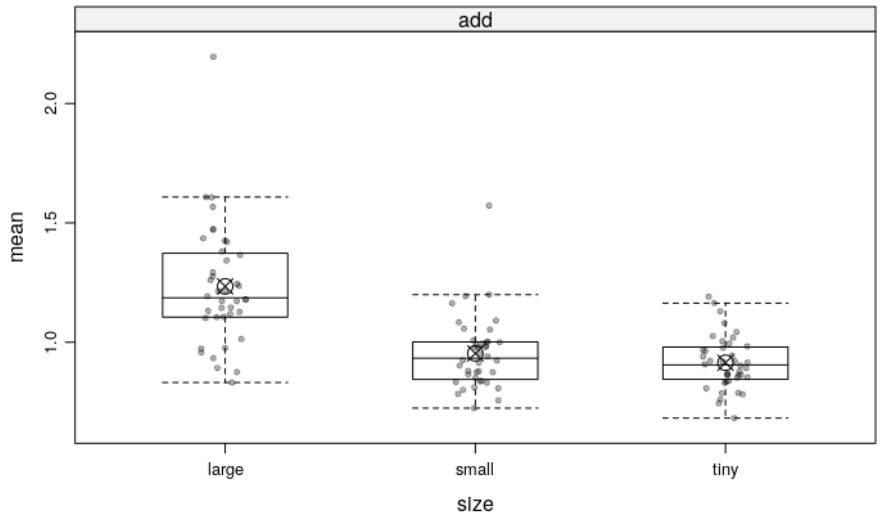

Figure 7.1: Distribution of response times for tiny ($mean = 0.91$, median=0.91), small ($mean = 0.95$, median=0.93) and large ($mean = 1.23$, median=1.19) addition problems.

The model that consists of the fixed problem size effect and the random subject effect was tested on type III sum-of-squares and revealed that the main effect of problem size is significant ($F(2,78)=131.06$, $p<0.001$).

The importance of the problem size is supported by the Bayes factor analysis. It showed that the model consisting of size and subjects described the data $8.17 \cdot 10^{21}$ times better than the model consisting of only subjects.

The result of the post-hoc test performed on the estimated marginal means of the mixed model is shown in Table 7.1. It revealed a significant time difference between large and tiny problems as well as between large and small tasks (both $p < 0.001$). The difference between small and tiny problems is $p < 0.05$. Therefore, hypothesis 1-3 are accepted.

Table 7.1: Simultaneous Tests for General Linear Hypothesis: Effects of the log-transformed problem size evaluated on response times of addition problems. Degrees of freedom are fixed at 78.

Contrast	Estimate in s	Std. Error in s	t-value	$Pr(>\|t\|)$
large-small	1.25	0.076	16.39	<0.001
large-tiny	1.44	0.076	18.90	<0.001
small-tiny	0.19	0.076	2.50	<0.05

7.1.2 Sensor-space

The sensor values of addition tasks were processed and averaged per region of interest (ROI) and hemisphere. Afterwards, a linear mixed model ($size*roi*hemi+(1|id)$) was fit with the processed data. A normality check indicated highly non-normal residuals. Thus, the model was fit with square root transformed ERD/S values. The presented test-statistics were then calculated with the Satterthwaite approximation for the degrees of freedom.

Theta band:
In the theta band, ANOVA-tests indicated significant differences for the main effects ROI (F(7,5529.1)=73.7, p<0.001), hemisphere (F(1, 5529.1)=7.26, p<0.01), size (F(2,5534.6)=80.61, p<0.001) and the interactions roi:hemi (F(7,5529.1)=2.05, p<0.05).

The post-hoc tests of square root transformed theta-bandpower values showed significant differences (p<0.001) between large and tiny (L-T) as well as between large and small (L-S) addition problems for all regions. Thus, hypothesis 5 and 6 are accepted. In more detail, these differences are found for the regions AF, C, CP, F, FC, P, PO (p<0.001) and T (p<0.05) for the contrast L-T. Large and small problems differ for the regions AF, C, F, FC, P, PO (p<0.001) and CP, T (p<0.01).
Table 7.2 shows that a significant difference between small and tiny (S-T) problems is found for the right (p<0.01), but not for the left hemisphere. Therefore, hypothesis 4 can be rejected.

Figure 7.2 presents the ERD/S values for all eight regions of interest and the problem sizes large (L), small (S) and tiny (T). While large problems show the lowest ERD/S for all regions, this value is highest for small size problems. P-values of significant difference are shown at the left upper corner for the contrasts large-tiny and large-small. No differences between small and tiny were significant.

Table 7.2: Simultaneous Tests for General Linear Hypothesis: Effects of the problem size and hemisphere evaluated on ERD/S values of the theta-band for addition problems.

Contrast	Estimate in %	Std. Error in %	z-value	$Pr(>\|z\|)$
large - small, l	-31.2	3.81	-8.183	<0.001
large - tiny, l	-27.8	4.0	-6.959	<0.001
small - tiny, l	3.4	3.8	0.891	0.37
large - small, r	-29.2	3.8	-7.656	<0.001
large - tiny, r	-35.4	4.0	-8.861	<0.001
small - tiny, r	-6.2	3.8	-1.640	0.12

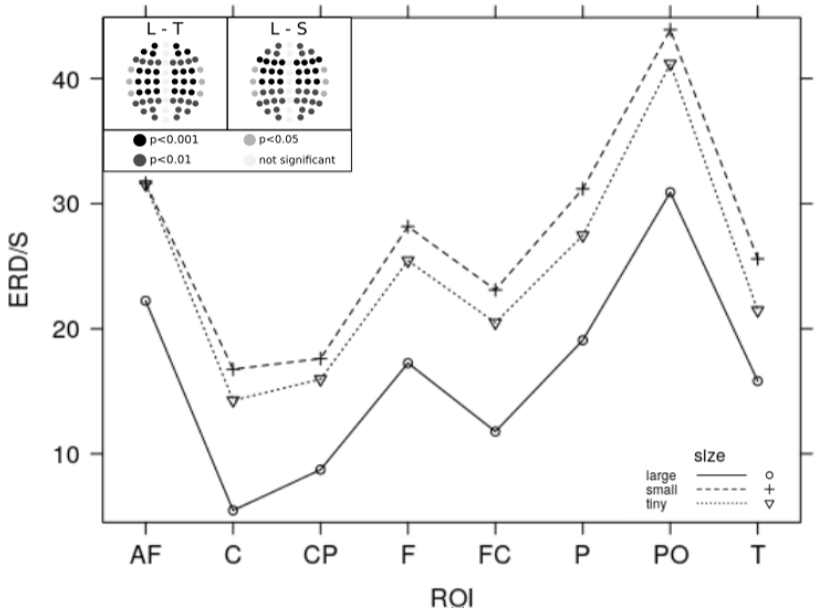

Figure 7.2: Median ERD/S values in % (Theta-band) for the interaction of problem sizes and ROI. The significance between large-tiny (L-T) and large-small (L-S) is shown in the subplot at the top.

Lower alpha band:
For the lower alpha band ANOVA-tests indicate significant differences for the main effects ROI ($F(7,5529)=16.52$, $p<0.001$), hemisphere ($F(1, 5529)=4.95$, $p<0.05$) and size ($F(2,5533)=43.94$, $p<0.001$).

Post-hoc tests performed on square root transformed lower-alpha ERD/S values reveal significant differences ($p<0.001$) between large and tiny and large and small sizes. This effect occurs, when ERD/S values are evaluated on the whole set of sensors, and when they are evaluated for both hemispheres individually too. The contrast between small and tiny problems becomes also significant ($p<0.01$) when ERD/S values are calculated for all sensor values and when they are evaluated only on the right hemisphere.
The contrast between large and tiny problem sizes is significant bilaterally for the regions C, CP, FC, T ($p<0.001$) and P ($p<0.01$) and PO ($p<0.05$) while large and small problems differ for the regions C, CP, FC ($p<0.01$) and P, T ($p<0.05$). Table 7.3 lists the post-hoc tests for the parieto-occipital region.

From the ERD/S values of all eight regions of interest and problem sizes (Figure 7.3) it is noteworthy that values are lowest for large problems, while tiny ones show the highest ERD/S ratio. The degree of significance for the contrasts large-

tiny (L-T) and large-small (L-S) is presented in the upper right corner of Figure 7.3.

Table 7.3: Simultaneous Tests for General Linear Hypothesis: Effects of the problem size, ROI and hemisphere evaluated on ERD/S values of the lower alpha band at parieto-occipital regions for addition problems.

Contrast	ROI	Estimate in %	Std. Error in %	z-value	$Pr(>\|z\|)$
large - small	PO	-9.7	7.6	-1.279	0.268
	PO, l	-18.6	10.7	-1.739	0.197
	PO, r	-0.08	10.7	-0.072	0.949
large - tiny	PO	-22.4	7.9	-2.819	$<$0.05
	PO, l	-29.4	11.2	-2.625	$<$0.05
	PO, r	-15.3	11.2	-1.364	0.321
small - tiny	PO	-12.7	7.6	-1.678	0.160
	PO, l	-10.8	10.7	-1.014	0.438
	PO, r	-14.5	10.7	-1.359	0.321

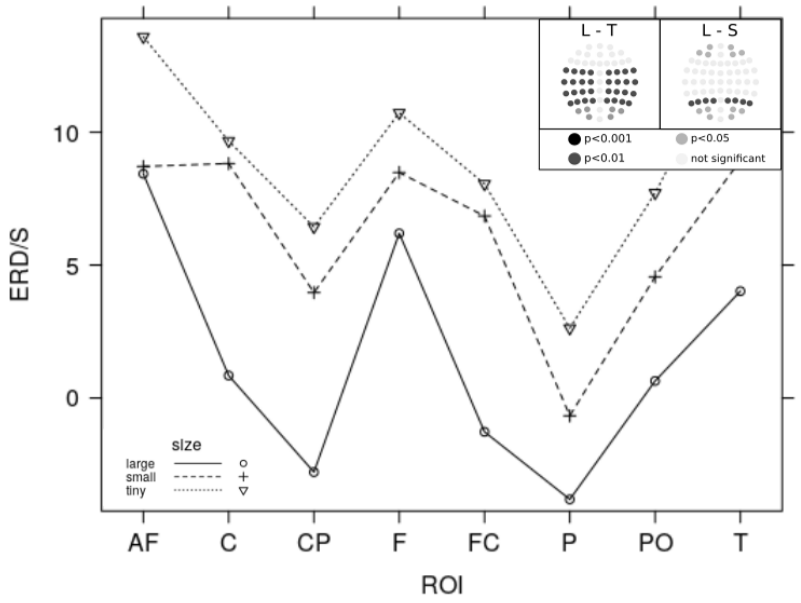

Figure 7.3: Median ERD/S values in % (Lower alpha band) for the interaction of problem sizes and ROI. The significance between large-tiny (L-T) and large-small (L-S) is shown in the subplot at the upper right corner.

Upper alpha band:
ANOVA-tests indicated significant differences for the main effects ROI ($F(7,5529)=61.28$, $p<0.001$), hemisphere ($F(1, 5529)=13.18$, $p<0.001$), size ($F(2,5534.3)=37.41$, $p<0.001$) and the interaction roi:hemi ($F(7,5529)=2.14$, $p<0.05$).

Post-hoc tests of square root transformed upper-alpha ERD/S values revealed a significant difference ($p<0.001$) between large and tiny as well as between large and small and tiny tasks. The significance was found for all sensors and on both hemispheres individually.
Moreover, the contrast between large and tiny problems is significant for the regions C, FC, P ($p<0.01$) and CP, PO, T ($p<0.05$); the contrast between large and small for the regions AF, C, F, FC ($p<0.01$) and CP, P ($p<0.05$). Small and tiny problems differ only in the PO region ($p<0.05$). Test statistics for this region are displayed in Table 7.4.

From ERD/S values of all eight regions of interest and problem sizes (figure 7.4), it can be seen that values are lowest for large problems, while tiny ones show the highest ERD/S ratio. The degree of significance for the contrasts large-tiny (L-T) and large-small (L-S) is presented in the lower left corner of Figure 7.4.

Table 7.4: Simultaneous Tests for General Linear Hypothesis: Effects of the problem size, ROI and hemisphere evaluated on ERD/S values of the upper alpha band at parieto-occipital regions for addition problems.

Contrast	ROI	Estimate in %	Std. Error in %	z-value	$Pr(>\|z\|)$
large - small	PO	-23	7.7	-0.307	0.828
	PO, l	-22	10.8	-0.204	0.875
	PO, r	-25	10.8	-0.230	0.875
large - tiny		-20.7	8.0	-2.581	$<$0.05
	PO, l	-18.2	11.3	-1.605	0.218
	PO, r	-23.2	11.3	-2.049	0.130
small - tiny	PO	-18.3	7.6	-2.402	$<$0.05
	PO, l	-16.0	10.8	-1.479	0.241
	PO, r	-20.7	10.8	-1.919	0.147

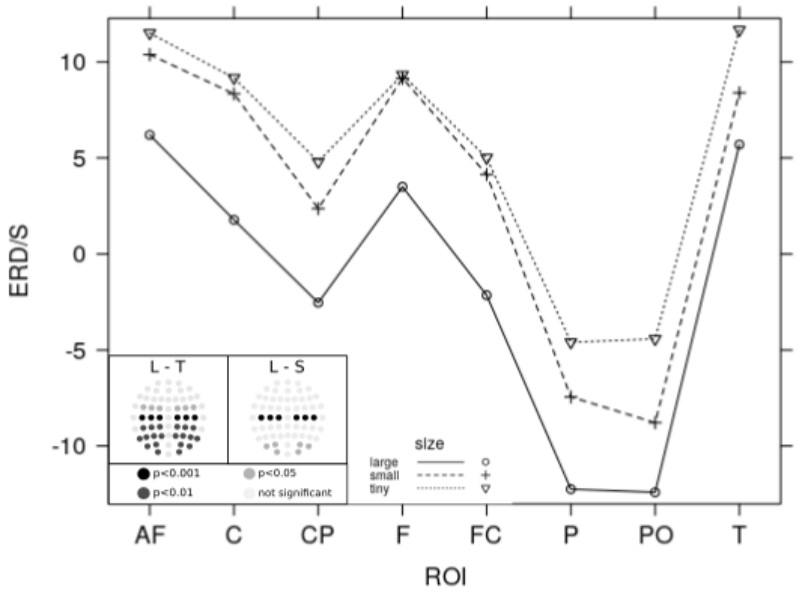

Figure 7.4: Median ERD/S values in % (Upper alpha band) for the interaction of problem sizes and ROI. The significance between large-tiny (L-T) and large-small (L-S) is shown in the subplot in the lower left corner.

A Bayesian repeated-measures ANOVA supports the found importance of the problem size effect onto ERD/S values. The model consisting problem size, ROI and hemisphere is $2.6 \cdot 10^{25}$ times better than the model without problem size. The multiplicative difference is $2.8 \cdot 10^9$ in the lower alpha band and $17.1 \cdot 10^9$ in the upper alpha band.

7.1.3 IC-space Analysis

The locations of the ICs were found with a dipole-fitting algorithm by the use of a four layer model that consists of skin, skull, cerebrospinal fluid and the cortex. Each of the 431 ICs was assigned to one of 10 clusters.
ICs in regions related to Visual Number Forming were mainly assigned to clusters 2 (16.3%), 4 (46.3%) and 11 (22.5%). Processes related to Auditory Number Form are well represented in group 11 (83.3%) and the ones for Numerical Quantity are found in Cluster 8 (35.2%) and in the groups 6 and 11 (both 22.2%). ICs related to the Episodic and Semantic memory are mostly in cluster 7 (47.1%) and 11 (23.5%). Sources activated in Salience / Attention control are found in group 11 (60%). Finally, working Memory / Cognitive control is almost equally distributed to clusters 3 (9.7%), 5 (10.2%), 6 (9.7%), 9 (21.0%), 10 (16.7%) and 11 (23.7%). The amount of ICs found for each Desikan-Killany region is listed in Tables 9.1 and 9.2 in the attachment section.

Table 7.5 shows the composition of each cluster. Clusters 2 and 4 mainly represent the Visual Number Form. Group 8 is representative for Numerical Quantity and group 7 for Episodic / Semantic memory. Independent components of the clusters 3, 5, 6, 9, 10 and 11 are largely found in regions related to working memory and cognitive control.

	Cluster									
	2	**3**	**4**	**5**	**6**	**7**	**8**	**9**	**10**	**11**
Visual Number Form	**54.2**	0.0	**66.1**	0.0	11.4	10.5	16.0	0.0	0.0	15.7
Auditory Number Form	0.0	0.0	0.0	3.1	2.9	0.0	0.0	0.0	0.0	8.7
Numerical Quantity	12.5	0.0	8.9	0.0	34.3	0.0	**76.0**	0.0	8.6	10.4
Episodic / Semantic	25.0	3.2	12.5	0.0	0.0	**63.2**	4.0	0.0	0.0	10.4
Salience / Attention control	0.0	3.2	0.0	6.3	0.0	0.0	0.0	0.0	2.9	5.2
Working Memory / Cognitive Control	4.2	**58.1**	10.7	**59.4**	**51.4**	26.3	0.0	**97.5**	**88.6**	**38.3**

Table 7.5: Neurocognitive functions as described by Fias et al. [136] of the clusters found by k-means. The clusters mainly include brain regions for the following functions: Clusters 2 and 4 for Visual Number Form. Cluster 8 for Numerical Quantity processing; Cluster 7 for Episodic / Semantic memory and clusters 3, 5, 6, 9, 10 and 11 contain mainly brain regions for Working Memory / Cognitive Control.

Visual number form

Cluster 2. The cluster #2 includes 24 ICs of 20 subjects. Dipoles are located mainly in the occipital lobe like the lateral occipital region (5 ICs), the cuneus (6 ICs), the pericalcarine (1 ICs), the lingual cortex (1 ICs), the superior (2 ICs), and the inferior (1 IC) parietal regions. Sources are also found in the parietal lobe involving the precuneus (6 ICs), the posterior cingulate (1 IC), the superior (2 ICs) and inferior parietal regions (1 IC) and one IC is found paracentral in the

frontal lobe. Assigning the regions to their corresponding neurocognitive systems shows that this cluster mainly represents regions related to the visual number form (54.2%). Other locations are linked to the episodic and semantic memory (25%), numerical quantity (12.5%) and the working memory and cognitive control (4.2%). The ERSP image in Figure 7.5 shows a significant ERD ($FDR = 0.05$) in the lower and upper alpha band that starts immediately after the task onset and lasts for the whole solving duration. The activation strength reaches -5.2 dB compared to the bias period. A comparison to other clusters shows that this alpha ERD is also significant compared to all working memory and cognitive control clusters (3, 5, 9, 10 and 11).

Cluster 4. The second cluster representing the visual number form is Cluster #4 and includes 31 ICs of 23 subjects. Most of the ICs are found in the lingual cortex (15 ICs), the fusiform area and lateral occipital regions (each has 9 ICs), and the pericalcerine (4 ICs). Others are in the inferior (4 ICs), the superior parietal regions (1), the precuneus (4 ICs), the parahippocampal (2 ICs), the middle temporal region (1 IC) and the cingulate comprises 6 ICs (isthmus: 5, posterior: 1). The regions are linked to the visual number form (66%), episodic and semantic (13%) as well as the working memory (11%). 9% are found in regions linked to numerical quantity.
The ERSP image in Figure 7.5 shows an immediate and significant ERS response ($FDR = 0.05$) in the frequency range of $2-9$ Hz and lasts for 400 ms. The response is followed by a strong (-3.6 dB) ERD in the lower and upper alpha band and an activation in the theta band. Both last for the whole solving process.
A comparison to other clusters reveals that the theta ERS in the early phase also becomes significant against the working memory and cognitive control clusters (3,6,9,10 and 11). The upper alpha ERD is significant compared to all working memory and cognitive control clusters in the middle of the task. In Figure 7.5 you can see from left to right in each row the cluster dipole locations (saggital-, superior view), the ERSP images that are time-locked to the task onset (equation presentation) and time-warped to the trial length. In this plot, nonsignificant differences (FDR=0.05) are masked with green.

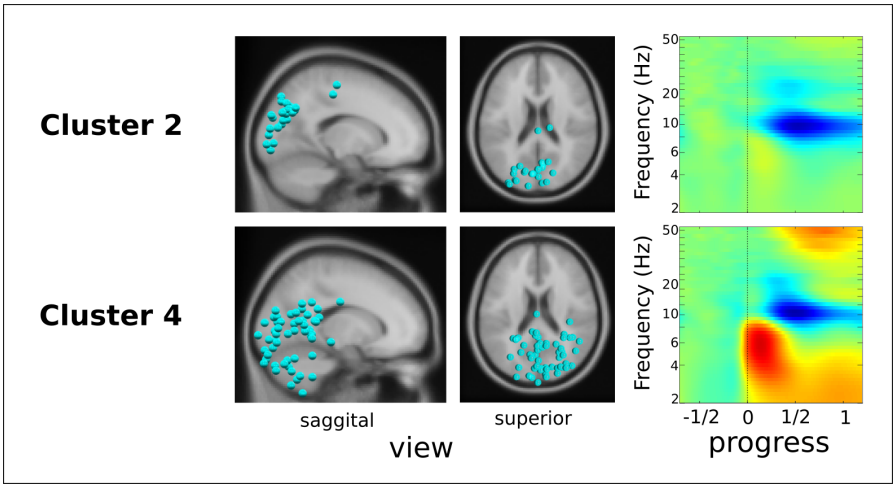

Figure 7.5: ERSP images for tiny addition tasks. From left to right. Cluster dipole locations (saggital-, superior view); ERSP images time-locked to the task onset (equation presentation) and time-warped to the median solving duration; normed to 1. Nonsignificant differences (FDR=0.05) are masked with green. The clusters contain mainly ICs of the numerical quantity processing system.

Numerical Quantity

Cluster 8. This cluster includes 25 ICs of 19 subjects and is mainly located in the parietal lobe. These are the interior (9 ICs) and superior parietal (2 ICs), supramarginal (8 ICs) regions and the precuneus (1 IC). 3 ICs are located lateral occipital and one is found in the lingual gyrus. They are mainly linked to numerical quantity (76%) and visual number form (16%).
The ERSP image in Figure 7.6 shows a significant ($FDR = 0.05$) immediate ERSP response in the 3-7Hz range that is followed by a significant ERD in the lower and upper alpha band. A comparison to other clusters reveals a difference to the working memory and cognitive control clusters 5 and 9. The difference gets significant in the alpha band from 1/4 to 1/2 of the task duration.

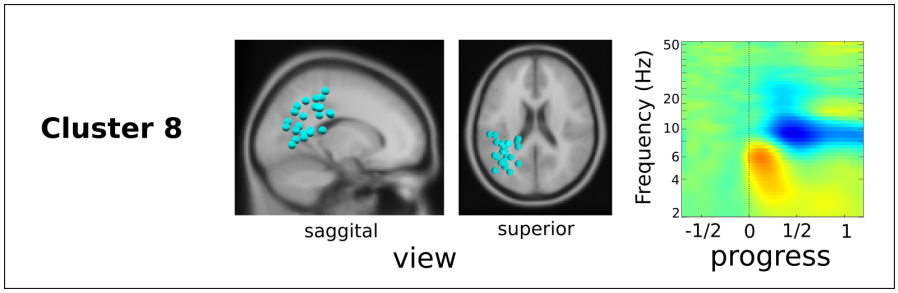

Figure 7.6: ERSP images for tiny addition tasks. From left to right. Cluster dipole locations (saggital-, superior view); ERSP images time-locked to the task onset (equation presentation) and time-warped to the median solving duration; normed to 1. Nonsignificant differences (FDR=0.05) are masked with green. The clusters contain mainly ICs of the numerical quantity processing system.

Episodic / Semantic Memory

Cluster 7. The cluster includes 38 ICs of 31 subjects and is mainly found in the precuneus (24 ICs). Others are in the cuneus (3 ICs), the pericalcerine (1 IC) and the cingulate (isthmus: 8 ICs, posterior: 2 ICs). These are linked to episodic and semantic memory (63%), working memory and cognitive control (26%) and the visual number forming (11%).
The ERSP in Figure 7.7 shows an immediate significant ERS response to the task onset in the $6-8\,\mathrm{Hz}$ frequency range. The ERS is followed by a significant ERD in the lower and upper alpha band that lasts for the whole task. A comparison to other clusters reveals a significant difference (FDR=0.05) to the working memory and cognitive control clusters 5 and 9 in the middle of the task at the theta, lower alpha and beta band.

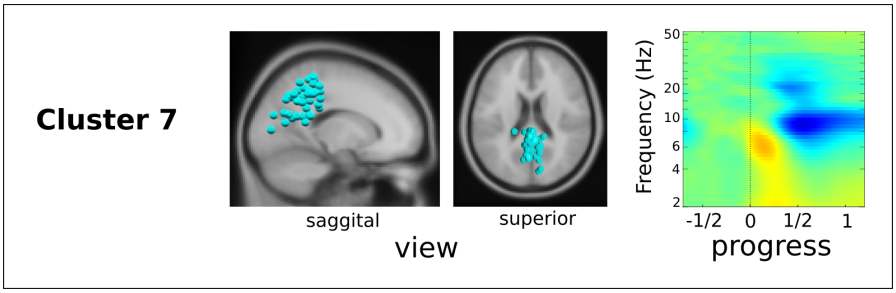

Figure 7.7: ERSP images for tiny addition tasks. From left to righ in each row: Cluster dipole locations (saggital-, superior view); ERSP images time-locked to the task onset (equation presentation) and time-warped to the median solving duration; normed to 1. Nonsignificant differences (FDR=0.05) are masked with green. The clusters contain mainly ICs of the episodic and semantic memory systems.

Working Memory / Cognitive Control

Cluster 3. This cluster consists of 31 ICs of 23 subjects and is mainly located precentral (11 ICs), the cinulate (posterior: 4 ICs, caudal anterior: 1 IC), superior frontal (1 IC), paracentral (7 ICs), the insula (1 IC) and precuneus (1 IC). The functions of these regions are linked to the episodic and semantic memory as well as to cognitive control and salience.
The ERSP image in Figure 7.8 of this cluster shows an immediate significant (FDR=0.05) ERS response in the $2-8\,\mathrm{Hz}$ range that lasts until 1 s after the tasks onset. It is followed by a significant (FDR=0.05) deactivation in the lower and upper alpha and beta band that peaks at $-1.9\,\mathrm{dB}$.

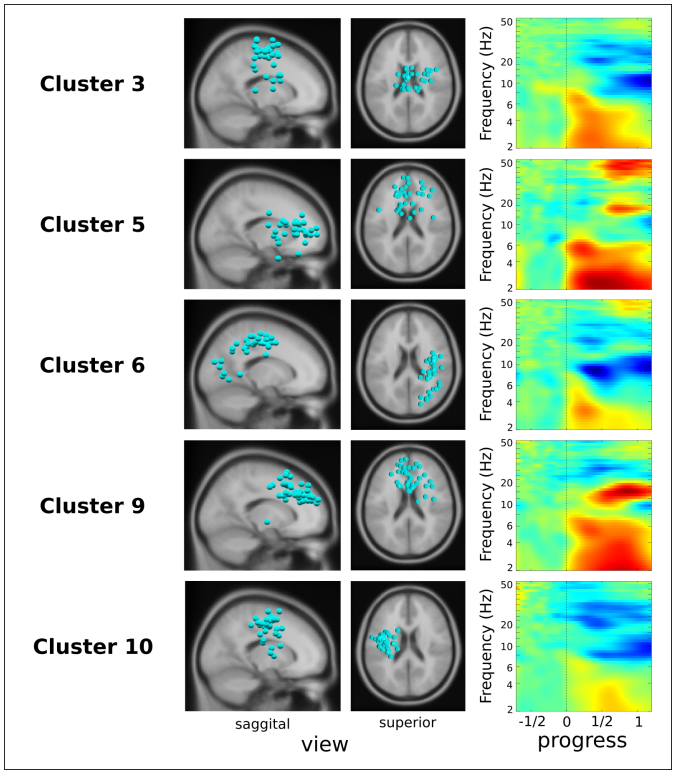

Figure 7.8: ERSP images for tiny addition tasks. From left to right in each row: Cluster dipole locations (saggital-, superior view); ERSP images time-locked to the task onset (equation presentation) and time-warped to the median solving duration; normed to 1. Nonsignificant differences (FDR=0.05) are masked with green. The clusters contain mainly ICs of working memory and cognitive control systems.

Cluster 5. The cluster includes 32 ICs of 21 subjects and consists of dipoles located in the cingulate (caudal anterior: 7 ICs, rostral anterior: 2 ICs), rostral middle frontal (4 ICs), superior frontal (3 ICs), lateral orbitofrontal (1 IC), caudal middle frontal (1 IC), superior temporal (1 IC) and the insula (2 ICs).
The regions are linked to the cognitive systems of working memory and cognitive control (59.4 %), salience and attention control (6.3 %) and auditory number form (3.1 %). The ERSP image in Figure 7.8 shows a strong significant activation of up to 1.3 dB over the whole solving process. A comparison to other clusters shows the lack of activation in the alpha band that becomes significant for the visual number form clusters (2 and 4), the episodic and semantic memory (7) and numerical quantity cluster (8). Further, the activation in the 2-3Hz frequency range becomes significant for clusters 2 and 4 and large problems.

Cluster 6. The cluster includes 35 ICs and 30 subjects. It contains regions in

the postcentral (10 ICs) and precentral (8 ICs), superior parietal (4 ICs), inferior parietal (3 ICs) areas as well as the supramarginal gyrus (5 ICs), the lingual cortex (1 IC), the lateral occipital region (2 ICs) and the fusiform gyrus (1 IC). These regions are related to working memory and cognitive control (51%) visual number form (11%), numerical quantity (34%) and auditory number form (3%). The ERSP image in Figure 7.8 shows a significant ($FDR = 0.05$) ERS activation in the frequency range of 2-4Hz peaking at 1/4 of the task and an alpha ERD starting after 1/4 of the task. A comparison to cluster 4 reveals the lack of activation in the 6-8Hz range immediately after the task onset.

Cluster 9. This cluster includes 40 ICs and 26 subjects and contains dipoles that are mainly located in the superior frontal lobe (27 ICs), the cingulate (caudal anterior: 4 ICs, posterior: 2 ICs,) as well as caudal (2 ICs) and rostral (2 ICs) middle frontal. Others are precentral (1 IC) and postcentral (1 IC).
These regions are linked to working memory and cognitive control (98%). The ERSP image in Figure 7.8 shows a significant ERS in the $2 - 8\,\mathrm{Hz}$ range over the whole solving process as well as an activation in the $12 - 16\,\mathrm{Hz}$ range.

Cluster 10. This cluster includes 35 ICs and 25 subjects and the dipoles are mainly located precentral (16 ICs) and postcentral (12 ICs). Others are in the posterior part of the cingulate (2 ICs), the caudal middle frontal region (1 IC), the pars opercularis (1 IC), the supramarginal gyrus (1 IC) and superior parietal (2 ICs).
The regions are mainly linked to working memory and cognitive control (87 %), numerical quantity (9 %) and salience and attention control (3 %). The ERSP image in Figure 7.8 shows a significant ($FDR = 0.05$) ERS in the middle of the task in the $2 - 4\,\mathrm{Hz}$ band as well as an ERD in the lower and upper alpha band starting after the first quartile of the task.

Cluster 11. This cluster includes 115 ICs and 35 subjects. It contains all ICs that do not fit exactly into one of the existing clusters. The largest amount of dipoles is located in regions related to working memory and cognitive control (39 %). The others are distributed to visual number forming (16 %) and auditory number forming (9 %), numerical quantity (10 %), episodic and semantic memory (10 %) and salience and attention control (5 %). The ERSP image in Figure 7.8 shows significant ERS in the theta band for the whole duration of the task as well as significant ERD in the lower and upper alpha band starting after 1/8 of the task.

ANOVA

The ANOVA shown in Table 7.6 reveals that ERD/S patterns differ significantly ($p<0.001$) between clusters for all frequency bands, that the effect of cluster:size is not significant. Exact median ERD/S values for all clusters and frequency bands are listed in Table 7.7.

		Theta			Lower alpha			Upper alpha		
Effect	NumDF	DenDF	F-value	$Pr(>F)$	DenDF	F-value	$Pr(>F)$	DenDF	F-value	$Pr(>F)$
cluster	9	715.32	3.2943	***	710.52	3.3232	***	711.32	4.0809	***
size	2	696.19	0.7333	0.48	695.65	1.9323	0.15	695.81	1.7526	0.17
cluster:size	18	696.19	0.7605	0.74	695.65	0.7654	0.74	695.81	0.5118	0.95

Table 7.6: Linear Mixed Model Anova Table (Type 3 tests, Satterthwaite-method), fitted by median bandpower values of the preprocessed data. The significance is coded for the fdr-adjusted p-values by '***': 0.001, '**': 0.01, '*': 0.05, '.': 0.1. The model was fit with log-transformed ERD/S values applied on data preprocessed with the adjust preprocessing pipeline.

	Theta			Lower alpha			Upper alpha		
Cluster	tiny	small	large	tiny	small	large	tiny	small	large
2	-3.10	0.80	1.36	12.91	20.78	13.46	4.45	-3.16	4.24
3	12.19	9.23	1.01	16.87	15.65	13.80	5.41	3.30	0.77
4	3.52	5.19	3.65	13.35	4.88	3.56	3.73	0.44	-4.69
5	11.56	-1.89	-3.02	17.03	19.25	17.17	8.44	-8.55	0.60
6	-1.36	-2.80	-4.90	20.83	22.18	11.68	-0.05	0.27	-2.81
7	-4.39	-2.63	-11.70	27.37	17.62	13.12	-0.01	-4.44	-8.15
8	-7.71	-4.92	-3.69	8.22	0.60	4.76	-6.45	-6.02	-5.66
9	-6.57	-9.75	-6.68	12.98	13.79	13.79	-0.23	-8.49	-1.00
10	1.43	-3.38	-3.78	15.53	7.22	17.34	13.26	2.66	9.32
11	1.24	-4.89	-8.48	20.83	22.20	10.00	2.85	-0.96	2.45

Table 7.7: Median ERD/S values in % for tiny, small and large problem sizes.

A look onto the theta-band shows that the clusters 3, 5 and 10 are of special interest. This is because the former two show a strong ERS, while cluster 10 is located near the left perisylvian region.
Post-hoc tests of the log-transformed theta-ERD/S values reveal that the large difference between tiny and small (2.96 and 13.45) as well as between large and tiny (11.18 and 14.58) problems in the theta-band of the clusters 3 and 5 is not significant.
The only significant difference ($p<0.05$) between large and small and small and tiny problems is found for cluster 8. Nevertheless, the effect of the size is marginal.

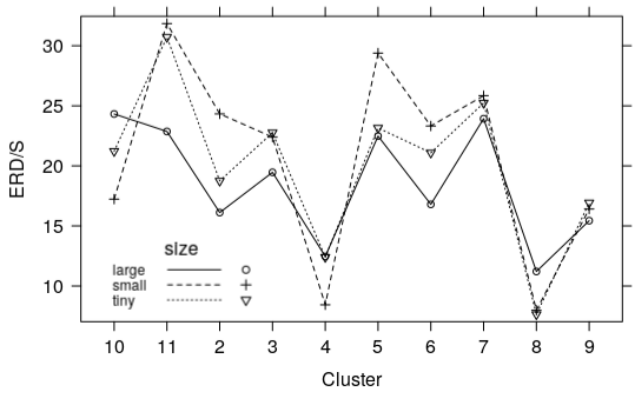

Figure 7.9: Median ERD/S values given in % in the theta-band for the interaction of problem sizes and cluster.

Continuing with the alpha-band, we see in Figure 7.5 that cluster 2 is located occipital, whereas clusters 4, 7, 8 (and partly cluster 6) are located parieto-occipital. The ERD/S values for each cluster are presented in Figures 7.10 and 7.11. Signficant differences between sizes are found in the clusters 3,4 and 5, but none of these clusters become significant in the post-hoc tests; neither in the lower, nor in the upper-alpha band. Also, differences ($p<0.05$) in the log-transformed upper alpha band.
Instead, significant differences ($p<0.05$) were found for cluster 10 between large and small as well as between small and tiny problems in the log-transformed lower-alpha band. The effect is large between tiny-small (8.31) and small-large (10.12), but marginal between tiny-large (1.81) problems.

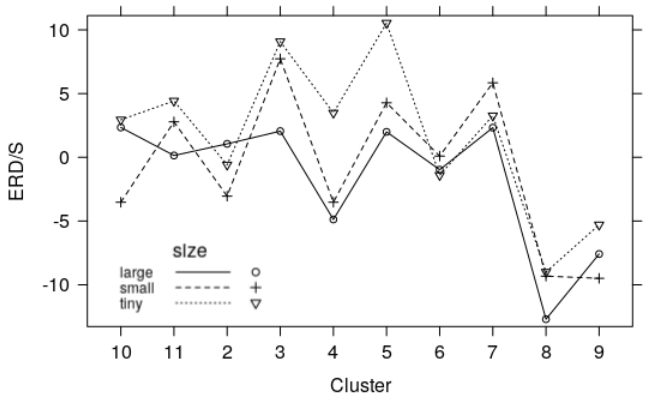

Figure 7.10: Median ERD/S values given in %(Lower alpha band) for the interaction of problem sizes and cluster.

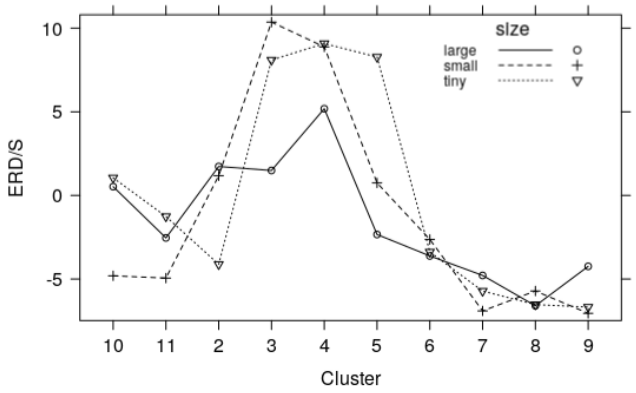

Figure 7.11: Median ERD/S values in % (Upper alpha band) for the interaction of problem sizes and cluster.

Time-Frequency Analysis

Time-frequency plots comparing problem sizes are shown in Figure 7.12. They show significant differences ($FDR = 0.05$) for both visual number form clusters (2 and 4), the episodic memory cluster (7) and one working memory / cognitive control cluster (6).
Starting with cluster 4, it can be seen that this cluster is located mainly in the lingual cortex, fusiform cortex as well as at lateral occiptial regions and shows significant differences ($FDR = 0.05$) in the theta and alpha band between large and tiny problems. Large problems elucidate a stronger alpha ERD and less theta ERS than tiny tasks in the second half of the solving process. Interestingly, a stronger

and longer lower alpha ERS is also found between small and tiny problems. Small problems tend to have a longer lower alpha ERS immediatly following the task onset. This becomes significant after one fourth of the trial. The second cluster links to visual number forming and is mainly located in the cuneus and at lateral occipital regions. It shows a higher alpha ERD for large problems than for tiny problems and becomes significant in the second half of the solving process. Cluster 7 which is located mainly in the precuneus is linked to episodic and semantic memory. It shows a stronger alpha ERD for large problems. Additionally, the deactivation in the smae time range becomes significant in the beta band too. The working memory cluster (6) located at right pre- and postcentral regions shows stronger lower alpha ERD for large operands compared to tiny ones.

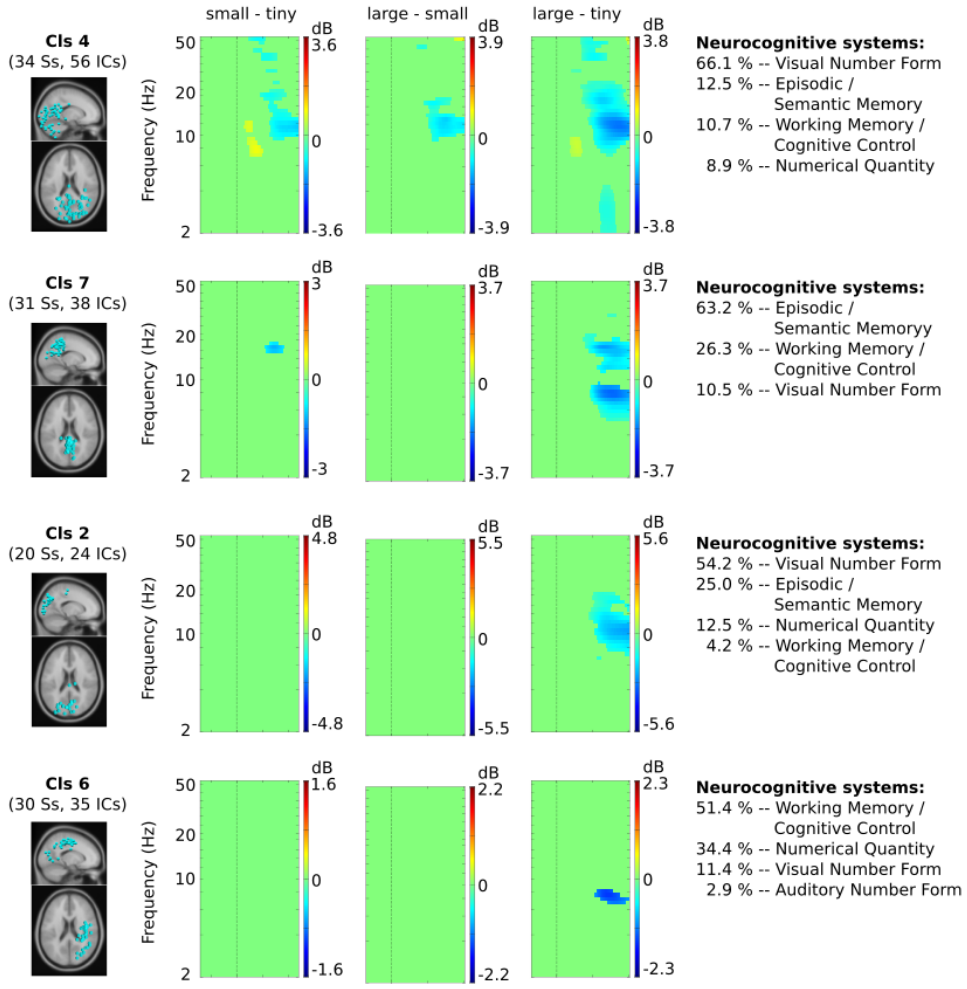

Figure 7.12: ERSP images for addition tasks. From left to right in each row: Cluster dipole locations (saggital-, superior view); difference ERSP images time-locked to the task onset (equation presentation) and time-warped to the trial length for: small-tiny trials; large-small trials; and large-tiny trials. Nonsignificant differences are masked in green. All four clusters show a significant decrease in alpha-band power for larger problem sizes. In cluster 4, the alpha-band power difference even becomes significant between tiny and small problems.

7.1.4 Are there differences between tiny, small and large addition problems?

The presented results allowed to check the hypothesis stated in 5.5. The results are as follows:
Hypothesis 1: There is a difference in response times between tiny and large problems.
Correct, large problems are solved $1.42\,\mathrm{s} + - 76\,\mathrm{ms}$ slower than tiny problems. Post-hoc tests showed a significant contrast ($p<0.001$) with a t-value of 16.39.
Hypothesis 2: There is a difference in response times between small and large problems.
Correct, the two categories differed by 1.25 s. Post-hoc tests found a significant difference ($p<0.001$) with a t-value of 18.88.
Hypothesis 3: There is a difference in response times between tiny and small problems.
Correct, the two categories differ by 190 ms. The contrast is signficiant ($p<0.05$) and result in a t-value of 2.5.
Hypothesis 4: Tiny problems show a higher left-hemispheric theta ERS than small problems.
Incorrect, the theta ERS of small problems is 3.4 % higher, but not signficant.
Hypothesis 5: Small problems show a higher left-hemispheric theta ERS than large problems.
Correct, small problems have a 31.2 % higher theta ERS value than large problems. The post-hoc test between large and small problems results in a z-value of -8.18 and proofs signficant difference $p<0.001$.
Hypothesis 6: Tiny problems show a higher left-hemispheric theta ERS than large problems.
Correct, the theta ERS of tiny problems is 27.8 % higher than the one measured on large problems. The post-hoc test between large-tiny problems resulted in a z-value of -6.96 and proofed signficant difference ($p<0.001$).
Hypothesis 7: Large problems show a lower alpha bandpower in the bilateral parieto-occipital regions than tiny problems. Correct for the lower alpha-band. z-value=3.912. $p<0.001$ and the left-hemispheric PO, z-value: -3.39, $p<0.01$.
Hypothesis 8: Large problems show a lower alpha bandpower in the bilateral parieto-occipital regions than small problems.
Incorrect, the bandpower in the bilateral PO region of large problems is 9.7 % lower, but the difference is insignificant.
Hypothesis 9: Small problems show a lower alpha bandpower in the bilateral parieto-occipital regions than tiny problems.
Incorrect, the lower alpha bandpower of small problems is 12.7 % lower than for tiny problems. Still, the difference is insignificant.

Hypothesis 10: At least one IC-Cluster is found in the left-hemispheric perisylvian region that shows enhanced activity in the theta-band for small problems.
Incorrect: Clusters 8 and 10 are spatially close to the left-hemispheric perisylvian region. Still, they do not show significant differences between tiny, small and large problem sizes. Theta-ERS as well as the theta-ERS difference between problem sizes is strongest in the frontal clusters 5 and 9. Unfortunately, the differences are non-significant ($p<0.05$)
Hypothesis 11: At least one IC-Cluster is found in the parieto-occipital region that shows enhanced upper-alpha ERD for large problems.
Correct: Cluster 2 is located occipital and the clusters 4, 6, 7 and 8 are found in parieto-occipital regions. Differences of ERD/S values in the alpha band do not become significant ($p<0.05$) when they are averaged over the whole solving duration. But, clusters 2, 4, 6 and 7 show significant differences ($FDR = 0.05$) between problem-sizes, when post-hoc tests are performed on the time-frequency bin level. This mainly occurs in the second half of the solving process.

7.2 Influence of strategies

7.2.1 Behavioral analysis

Subjects required a median response time of 1.15s to answer large addition problems through retrieval strategies and were slightly slower (1.34s) to solve them procedurally. The distribution of response times is shown in Figure 7.13. One extreme outlier is apparent at both classes.

The model that consists of the fixed effect of strategies and the random factor subject variance was tested on type III sum-of-squares and revealed that the main effect of strategies is significant ($F(1, 483.35)=26.32$, $p<0.001$). This is supported by the post-hoc test as shown in Table 7.8. Therefore, hypothesis 12 is accepted. This is coherent with the result of the Bayes factor analysis which says that the data are described $27 \cdot 10^3$ times better, when the effect of strategies is added to subjects.

Table 7.8: Simultaneous Tests for General Linear Hypothesis: Effects of strategies evaluated on ERD/S values of response times.

Contrast	Estimate in ms	Std. Error in ms	t-value	$Pr(>\|t\|)$
procedural-retrieval	150	29	5.124	<0.001

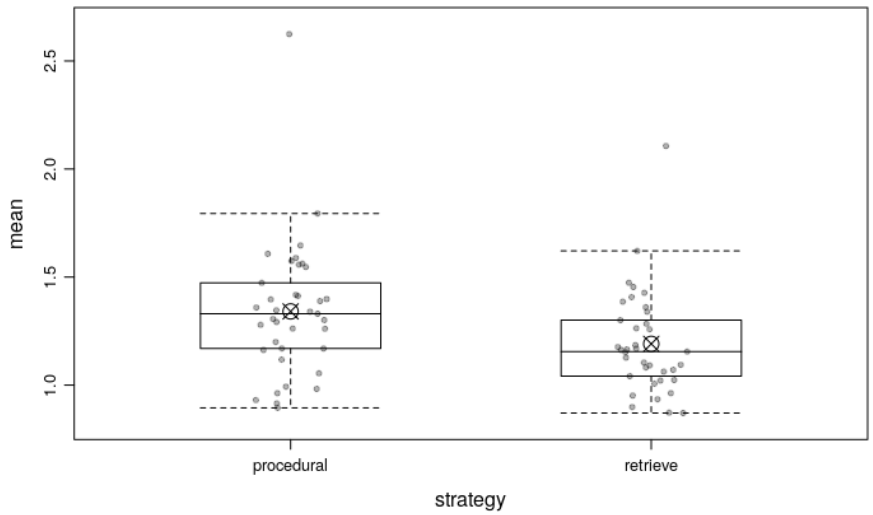

Figure 7.13: Distribution of response times for retrieval ($\mu = 1.21$, median=1.15) and procedural strategies ($\mu = 1.42$, median=1.34) of large addition problems.

7.2.2 Sensor-space

The sensor values were averaged over regions of interest and hemisphere. Afterwards, a linear mixed model ($strategy * roi * hemi + (1|id)$) was fit with the processed and square root transformed data. The presented test-statistics were calculated with the Satterthwaite approximation for the degrees of freedom.

Theta band:
ANOVA-tests indicated significant differences for ROI ($F(7,10953)=103.64$, $p<0.001$), hemisphere ($F(1,10953)=21.28$, $p<0.001$), strategy ($F(1,10973)=66.66$, $p<0.001$) and the interactions roi:hemi ($F(7,10953)=4.15$, $p<0.001$) and roi:strategy ($F(7,10953)=2.27$, $p<0.05$).

Post-hoc tests of square root transformed theta-bandpower values showed significant differences ($p<0.001$) between retrieved and procedurally solved strategies as well as in both hemispheres as shown in Table 7.9. Regarding regions of interest, procedure differed from retrieve in AF, CP, P, PO ($p<0.001$), F ($p<0.01$) and C ($p<0.05$). The ERD/S values are plotted in Figure 7.14.

Table 7.9: Simultaneous Tests for General Linear Hypothesis: Effects of strategy and hemisphere evaluated on ERD/S values of the theta band for large addition problems.

Contrast	Estimate in %	Std. Error in %	z-value	$Pr(>\|z\|)$
procedure - retrieve	-14.0	1.72	-8.165	<0.001
procedure - retrieve, l	-12.8	2.38	-5.390	<0.001
procedure - retrieve, r	-15.2	2.38	-6.364	<0.001

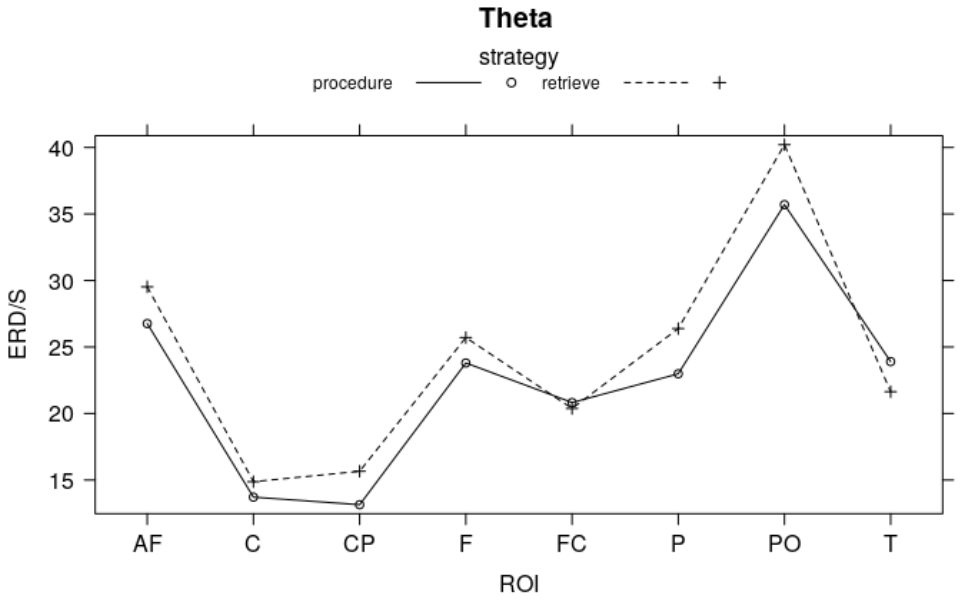

Figure 7.14: Median ERD/S values in % (Theta-band) for the interaction of strategies and ROI of large problems.

Lower alpha band:
ANOVA-tests indicated significant differences for the main effects ROI ($F(7,10953)=42.53$, $p<0.001$), hemisphere ($F(1,10953)=19.70$, $p<0.001$) and strategy ($F(1,10970)=7.12$, $p<0.01$).

Results of post-hoc tests showed significant differences between procedure and retrieve ($p<0.01$) on the whole scalp and on the right hemisphere ($p<0.05$). Significant differences for individual regions (e.g. bilateral parieto-occipital) were not found as shown in Figure 7.14 and Table 7.10. Thus, hypothesis 3 could be rejected.

Table 7.10: Simultaneous Tests for General Linear Hypothesis: Effects of the strategy, ROI and hemisphere evaluated on ERD/S values of the lower alpha band at parieto-occipital regions for large addition problems.

Contrast	ROI	Estimate in %	Std. Error in %	z-value	$Pr(>\|z\|)$
procedure - retrieve	PO	-11.5	4.7	-2.463	0.110
procedure - retrieve	PO, l	-13.0	6.5	-1.975	0.615
procedure - retrieve	PO, r	-9.99	6.59	-1.517	0.615

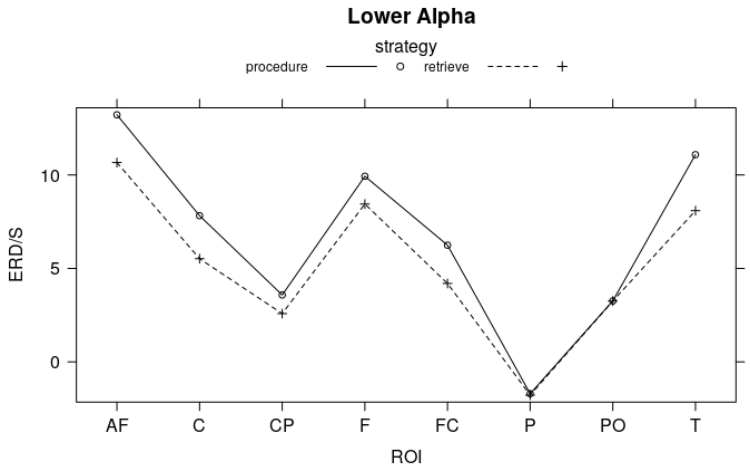

Figure 7.15: Median ERD/S values in % (Lower alpha band) for the interaction of strategies and ROI of large problems.

Upper alpha band:
ANOVA tests indicated significant differences for the main effects ROI ($F(7,10953)=133.05$, $p<0.001$), hemisphere ($F(1,10953)=21.26$, $p<0.001$) and strategy ($F(1,10971)=18.54$, $p<0.001$).

Post-hoc tests performed on the square-root transformed upper-alpha ERD/S values showed differences between the two strategies ($p<0.001$), as well as on both hemispheres ($p<0.01$) and for the regions AF and PO ($p<0.05$). Table 7.11 shows the test results of the parieto-occipital region and Figure 7.16 the comparison of both strategies over all bilateral regions.

Table 7.11: Simultaneous Tests for General Linear Hypothesis: Effects of the strategy, ROI and hemisphere evaluated on ERD/S values of the upper alpha band at parieto-occipital regions for large addition problems.

Contrast	ROI	Estimate in %	Std. Error in %	z-value	$Pr(>\|z\|)$
procedure - retrieve	PO	-12.00	4.6	-2.589	<0.05
procedure - retrieve	PO, l	-15.6	6.5	-2.388	0.14
procedure - retrieve	PO, r	-8.3	6.5	-1.282	0.370

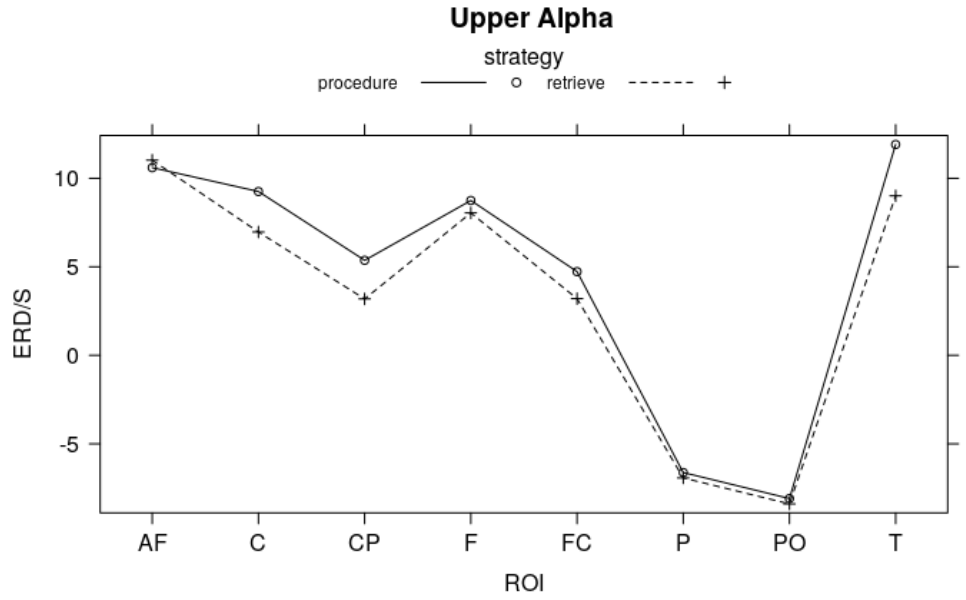

Figure 7.16: Median ERD/S values in % (Lower alpha band) for the interaction of strategies and ROI of large problems.

7.2.3 IC-space Analysis

The results of the k-means clustering are shown in Figure 7.17. This plot shows the location of the ICs on the left side (saggital and superior view) and the event-related spectral perturbations of the retrieved tasks on the right. The temporal axis is time-warped to the length of the solving process. Hence, all trials last from 0 to the right side of the plotted image. A look onto the theta-band reveals that information in this band is contained in clusters 3, 6 and 7. It is interesting that all of the contained ICs are located in the occipital and parieto-occipital regions. Further, they share a theta-ERS activation at the very beginning of the task which is most prominent in cluster 3 and 6 (1.7dB). This activation disappears after 3/8 of the solving process at clusters 6 and 7 and remains over the whole solving process at cluster 3.
Additionally, it is noteworthy that cluster 4 contains information in the delta band. Delta ERS is apparent at the first and the last 1/3 of the solving process.
Finally, alpha ERD is found for all clusters over the whole solving process.

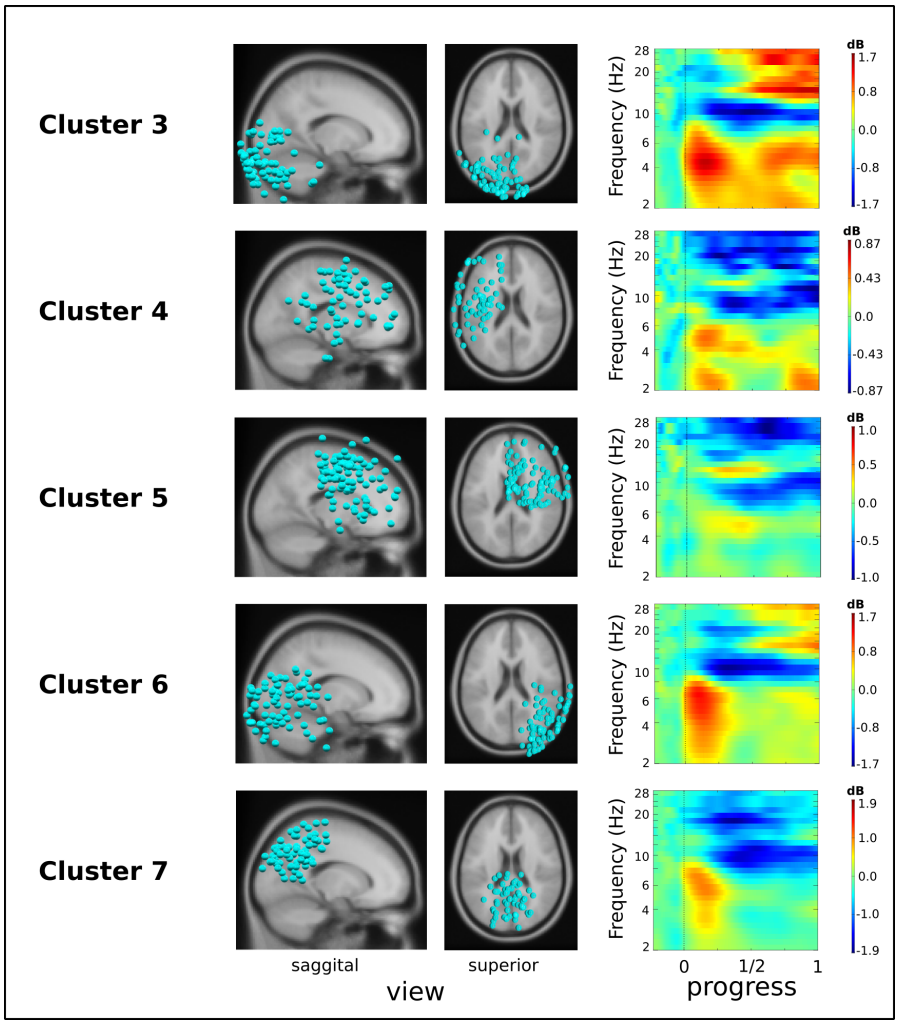

Figure 7.17: ERSP images for retrieval tasks. From left to right in each row: Cluster dipole locations (saggital-, superior view); ERSP images time-locked to the task onset (equation presentation) and time-warped to the median solving duration; normed to 1. Nonsignificant differences (FDR=0.05) are masked with green. The clusters contain mainly ICs of the visual number form processing system.

7.2.4 Are there differences between recalled and procedurally solved strategies at large problems?

The results displayed in this chapter allowed to validate the hypothesis stated in 5.5 and are as follows:
Hypothesis 12: There is a difference in response times between recalled and procedurally solved problems.
Correct, procedurally solved trials are solved 150 ms +- 29 ms slower than retrieved problems. The post-hoc test results in a t-value of 5.12 and is $p<0.001$ significant.
Hypothesis 13: Recalled problems show a higher left-hemispheric theta ERS than small problems.
Correct, the theta ERS is on the left hemisphere 12.8 % higher for retrieved problems than for procedurally solved ones. The post-hoc test is significant $p<0.001$ and resulted in a z-value of -5.39 for procedure-retrieve.
Hypothesis 14: Procedurally solved problems show a lower alpha bandpower in the bilateral parieto-occipital regions than tiny problems.
Incorrect, t-value:-0.02 and $p = 0.99$ for the lower alpha band and t-value:0.07 and $p = 0.95$ for the upper alpha band.
Hypothesis 15: At least one IC-Cluster is found in the left-hemispheric perisylvian region that shows enhanced activity in the theta-band for recalled problems than for procedurally solved ones.
Incorrect, Cluster 3 shows the strongest theta ERS and cluster 4 is located near the left perisylvian region, but none of them shows significant differences between tasks that were solved with retrieved and procedurally solved strategies.
Hypothesis 16: At least one IC-Cluster is found in the parieto-occipital region that shows enhanced upper-alpha ERD for procedurally solved problems (over recalled ones).
Incorrect, cluster 7 is located in the parieto-occipital region and shows alpha ERD. Still, there is no significant difference between retrieved and procedurally solved tasks.

7.3 Interaction of problem-size and strategies

The sensor values were processed and averaged per ROI and hemisphere. Afterwards, a linear mixed model ($op*strategy*size*roi*hemi+(1|id)$) was fit with the processed data. A normality check indicated highly non-normal residuals. Thus, the model was fit with square root transformed ERD/S values. The presented test-statistics were then calculated with the Satterthwaite approximation for the degrees of freedom.

Theta band:
ANOVA-tests indicated significant differences for the main effects strategy ($F(1,37255)=4.77$, $p<0.05$), size ($F(2,37244)=229.82$, $p<0.001$), ROI ($F(7,37241)=111.26$, $p<0.001$), hemisphere ($F(1,37241)=90.70$, $p<0.001$) and the interactions op:strategy ($F(1,37246)=5.79$, $p<0.05$), strategy:size ($F(2,37244)=8.56$, $p<0.001$) and op:strategy:size ($F(2,37243)=7.08$, $p<0.001$) in the theta band.

Figure 7.18 presents the difference of ERD/S values for addition problems of different sizes for all regions of interest. Large problems show the lowest ERD/S values, while tiny and small ones elicidate larger values. It appears that small problems have a higher ERS, but this difference is not significant. Retrieved problems have a slightly higher ERS value for all problem sizes. This difference becomes significant at small problems ($p<0.001$) for the regions F, FC, PO ($p<0.05$) and large problems ($p<0.05$).

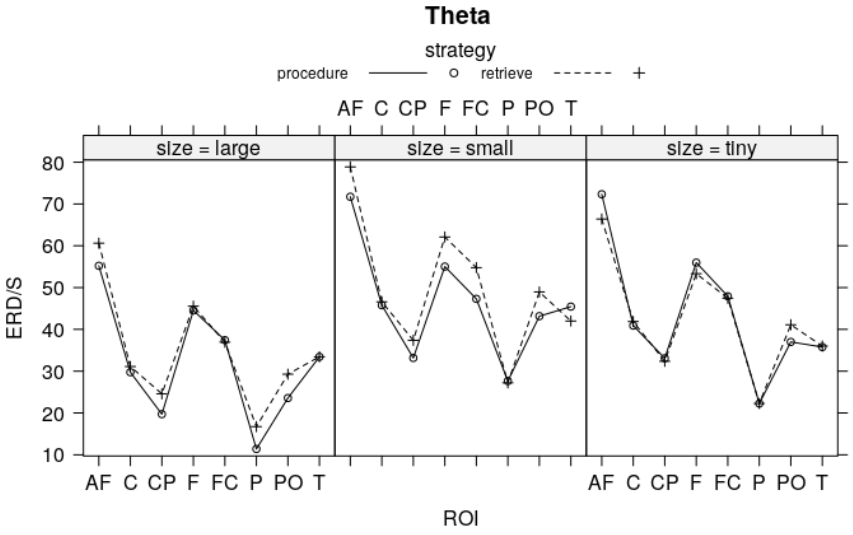

Figure 7.18: Median ERD/S values in % (Theta-band) for the interaction of problem sizes, strategy and ROI.

Post-hoc tests showed significant differences ($p<0.05$) between retrieved and procedurally solved problems. More detailed insights revealed differing ERD/S values between both strategies also for large ($p<0.05$) and small ($p<0.001$) problems. Further, for multiplication tasks ($p<0.05$) and in more detail for small multiplication problems ($p<0.001$).

Size differed between large and small as well as between large and tiny problems ($p<0.001$) whereas apart from one excpetion, no difference was found for the contrast small-tiny. Table 7.12 shows that this is true for all regions of interest on both hemispheres, except from the contrast large-tiny in the left temporal region. Controlling for strategy, the ERD/S values differed between large and small ($p<0.001$) and large and tiny problems ($p<0.001$) for retrieved and procedurally solved tasks; tiny problems differed from small ones ($p<0.01$).

		left hemisphere				right hemisphere			
Contrast	ROI	Estimate in %	Std. Error in %	z-value	$Pr(>\|z\|)$	Estimate	Std. Error	z-value	$Pr(>\|z\|)$
large - small	AF	-23.5	4.3	-5.423	***	-20.8	4.3	-4.804	***
large - tiny	AF	-27.5	6.2	-4.440	***	-31.2	6.2	-5.033	***
small - tiny	AF	-4.0	6.6	-0.597	0.634	-10.3	6.6	-1.557	0.167
large - small	C	-24.1	4.3	-5.550	***	-21.6	4.3	-4.976	***
large - tiny	C	-24.4	6.2	-3.935	***	-25.6	6.2	-4.144	***
small - tiny	C	-0.3	6.6	-0.042	0.966	-4.1	6.6	-0.613	0.634
large - small	CP	-18.0	4.3	-4.146	***	-21.7	4.3	-4.991	***
large - tiny	CP	21.9	6.2	-3.538	***	-27.9	6.2	-4.510	***
small - tiny	CP	-3.9	6.6	-0.591	0.634	-6.3	6.6	-0.946	0.424
large - small	F	-18.9	4.3	-4.355	***	-16.1	4.3	-3.715	***
large - tiny	F	-21.6	6.2	-3.493	***	-27.3	6.2	-4.418	***
small - tiny	F	-2.7	6.6	-0.412	0.742	-11.2	6.6	-1.696	0.131
large - small	FC	-20.2	4.3	-4.646	***	-19.4	4.3	-4.481	***
large - tiny	FC	-23.7	6.2	-3.828	***	-27.5	6.2	-4.448	***
small - tiny	FC	-3.5	6.6	-0.534	0.662	-8.1	6.6	-1.222	0.296
large - small	P	-22.5	4.3	-5.175	***	-18.3	4.3	-4.213	***
large - tiny	P	-12.2	6.2	-1.969	0.073	-19.4	6.2	-3.132	**
small - tiny	P	10.3	6.6	1.549	0.167	-1.1	6.6	-0.168	0.885
large - small	PO	-30.4	4.3	-7.015	***	-22.3	4.3	-5.146	***
large - tiny	PO	-23.9	6.2	-3.854	***	-30.1	6.2	-4.866	***
small - tiny	PO	6.6	6.6	0.993	0.405	-7.8	6.6	-1.177	0.310
large - small	T	-14.6	4.3	-3.361	**	-15.4	4.3	-3.553	***
large - tiny	T	-13.0	6.2	-2.107	0.054	-17.4	6.2	-2.816	**
small - tiny	T	1.5	6.6	0.233	0.852	-2.0	6.6	-0.305	0.811

Table 7.12: Median ERD/S differences of the theta band between problem sizes for all ROIs on both hemishpheres.

Lower alpha band:
ANOVA-tests indicated significant differences for the main effects operation ($F(1,37244)=23.48$, $p<0.001$), size ($F(2,37243)=236.96$, $p<0.001$), hemisphere ($F(1,37241)=50.06$, $p<0.001$), ROI ($F(7,37241)=11.04$, $p<0.001$) and the interactions op:strategy ($F(1,37245)=44.02$, $p<0.001$), strategy:size ($F(2,37243)=15.68$, $p<0.001$) and hemi:roi ($F(7,37241)=4.19$, $p<0.001$) in the lower alpha band.

Figure 7.19 presents the difference of lower alpha ERD/S values for addition problems of different sizes for all regions of interest.

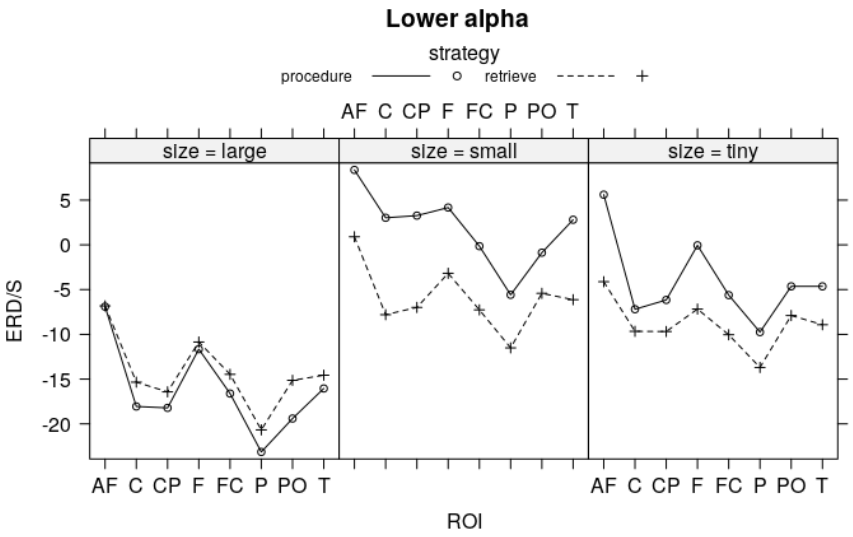

Figure 7.19: Median ERD/S values in % (Lower alpha band) for the interaction of problem sizes and ROI.

Post-hoc tests revealed significant differences between retrieved and procedurally solved addition and multiplication problems (both $p<0.001$). Differences between strategies were also found for large ($p<0.001$) and small ($p<0.01$) tasks.

Size differed between large and small ($p<0.001$) and large and tiny problems ($p<0.001$). The contrast large-small and large-tiny was also found for procedure only and retrieve only tasks. Table 7.13 shows that this is also true for all regions of interest on both hemispheres, except from the right hemispheric AF ($p<0.05$) and F ($p<0.05$) regions.

		left hemisphere				right hemisphere			
Contrast	ROI	Estimate in %	Std. Error in %	z-value	$Pr(>\|z\|)$	Estimate	Std. Error	z-value	$Pr(>\|z\|)$
large - small	AF	-0.198	0.041	-4.844	***	-0.111	0.041	-2.717	*
large - tiny	AF	-0.224	0.058	-3.838	***	-0.151	0.058	-2.585	*
small - tiny	AF	-0.026	0.063	-0.414	0.84	-0.040	0.063	-0.635	0.74
large - small	C	-0.216	0.041	-5.283	***	-0.208	0.041	-5.087	***
large - tiny	C	-0.216	0.058	-3.696	***	-0.189	0.058	-3.230	**
small - tiny	C	0.000	0.063	0.006	0.99	0.020	0.063	0.313	0.86
large - small	CP	-0.218	0.041	-5.320	***	-0.252	0.041	-6.159	***
large - tiny	CP	-0.227	0.058	-3.881	***	-0.214	0.058	-3.672	***
small - tiny	CP	-0.009	0.063	-0.143	0.91	0.038	0.063	0.602	0.75
large - small	F	-0.211	0.041	-5.154	***	-0.117	0.041	-2.853	**
large - tiny	F	-0.231	0.058	-3.949	***	-0.134	0.058	-2.302	*
small - tiny	F	-0.020	0.063	-0.314	0.86	-0.018	0.063	-0.283	0.87
large - small	FC	-0.204	0.041	-4.988	***	-0.151	0.041	-3.680	***
large - tiny	FC	-0.215	0.058	-3.687	***	-0.166	0.058	-2.840	**
small - tiny	FC	-0.011	0.063	-0.178	0.90	-0.015	0.063	-0.244	0.88
large - small	P	-0.194	0.041	-4.738	***	-0.261	0.041	-6.377	***
large - tiny	P	-0.227	0.058	-3.880	***	-0.200	0.058	-3.416	**
small - tiny	P	-0.033	0.063	-0.523	0.78	0.062	0.063	0.984	0.47
large - small	PO	-0.245	0.041	-5.982	***	-0.240	0.041	-5.873	***
large - tiny	PO	-0.276	0.058	-4.730	***	-0.276	0.058	-4.726	***
small - tiny	PO	-0.031	0.063	-0.502	0.78	-0.036	0.063	-0.570	0.76
large - small	T	-0.223	0.041	-5.443	***	-0.189	0.041	-4.611	***
large - tiny	T	-0.243	0.058	-4.165	***	-0.175	0.058	-2.999	**
small - tiny	T	-0.020	0.063	-0.327	0.86	0.014	0.063	0.217	0.88

Table 7.13: Median ERD/S differences of the lower alpha band between problem sizes for all ROIs on both hemishpheres.

Upper alpha band:
ANOVA-tests indicated significant differences for the main effects operation ($F(1,37244)=23.15$, $p<0.001$), size ($F(2,37243)=250.58$, $p<0.001$), hemisphere ($F(1,37241)=24.68$, $p<0.001$), ROI ($F(7,37241)=6.30$, $p<0.001$) and the interactions op:strategy ($F(1,37245)=24.66$, $p<0.001$) and strategy:size ($F(2,37244)=5.94$, $p<0.01$).

Figure 7.20 presents the difference of upper alpha ERD/S values for addition problems of different sizes for all ROIs.

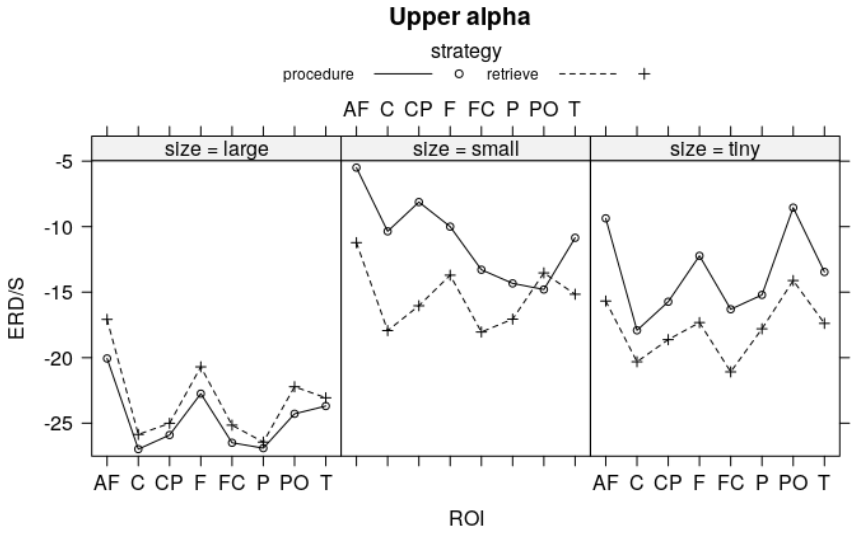

Figure 7.20: Median ERD/S values in % (Upper alpha band) for the interaction of problem sizes and ROIs. The significance between large-tiny (L-T) and large-small (L-S) is shown in the subplot in the lower left corner.

Post-hoc tests revealed significant differences between retrieved and procedurally solved addition and multiplication problems (both $p<0.001$). Differences between strategies were also found for large problems ($p<0.001$).

Regarding problem size, differences between large and small ($p<0.001$), large and tiny tasks ($p<0.001$) and small and tiny ($p<0.05$) were found. The contrast large-small and large-tiny is also significantly different for procedure and retrieve only problems ($p<0.001$). Table 7.14 shows that these contrasts are also significantly different for all individual regions of both hemispheres.

		left hemisphere				right hemisphere			
Contrast	ROI	Estimate in %	Std. Error in %	z-value	$Pr(>\|z\|)$	Estimate	Std. Error	z-value	$Pr(>\|z\|)$
large – small	AF	-0.232	0.041	-5.582	***	-0.147	0.041	-3.533	***
large – tiny	AF	-0.223	0.059	-3.760	***	-0.210	0.059	-3.543	***
small – tiny	AF	0.009	0.063	0.143	0.942	-0.063	0.063	-0.996	0.425
large – small	C	-0.259	0.041	-6.243	***	-0.189	0.041	-4.564	***
large – tiny	C	-0.261	0.059	-4.408	***	-0.214	0.059	-3.615	***
small – tiny	C	-0.002	0.063	-0.031	0.976	-0.025	0.063	-0.389	0.797
large – small	CP	-0.267	0.041	-6.429	***	-0.228	0.041	-5.490	***
large – tiny	CP	-0.274	0.059	-4.637	***	-0.231	0.059	-3.910	***
small – tiny	CP	-0.008	0.063	-0.122	0.942	-0.004	0.063	-0.058	0.974
large – small	F	-0.209	0.041	-5.029	***	-0.157	0.041	-3.774	***
large – tiny	F	-0.221	0.059	-3.734	***	-0.232	0.059	-3.915	***
small – tiny	F	-0.012	0.063	-0.195	0.942	-0.075	0.063	-1.187	0.323
large – small	FC	-0.223	0.041	-5.368	***	-0.160	0.041	-3.853	***
large – tiny	FC	-0.231	0.059	-3.899	***	-0.220	0.059	-3.711	***
small – tiny	FC	-0.008	0.063	-0.128	0.942	-0.060	0.063	-0.944	0.448
large – small	P	-0.176	0.041	-4.243	***	-0.237	0.041	-5.701	***
large – tiny	P	-0.204	0.059	-3.453	***	-0.263	0.059	-4.440	***
small – tiny	P	-0.028	0.063	-0.447	0.786	-0.026	0.063	-0.415	0.794
large – small	PO	-0.155	0.041	-3.743	***	-0.214	0.041	-5.150	***
large – tiny	PO	-0.258	0.059	-4.353	***	-0.328	0.059	-5.536	***
small – tiny	PO	-0.102	0.063	-1.616	0.150	-0.114	0.063	-1.800	0.105
large – small	T	-0.223	0.041	-5.370	***	-0.159	0.041	-3.841	***
large – tiny	T	-0.263	0.059	-4.443	***	-0.193	0.059	-3.255	**
small – tiny	T	-0.040	0.063	-0.635	0.664	-0.033	0.063	-0.526	0.737

Table 7.14: Median ERD/S differences of the upper alpha band between problem sizes for all ROIs on both hemishpheres.

The Bayesian ANOVA revealed that the model for hemisphere and size describes the data $9.0 \cdot 10^{43}$ times better than hemisphere alone. The inclusion of size to the ROI model improves it by a factor of $5.95 \cdot 10^{44}$. Further, the inclusion of size to a model including ROI and hemisphere improves the performance by a factor of $7.14 \cdot 10^{44}$.

7.4 Interaction of problem-size, strategies and n+1

The sensor values were processed and averaged per ROI and hemisphere. Afterwards, a linear mixed model ($op*strategy*sum*add1s*hemi*roi*(1|id)$) was fit with the processed data. A normality check indicated highly non-Normal residuals. Thus, the model was fit with square root transformed ERD/S values. The presented test-statistics were then calculated with the Satterthwaite approximation for degrees of freedom.

Theta band:

ANOVA-tests indicated significant differences for the main effects strategy ($F(1,37182)=5.91$, $p<0.5$), sum ($F(1,37179)=7.22$, $p<0.01$), 1-task ($F(1,37179)=39.41$, $p<0.001$), hemi ($F(1,37177)=31.22$, $p<0.001$), ROI ($F(7,37177)=17.88$, $p<0.001$) and the interactions op:strategy ($F(1,37180)=4.40$, $p<0.05$), strategy:add1s ($F(1,37180)=6.84$, $p<0.01$), sum:add1s ($F(1,37178)=15.41$, $p<0.001$), strategy:roi ($F(7,37177)=2.32$, $p<0.05$), op:strategy:add1s ($F(1,37180)=6.74$, $p<0.01$), op:add1s:roi ($F(7,37177)=2.70$, $p<0.05$).

Figure 7.21 shows the problem size effect in the theta band. Tasks with a sum of 3 show the lowest theta ERS, while tasks with 10 have the highest value.

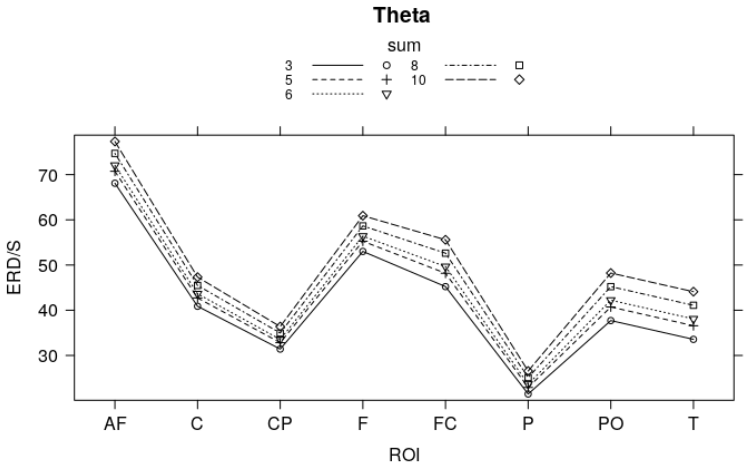

Figure 7.21: Problem size effect in the theta band for operand sums 3-10 displayed for all 8 bilateral ROIs.

The difference of strategies and the factor +1 is shown for different problem sums in Figure 7.22. It is low at tiny problems and increases for larger problems.

Post-hoc tests showed significant differences between self-reported strategies of sensors of the whole scalp ($p<0.05$) and for those in the parieto-occipital re-

gion ($p<0.05$). Additionally, for self-reported strategies at multiplication problems ($p<0.05$) and 1-tasks ($p<0.05$).
1-tasks are significantly different from tasks that do not include an operator 1 ($p<0.001$). In more detail, this effect was found for addition problems for the regions AF, F ($p<0.001$), C, FC, PO ($p<0.01$) and CP, P ($p<0.05$). Multiplication problems showed this effect only in the parietal region ($p<0.05$).

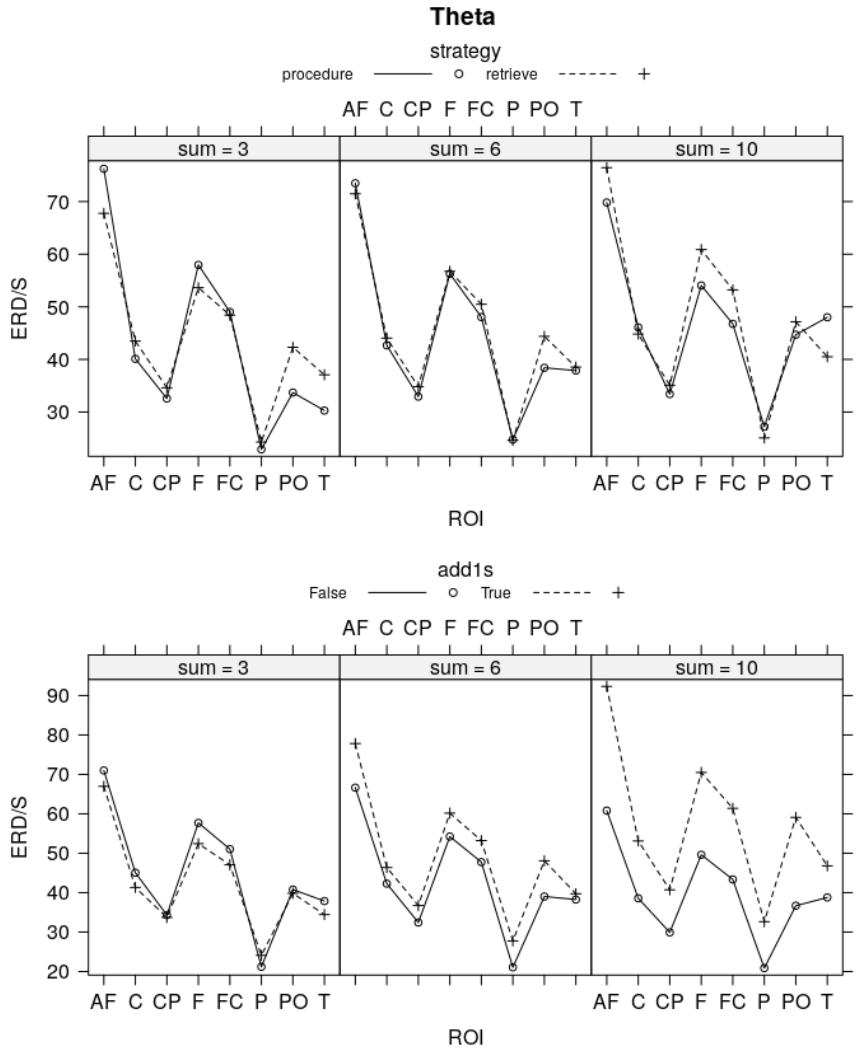

Figure 7.22: Differences between strategies (top) and n+1/n+m (bottom) in the theta band.

Lower alpha band:
ANOVA-tests indicate significant differences for the main effects

operation (F(1,37179)=11.24, p<0.001), sum (F(1,37178)=16.04, p<0.001), 1-task
(F(1,37179)=21.36, p<0.001), hemisphere (F(1,37177)=5.67, p<0.05), ROI (F(1,37177)=4.20, p<0.001) and the interactions op:strategy (F(1,37179)=10.33, p<0.01), strategy:sum (F(1,37178)=5.9, p<0.01), operation:1-task (F(1,37179)=12.79, p<0.001), sum:1-task (F(1,37178)=18.97, p<0.001), strategy:roi (F(7,37177)=2.34, p<0.05), op:strategy:sum (F(1,37178)=4.64, p<0.05), op:strategy:1-task (F(1,37179)=12.54, p<0.001), strategy:1-task:hemi (F(1,37177)=4.30, p<0.05), strategy:1-task:roi (F(7,37177)=2.56, p<0.05).

Figure 7.23 shows the problem size effect in the theta band. Tasks with a sum of 3 show the lowest alpha ERD, while tasks with 10 have the highest value.

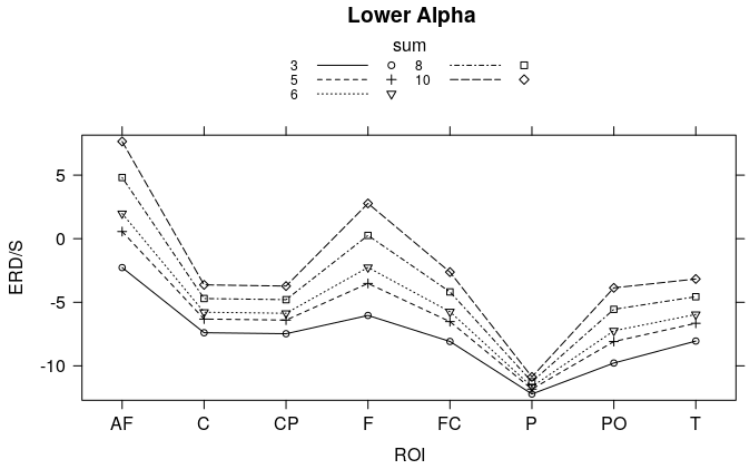

Figure 7.23: Problem size effect in the lower alpha band for operand sums 3-10 displayed for all 8 bilateral ROIs.

The difference of strategies and the factor +1 is shown for different problem sums in Figure 7.24. The difference is low at tiny problems, and increases for larger problems.

Post-hoc tests showed significant differences between self-reported strategies at addition tasks (p<0.001) and in more detail at $n + 1$ tasks (p<0.001), $n \cdot m$ (p<0.01) and $n \cdot 1$ (n<0.05) tasks. ERD/S values of the procedure strategy were significantly higher than those from retrieved answers. This effect was found in the left hemisphere (p<0.001) and in the AF region for tasks that did not include an operator of 1.

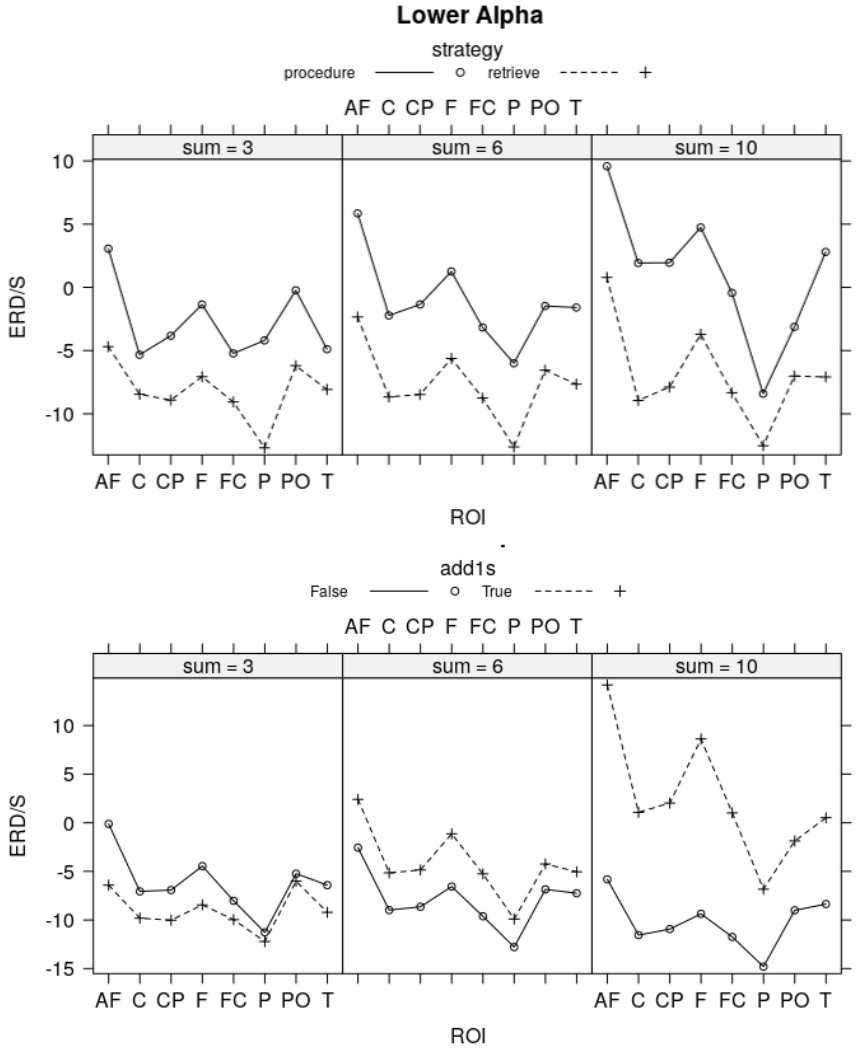

Figure 7.24: Differences between strategies (top) and n+1/n+m (bottom) in the lower alpha band.

Upper alpha band:
ANOVA-tests indicated significant differences for the main effects operation ($F(1,37179)=7.73$, $p<0.01$), sum ($F(1,37179)=20.72$, $p<0.001$), 1-tasks ($F(1,37179)=20.72$, $p<0.001$), ROI ($F(7,37177)=2.05$, $p<0.05$) and the interactions operation:strategy ($F(1,37179)=4.74$, $p<0.05$), strategy:sum ($F(1,37178)=5.89$, $p<0.05$), sum:1-tasks ($F(1,37178)=12.01$, $p<0.001$), strategy:roi ($F(7,37177)=2.05$, $p<0.05$), 1-tasks:roi ($F(7,37177)=2.04$, $p<0.05$), hemisphere:roi ($F(7,37177)=3.79$, $p<0.001$), op:strategy:sum ($F(1,37178)=6.89$, $p<0.01$) and op:1-task:hemisphere ($F(1,37177)=4.42$, $p<0.05$).

The difference of strategies and the factor +1 is shown for different problem sums in Figure 7.25. The difference is low at tiny problems, and increases for larger problems.

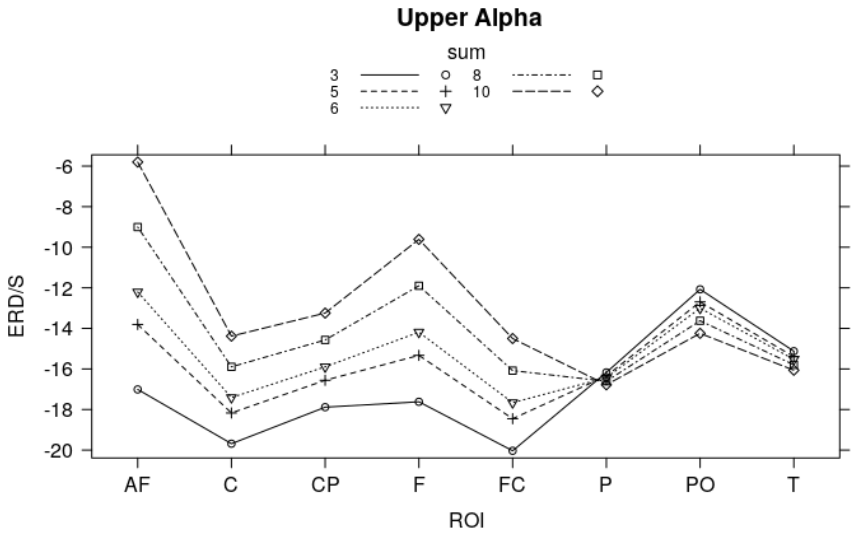

Figure 7.25: Problem size effect in the upper alpha band for operand sums 3-10 displayed for all 8 bilateral ROIs.

The difference of strategies and the factor +1 is shown for different problem sums in Figure 7.26. The difference is low at tiny problems, and increases for larger problems.

Post-hoc tests showed significant differences between the strategies retrieve and procedure in the bilateral parieto-occipital region ($p<0.05$). Tasks involving 1 were significantly different from others in general ($p<0.001$) and for the regions C, CP ($p<0.01$) and FC ($p<0.05$). These two types of problems differed in the left and in the right hemisphere (both $p<0.001$) for addition tasks, but not for multiplications.

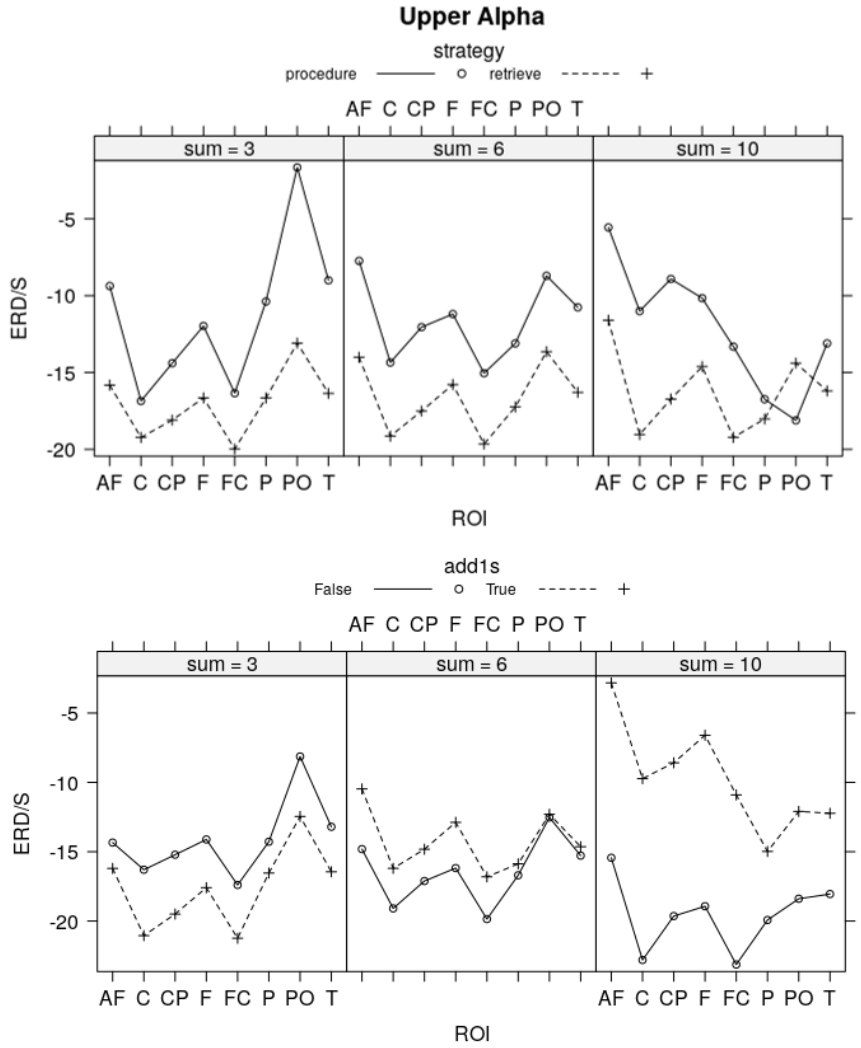

Figure 7.26: Differences between strategies (top) and n+1/n+m (bottom) in the upper alpha band.

8 Discussion

8.1 Analysis of the problem-size effect

The most consistently found effect that is observable in this work is the problem size effect. It states that reaction times and the use of procedural solution strategies increase with increasing problem size [35], [36], [137]. In this study, we analyzed patterns between tiny, small, and large problems. Problems with both operands below 5 are considered as tiny. Problems with an operand-sum above ten are considered as large, and small problems lay in between.
Considering reaction times, we expected that large problems are solved slower than small problems, and those small problems are calculated slower than tiny ones.
The comparison of the problem size categories revealed a significant difference between large and tiny problems and between large and small tasks. Additionally, the contrast in response times between tiny and small sizes is significant too.

Regarding EEG-oscillations, we expected effects in the theta- and alpha band. In the alpha band, band power does correlate inversely with the invested cognitive demand [56], and deactivations occur whenever information from the knowledge system is accessed [75], [76]. The knowledge system comprises the procedural memory system. As important anatomical structures for solving arithmetical problems include the visual areas e.g., V1, the angular gyrus, and the fusiform gyrus, we assumed that changes are observable mainly in the occipital and parieto-occipital regions of the brain. Changes in the theta-band are mainly observed together with cognitive processes like the working memory [58], [59], attention control [60]–[62] or during information encoding. Additionally, arithmetical facts are recalled by the use of the lexical system involving the left cortico-subcortico-loop. Thus, differences in the theta band are mainly expected in the left central and frontocentral regions.
Taken together, we expected that small problems elucidate higher theta ERS and lower alpha ERD than large problems.
In the analysis, we found differences between problem sizes in the theta, lower

alpha, and upper alpha band. A closer look revealed that these differences also exist on more detailed scales like the individual hemispheres and regions of interest. Exceptions from this simplified observation were found in the theta band for the contrast of tiny and small problems. Here, the significant difference appeared only in the right hemisphere. Other oddities were found in the alpha band for the difference of small and tiny problems in the anterio-frontal and frontal regions, as well as parietal and parieto-occipital in the lower alpha band, and temporal in the upper alpha band. Also, for the contrast of small and tiny problems in the central, frontal, fronto-central, and temporal regions as well as anterio-frontal, centro-parietal, and parietal in the upper alpha band.
Hence, we could replicate results of [4], [5] who found a higher left-hemispheric theta ERS for small (operand sum < 10) compared to large (operand sum ≥ 10) problems and a stronger lower-alpha ERD for large problems. Contradicting our expectations, the difference in left-hemispheric theta ERS was not significant between tiny and small problems. Theta ERS is linked to memory encoding and retrieval [65]–[67] and may reflect mathematical fact retrieval [3], [4], [68], [69]. Consequently, the missing significant difference between tiny and small problems suggests that both classes of problems are solved through the same underlying process.

Through the independent component analysis, we expected to find at least one cluster that contains mainly alpha ERD and is located in the bilateral parieto-occipital region and one cluster that contains mainly theta ERS and is located in the left-hemispheric perisylvian region.
The analysis of ERD/S values evaluated on independent components allowed to identify four clusters located in the parieto-occipital, parietal, and centro-parietal regions that showed significant differences between large and tiny problem sizes in the second half of the solving process. Two of them showed the differences also between small and tiny problems and one for the contrast of large and small problems too. Further, we found three clusters that are located in the frontal and fronto-central region and showed large activations in the theta-band. Significant differences were found between large and tiny and large and small problems. The evaluation of individual time-frequency bins even allowed us to identify differences between tiny and small problems.

8.2 Strategy differences

The current belief that tiny problems are solved through a recall from long-term memory was challenged in a newer behavioral study [7]. The authors claim that problems with operands below four would be solved through fast automated, and

unconscious processes.
We followed this hypothesis and contrasted the behavioral and neurological patterns with these tiny and small problems. Furthermore, we compared these findings to differences between self-reported retrieval and procedural and counting strategies.

8.2.1 Differences between reconstructive and reproductive strategies

We analyzed patterns between self-reported reconstructive and reproductive strategies. Reproductive processes refer to a recall from long-term memory, while reconstructive strategies describe problem transformations that are applied before the answer is recalled. Reconstructive strategies consist of problem transformations, counting, and other procedural strategies. They comprise additional steps required before the actual solution is retrieved. Hence, we assumed that the application of these strategies leads to longer calculation times. Indeed, we could experimentally prove the assumption and found that response times are, on average 150 ms longer for procedurally solved problems compared to retrieved tasks. This finding is in line with the current literature and was amongst others, also observed by Grabner et al. [5]. For reasons described in 8.1, we expected effects in the theta- and alpha band. This is, procedurally solved problems show a lower bilateral alpha ERD while retrieved tasks elucidate a higher theta ERS. Mainly, in the central and fronto-central regions of the left hemisphere.
Indeed, we could find significant differences in the theta-band in the left hemisphere. Retrieved strategies elucidated a theta ERS that is 12.8 % higher than at procedural problems. Furthermore, a look into the alpha band showed a by 12.0 % significantly lower alpha ERD value for procedurally solved problems than for retrieved ones. To conclude, we could replicate the results of [5] in the theta and upper-alpha band.

8.3 Comparison of sensor and source space

Two main effects were analyzed in the sensor and the source space and allowed to make a qualitative comparison.
Regarding problem size, we found differences in the sensor and the source space that are very similar. In the sensor space, we found that tiny and small problems compared to large problems become significantly different, but that the differences are not significant between tiny and small problems. This is true for the theta and alpha band and is consistent with findings of [4], [5].
The analysis of activations on the independent components showed differences be-

tween problem sizes for particular clusters. These are clusters 6 and 11 for the theta-band and clusters 3, 4, and 5 for the alpha band. The differences become significant between tiny and large problems, but not between tiny and small ones. Therefore, advances of the IC-space analysis compared to the sensor-space analysis are limited. We calculated the test-statistics for 5 and 10 clusters. Five clusters have the advantage that all subjects are included in most clusters, which is not given for 10 clusters. The bespoken cluster number 5, for example, comprises only 32 ICs of 21 subjects. This makes it difficult to make conclusions of the whole population, but allowed to find more precise and segregated locations of the clusters as well as more detailed ERSP patterns. This is the reason why the 10-cluster setup is presented in this thesis.
The analysis of strategies showed similar results. We did find differences between strategies in the theta-band. Unfortunately, these differences did not become significant in the source space.
Taken together, the advances of the IC-space analysis are limited and in our opinion not worth the additional required computation time.

8.4 Conclusion

In conclusion, we could replicate the problem size effect; Tiny and small problems differed from large ones in the theta-, the lower- and the upper-alpha band such that smaller problems elucidated higher theta ERS values, but less deactivation in the alpha band. This effect was found by the analysis of sensor values and also by the analysis of the independent components ERSPs. We could also identify differences between strategies in behavioral data and EEG-oscillations. Significant differences were mainly found in the theta-band and for the whole scalp when sensor values were evaluated, but not for the IC-space analysis. A comparison between those methods showed that both find similar effects. But, dealing with ICs requires additional steps like performing the ICA, fitting dipoles, and clustering. Each of these steps comes with additional parameters that have to be found and additional computation time. Together with the imprecise found locations of IC-clusters, we conclude that the analysis on the sensor space is fully sufficient in most cases.
Besides the comparison of the two analysis methods, we could compare tiny addition problems to small addition and tiny multiplication problems and found no significant differences in their EEG oscillations. Thus, we found no support for Uittenhove's model of fast unconscious and automated procedures for tiny problems.

9

Attachments

Table 6.6 shows the names, the ids, the hemisphere and lobe of all Desikan-Killany regions for which ICs were found. Moreover, it lists how many ICs included in these regions were assigned to each cluster. ICs in regions related to Visual Number Forming were mainly assigned to clusters 2 (16.3%), 4 (46.3%) and 11 (22.5%). Processes related to Auditory Number Form are well represented in group 11 (83.3%) and the ones for Numerical Quantity are found in Cluster 8 (35.2%) and in the groups 6 and 11 (both 22.2%). ICs related to the Episodic and Semantic memory are mostly in cluster 7 (47.1%) and 11 (23.5%). Sources activated in Salience / Attention control are found in group 11 (60%). Finally, working Memory / Cognitive control is almost equally distributed to clusters 3 (9.7%), 5 (10.2%), 6 (9.7%), 9 (21.0%), 10 (16.7%) and 11 (23.7%).

				Cluster									
	#	**Hemi**	**Lobe**	**2**	**3**	**4**	**5**	**6**	**7**	**8**	**9**	**10**	**11**
Visual Number Form													
Pericalcarine	22	L	Occipital	1	0	2	0	0	0	0	0	0	1
Pericalcarine	122	R	Occipital	0	0	2	0	0	1	0	0	0	1
Cuneus	6	L	Occipital	2	0	0	0	0	1	0	0	0	0
Cuneus	106	R	Occipital	4	0	0	0	0	2	0	0	0	1
Lingual	14	L	Occipital	1	0	6	0	0	0	1	0	0	2
Lingual	114	R	Occipital	0	0	9	0	1	0	0	0	0	2
Lateral Occipital	12	L	Occipital	5	0	2	0	0	0	3	0	0	1
Lateral Occipital	112	R	Occipital	0	0	7	0	2	0	0	0	0	2
Fusiform	8	L	Temporal	0	0	3	0	0	0	0	0	0	4
Fusiform	108	R	Temporal	0	0	6	0	1	0	0	0	0	4
Clusters contain % of Visual Number Form				16.3	0.0	**46.3**	0.0	5.0	5.0	5.0	0.0	0.0	22.5
Auditory Number Form													
Superior Temporal	31	L	Temporal	0	0	0	1	0	0	0	0	0	4
Superior Temporal	131	R	Temporal	0	0	0	0	0	0	0	0	0	1
Banks of Superior Temporal Sulcus	2	L	.	0	0	0	0	0	0	0	0	0	1
Banks of Superior Temporal Sulcus	102	R	.	0	0	0	0	1	0	0	0	0	4
Clusters contain % of Auditory Number Form				0.0	0.0	0.0	8.3	8.3	0.0	0.0	0.0	0.0	**83.3**
Numerical Quantity													
Superior parietal	30	L	Parietal	1	0	0	0	0	0	2	0	2	1
Superior parietal	130	R	Parietal	1	0	1	0	4	0	0	0	0	3
Inferior parietal	9	L	Parietal	1	0	0	0	0	0	9	0	0	1
Inferior parietal	109	R	Parietal	0	0	4	0	3	0	0	0	0	4
Supramarginal	32	L	Parietal	0	0	0	0	0	0	8	0	1	1
Supramarginal	132	R	Parietal	0	0	0	0	5	0	0	0	0	2
Clusters contain % of Numerical Quantity				5.6	0.0	9.3	0.0	22.2	0.0	**35.2**	0.0	5.6	22.2
Episodic / Semantic													
Inferior temporal	10	L	Temporal	0	0	0	0	0	0	0	0	0	1
Inferior temporal	110	R	Temporal	0	0	0	0	0	0	0	0	0	4
Middle Temporal	16	R	Temporal	0	0	1	0	0	0	0	0	0	1
Parahippocampal	17	L	Temporal	0	0	2	0	0	0	0	0	0	0
Precuneus	26	L	Parietal	1	1	0	0	0	10	1	0	0	5
Precuneus		R	Parietal	5	0	4	0	0	14	0	0	0	1
Clusters contain % of Episodic / Semantic				11.8	2.0	13.7	0.0	0.0	**47.1**	2.0	0.0	0.0	23.5

Table 9.1: Amount of independent components found for each Desikan-Killany region; regions are grouped by neurocognitive processes as described in [136].

				Cluster									
	#	**Hemi**	**Lobe**	**2**	**3**	**4**	**5**	**6**	**7**	**8**	**9**	**10**	**11**
Salience / Attention control													
Insula		L		0	0	0	0	0	0	0	0	0	3
Insula		R		0	1	0	2	0	0	0	0	0	0
Pars triangularis	21	L	Frontal	0	0	0	0	0	0	0	0	0	2
Pars Opercularis	19	L	Frontal	0	0	0	0	0	0	0	0	1	1
Clusters contain % of Salience / Attention control				0.0	10.0	0.0	20.0	0.0	0.0	0.0	0.0	10.0	**60.0**
Working Memory / Cognitive Control													
Postcentral	23	L	Parietal	0	0	0	0	0	0	0	0	12	4
Postcentral		R	Parietal	0	0	0	0	10	0	0	1	0	2
Precentral	25	L	Frontal	0	2	0	0	0	0	0	0	16	4
Precentral		R	Frontal	0	9	0	1	8	0	0	1	0	8
Isthmus of Cingulate	11	L	Parietal	0	0	5	0	0	4	0	0	0	1
Isthmus of Cingulate	111	R	Parietal	0	0	0	0	0	4	0	0	0	1
Posterior Cingulate	24	L	Parietal	0	3	1	0	0	1	0	1	2	1
Posterior Cingulate	124	R	Parietal	1	1	0	0	0	1	0	1	0	2
Caudal Anterior Cingulate	3	L	Frontal	0	0	0	4	0	0	0	3	0	1
Caudal Anterior Cingulate	103	R	Frontal	0	1	0	3	0	0	0	1	0	1
Rostral Anterior Cingulate	27	L	Frontal	0	0	0	2	0	0	0	0	0	0
Rostral Middle Frontal	28	L	Frontal	0	0	0	1	0	0	0	2	0	2
Rostral Middle Frontal		R	Frontal	0	0	0	3	0	0	0	0	0	0
Superior frontal	29	L	Frontal	0	1	0	2	0	0	0	15	0	5
Superior frontal		R	Frontal	0	1	0	1	0	0	0	12	0	4
Lateral Orbitofrontal	113	R	Frontal	0	0	0	0	0	0	0	0	0	2
Lateral Orbitofrontal	15	L	Frontal	0	0	0	1	0	0	0	0	0	1
Caudal Middle Frontal	4	L	Frontal	0	0	0	0	0	0	0	0	1	1
Caudal Middle Frontal		R	Frontal	0	0	0	1	0	0	0	2	0	4
Clusters contain % of Working menory / cognitive control				0.5	9.7	3.2	10.2	9.7	5.4	0.0	21.0	16.7	23.7

Table 9.2: Amount of independent components found for each Desikan-Killany region; regions are grouped by neurocognitive processes as described in [136].

Bibliography

[1] G. Pfurtscheller and F. Lopes da Silva, "Event-related desynchronization (ERD) and event-related synchronization", in *Electroencephalography: Basic Principles, Clinical Applications and Related Field*, E. In, E. Niedermeyer, and F. Lopes da Silva, Eds., 5th ed, Philadelphia, PA: Lippincott, Williams & Wilkins, 2005, pp. 1003–1016.

[2] C. Neuper and G. Pfurtscheller, "Event-related dynamics of cortical rhythms: Frequencyspecific features and functional correlates", *International Journal of Psychophysiology*, vol. 43, no. 1, pp. 41–58, 2001. [Online]. Available: `https://doi.org/10.1016/S0167-8760`.

[3] W. Klimesch, B. Schack, and P. Sauseng, "The Functional Significance of Theta and Upper Alpha Oscillations", *Experimental Psychology*, vol. 52, no. 2, pp. 99–108, 2005. [Online]. Available: `https://doi.org/10.1027/1618-3169.52.2.99`.

[4] B. De Smedt, R. Grabner, and B. Studer, "Oscillatory EEG correlates of arithmetic strategy use in addition and subtraction", *Experimental Brain Research*, vol. 195, no. 4, pp. 635–642, 2009.

[5] R. Grabner and B. De Smedt, "Oscillatory EEG correlates of arithmetic strategies: A training study", *Frontiers in Psychology*, vol. 3, pp. 1–11, 2012.

[6] P. Barrouillet and C. Thevenot, "On the problem-size effect in small additions: Can we really discard any counting-based account?", *Cognition*, vol. 128, no. 1, pp. 35–44, 2013.

[7] K. Uittenhove, C. Thevenot, and P. Barrouillet, "Fast automated counting procedures in addition problem solving: When are they used and why are they mistaken for retrieval?", *Cognition*, vol. 146, pp. 289–303, 2016. [Online]. Available: https://doi.org/10.1016/j.cognition.2015.10.008.

[8] H. Kahn and H. Whitaker, "Acalculia: An historical review of localization", *Brain and Cognition*, vol. 17, pp. 102–115, 1991. [Online]. Available: https://doi.org/10.1016/0278-2626(91)90071-F.

[9] D. S. Henschen, "Über Sprach-, Musik- und Rechenmechanismen und ihre Lokalisationen im Großhirn.", 1919.

[10] L. Zago, L. Petit, M. Turbelin, F. Andersson, M. Vigneau, and N. Tzourio-Mazoyer, "How verbal and spatial manipulation networks contribute to calculation: An fMRI study", *Neuropsychologia*, vol. 46, no. 9, pp. 2403–2414, 2008. DOI: https://doi.org/10.1016/j.neuropsychologia.2008.03.001. [Online]. Available: https://doi.org/10.1016/j.neuropsychologia.2008.03.001.

[11] O. Gruber, P. Indefrey, H. Steinmetz, and A. Kleinschmidt, "Dissociating neural correlates of cognitive components in mental calculation", *Cerebral Cortex*, vol. 11, no. 4, pp. 350–359, 2001. DOI: https://doi.org/10.1093/cercor/11.4.350. [Online]. Available: https://doi.org/10.1093/cercor/11.4.350.

[12] O. Simon, J. Mangin, L. Cohen, D. Le Bihan, and S. Dehaene, "Topographical layout of hand, eye, calculation, and language-related areas in the human parietal lobe", *Neuron*, vol. 33, no. 3, pp. 475–487, 2002. DOI: https://doi.org/10.1016/S0896-6273(02)00575-5. [Online]. Available: https://doi.org/10.1016/S0896-6273(02)00575-5.

[13] V. Menon, K. Mackenzie, S. Rivera, and A. Reiss, "Prefrontal cortex involvement in processing incorrect arithmetic equations: Evidence from event-related fMRI", *Human Brain Mapping*, vol. 16, no. 2, pp. 119–130, 2002. DOI: https://doi.org/10.1002/hbm.10035+. [Online]. Available: https://doi.org/10.1002/hbm.10035.

[14] F. Krueger, M. V. Spampinato, M. Pardini, S. Pajevic, J. N. Wood, G. H. Weiss, S. Landgraf, and J. Grafman, "Integral calculus problem solving: An fMRI investigation", *Neuroreport*, vol. 19, no. 11, p. 1095, 2008.

[15] V. Menon, S. Rivera, C. White, G. Glover, and A. Reiss, "Dissociating prefrontal and parietal cortex activation during arithmetic processing", *NeuroImage*, vol. 12, no. 4, pp. 357–365, 2000. DOI: https://doi.org/10.1006/nimg.2000.0613. [Online]. Available: https://doi.org/10.1006/nimg.2000.0613.

[16] L. Zago, M. Pesenti, E. Mellet, F. Crivello, B. Mazoyer, and N. Tzourio-Mazoyer, "Neural correlates of simple and complex mental calculation", *Neuroimage*, vol. 13, pp. 314–327, 2001. DOI: https://doi.org/10.1006/nimg.2000.0697. [Online]. Available: https://doi.org/10.1006/nimg.2000.0697.

[17] M. Rosenberg-Lee, M. Lovett, and J. Anderson, "Neural correlates of arithmetic calculation strategies", *Cognitive Affective Behavioural Neuroscience*, vol. 9, no. 3, pp. 270–285, 2009. DOI: https://doi.org/10.3758/CABN.9.3.270. [Online]. Available: https://doi.org/10.3758/CABN.9.3.270.

[18] V. Menon, "Arithmetic in the child and adult brain", *Handbook of Mathematical Cognition*, 2015.

[19] E. Kirk and M. Ashcraft, "Telling Stories: The Perils and Promise of Using Verbal Reports to Study Math Strategies", *Journal of Experimental Psychology: Learning, Memory and Cognition*, vol. 27, no. 1, pp. 157–175, 2001. DOI: http://dx.doi.org/10.1037/0278-7393.27.1.157. [Online]. Available: http://dx.doi.org/10.1037/0278-7393.27.1.157.

[20] B. Smith-Chant and J. LeFevre, "Doing as they are told and telling it like it is: Self-reports in mental arithmetic", *M&C*, vol. 31, pp. 516–528, 2003.

[21] T. Hinault, P. Lemaire, and N. Phillips, "Aging and sequential modulations of poorer strategy effects: An EEG study in arithmetic problem solving", *Brain Res*, vol. 1630, pp. 144–158, 2016. DOI: https://doi.org/10.1016/j.brainres.2015.10.057. [Online]. Available: https://doi.org/10.1016/j.brainres.2015.10.057.

[22] L. Wang, J. Q. Gan, L. Zhang, and H. Wang, "Differential recruitment of brain networks in single-digit addition and multiplication: Evidence from EEG oscillations in theta and lower alpha bands", en, *International Journal of Psychophysiology*, vol. 128, pp. 81–92, Jun. 2018, ISSN: 01678760. DOI: 10.1016/j.ijpsycho.2018.04.005. [Online]. Available: https://linkinghub.elsevier.com/retrieve/pii/S0167876017304804 (visited on 07/01/2019).

[23] Y. Chen and J. Campbell, "Operator and operand preview effects in simple addition and multiplication: A comparison of Canadian and Chinese adults", *Journal of Cognitive Psychology*, vol. 27, no. 3, pp. 326–334, 2015. [Online]. Available: https://doi.org/10.1080/20445911.2014.999685.

[24] ——, "Operator priming and generalization of practice in adults' simple arithmetic", *Journal of Experimental Psychology: Learning, Memory, and Cognition*, vol. 42, pp. 627–635, 2016. DOI: doi:10.1037/xlm0000196.

[25] A. Metcalfe and J. Campbell, "Adults' strategies for simple addition and multiplication: Verbal self-reports and the operand recognition paradigm", *J. Exp. Psychol. Learn. Mem. Cogn*, vol. 37, pp. 661–672, 2011. DOI: http://dx.doi.org/10.1037/a0022218. [Online]. Available: http://dx.doi.org/10.1037/a0022218.

[26] M. Fayol and C. Thevenot, "The use of procedural knowledge in simple addition and subtraction problems", *Cognition*, vol. 123, pp. 392–403, 2012. DOI: https://doi.org/10.1016/j.cognition.2012.02.008. [Online]. Available: https://doi.org/10.1016/j.cognition.2012.02.008.

[27] J. Campbell and Q. Xue, "Cognitive Arithmetic Across Cultures", *Journal of Experimental Psychology: General*, vol. 130, no. 2, pp. 299–315, 2001. [Online]. Available: https://doi.org/10.1037/00963445.130.2.299.

[28] S. Duverne and P. Lemaire, "Arithmetic split effects reflect strategy selection: An adult age comparative study in addition comparison and verification tasks", *Can. J. Exp. Psychol. (Revue Canadienne de Psychologie Expérimentale)*, vol. 59, no. 4, pp. 262–278, 2005. [Online]. Available: http://dx.doi.org/10.1037/h0087479..

[29] K. Uittenhove and P. Lemaire, *Numerical Cognition during Cognitive Aging*. In: Cohen, 2014.

[30] P. Lemaire, *Cognitive Aging: The Role of Strategies*. New York, NY: Psychology Press, 2015. [Online]. Available: https://sci-hub.tw/https://doi.org/10.4324/9781315650999.

[31] I. Imbo and A. Vandierendonck, "The development of strategy use in elementary school children: Working memory and individual differences", *J. Exp. Child Psychol*, vol. 96, no. 4, pp. 284–309, 2007. [Online]. Available: http://dx.doi.org/10.1016/j.jecp.2006.09.001..

[32] P. Lemaire and L. Reder, "What effects strategy selection in arithmetic? The example of parity and five effects on product verification", *Mem. Cogn*, vol. 27, no. 2, pp. 364–382, 1999. [Online]. Available: http://dx.doi.org/10.3758/BF03211420..

[33] P. Lemaire and R. Siegler, "Four aspects of strategic change: Contributions to children's learning of multiplication", *J. Exp. Psychol. Gen*, vol. 124, no. 1, pp. 83–97, 1995. [Online]. Available: http://dx.doi.org/10.1037/0096-3445.124.1.83..

[34] T. Hinault and P. Lemaire, *What does EEG tell us about arithmetic strategies? A review*. 2016.

[35] R. Grabner and B. De Smedt, "Neurophysiological evidence for the validity of verbal strategy reports in mental arithmetic", *Biological Psychology*, vol. 87, no. 1, pp. 128–136, 2011.

[36] J.-A. LeFevre, J. Bisanz, K. Daley, L. Buffone, S. Greenham, and G. Sadesky, "Multiple Routes to Solution of Single-Digit Multiplication Problems", *Journal of Experimental Psychology: General*, vol. 125, no. 3, pp. 284–306, 1996. [Online]. Available: https://doi.org/10.1037/00963445.125.3.284.

[37] J.-A. LeFevre, G. Sadesky, and J. Bisanz, "Selection of Procedures in Mental Addition: Reassessing the Problem Size Effect in Adults", *Journal of Experimental Psychology: Learning, Memory and Cognition*, vol. 22, no. 1, pp. 216–230, 1996. [Online]. Available: https://doi.org/10.1037/02787393.22.1.216.

[38] C. Thevenot, P. Barrouillet, and M. Fayol, "Algorithmic solution of arithmetic problems and operands-answer associations in long-term memory", *Quarterly Journal of Experimental Psychology*, vol. 54, no. 2, pp. 599–611, 2001. [Online]. Available: https://doi.org/10.1080/713755966.

[39] P. Barrouillet and M. Fayol, "From algorithmic computing to direct retrieval: Evidence from number and alphabetic arithmetic in children and adults. Memory and", *Cognition*, vol. 26, no. 2, pp. 355–368, 1998. [Online]. Available: https://doi.org/10.3758/BF03201146.

[40] J. Campbell and J. Timm, "Adults' strategy choices for simple addition: Effects of retrieval interference", *Psychonomic Bulletin and Review*, vol. 7, no. 4, pp. 692–699, 2000. [Online]. Available: https://doi.org/10.3758/BF03213008.

[41] J. Campbell, "Architectures for numerical cognition", *Cognition*, vol. 53, pp. 1–44, 1994.

[42] J. Campbell, "Handbook of Mathematical Cognition", *Cogn*, vol. 30, no. 6, J. Campbell, Ed., pp. 988–994, 2005. [Online]. Available: http://dx.doi.org/10.3758/BF03195782..

[43] M. McCloskey, "Cognitive mechanisms in numerical processing: Evidence from acquired dyscalculia", *Cognition*, vol. 44, pp. 107–157, 1992. [Online]. Available: http://dx.doi.org/10.1016/00100277.

[44] M. McCloskey and P. Macaruso, *Architecture of cognitive numerical processing mechanisms: contrasting perspectives on theory development and evaluation*. 1994.

[45] ——, "Representing and using numerical information", *Am*, 1995.

[46] D. Ansari, "Does the Parietal Cortex Distinguish between "10," "Ten," and Ten Dots?", en, *Neuron*, vol. 53, no. 2, pp. 165–167, Jan. 2007, ISSN: 08966273. DOI: 10.1016/j.neuron.2007.01.001. [Online]. Available: https://linkinghub.elsevier.com/retrieve/pii/S0896627307000049 (visited on 08/08/2019).

[47] S. Dehaene, "Varieties of numerical abilities", *Cognition*, vol. 44, pp. 1–42, 1992.

[48] S. Dehaene and L. Cohen, "Towards an anatomical and functional model on number processing", *Math. Cogn*, vol. 1, pp. 83–120, 1995.

[49] S. Dehaene, M. Piazza, P. Pinel, and L. Cohen, "Three parietal circuits for number processing", *Cognition*, vol. 20, pp. 487–506, 2003.

[50] S. Dehaene and L. Cohen, "Cerebral pathways for calculation: Double dissociation between rote verbal and quantitative knowledge of arithmetic", *Cortex*, vol. 33, no. 2, pp. 219–250, 1997.

[51] J. Campbell and L. Epp, "An encoding-complex approach to numerical cognition in Chinese-English bilinguals", *Can. J. Exp. Psychol*, vol. 58, pp. 229–244, 2004.

[52] J. Campbell and J. Clark, "Numerical Cognition: An Encoding-Complex Perspective", *The Nature and Origins of Mathematical Skills. Elsevier Science*, J. Campbell, Ed., pp. 457–491, 1992.

[53] B. Pakkenberg and H. Gundersen, "BNeocortical neuron number in humans: Effect of sex and", *Comparat. Neurol*, vol. 384, no. 2, pp. 312–320, 1997.

[54] T. Hinault, S. Dufau, and P. Lemaire, *Sequential modulations of poorer-strategy effects during strategy execution: an event-related potential study in arithmetic. Brain Cogn.* 2014.

[55] ——, "Strategy combination in human cognition: A behavioral and ERP study in arithmetic", *Psychon. Bull. Rev*, 2014. [Online]. Available: http://dx.doi.org/10.3758/.

[56] G. Pfurtscheller and F. Lopes, "Event-related EEG/MEG synchronization and desynchronization: Basic principles", *Clinical Neurophysiology*, vol. 110, pp. 1842–1857, 1999. [Online]. Available: https://doi.org/10.1016/S1388-2457.

[57] M. Bastiaansen, P. Hagoort, N. Christa, and K. Wolfgang, "Oscillatory neuronal dynamics during language comprehension", *Progress in Brain Research*, vol. 159, pp. 179–196, 2006.

[58] P. Sauseng, W. Klimesch, M. Doppelmayr, S. Hanslmayr, M. Schabus, and W. Gruber, "Theta coupling in the human electroencephalogram during a working memory task", *Neurosci. Lett*, vol. 354, pp. 123–126, 2004.

[59] P. Sauseng, B. Griesmayr, R. Freunberger, and W. Klimesch, "Control mechanisms in working memory: A possible function of EEG theta oscillations", *Neurosci. Biobehav. Rev*, vol. 34, pp. 1015–1022, 2010.

[60] M. Deiber, P. Missonnier, O. Bertrand, G. Gold, L. Fazio-Costa, V. Ibanez, and P. Giannakopoulos, "Distinction between perceptual and attentional processing in working memory tasks: A study of phase-locked and induced oscillatory brain dynamics", *J. Cogn. Neurosci*, vol. 19, pp. 158–172, 2007.

[61] P. Sauseng, J. Hoppe, W. Klimesch, C. Gerloff, and F. Hummel, "Dissociation of sustained attention from central executive functions: Local activity and interregional connectivity in the theta range", *European Journal of Neuroscience*, vol. 25, pp. 587–593, 2007.

[62] M. Clayton, N. Yeung, and R. Cohen Kadosh, "The roles of cortical oscillations in sustained attention", *Trends Cogn. Sci*, vol. 19, pp. 188–195, 2015.

[63] T. Harmony, T. Fernández, J. Silva, J. Bosch, P. Valdés, A. Fernández-Bouzas, L. Galán, E. Aubert, and D. Rodrıéguez, "Do specific EEG frequencies indicate different processes during mental calculation?", *Neuroscience letters*, vol. 266, no. 1, pp. 25–28, 1999.

[64] S. Micheloyannis, V. Sakkalis, M. Vourkas, C. Stam, and P. Simos, "Neural networks involved in mathematical thinking: Evidence from linear and nonlinear analysis of electroencephalographic activity", *Neuroscience Letters*, vol. 373, no. 3, pp. 212–217, 2005. [Online]. Available: `https://doi.org/10.1016/j.neulet.2004.10.005`.

[65] A. Burgess and J. Gruzelier, "Short duration power changes in the EEG during recognition memory for words and faces", *Psychophysiology*, vol. 37, no. 5, pp. 596–606, 2000. [Online]. Available: `https://doi.org/10.1017/S0048577200981356`.

[66] O. Jensen and C. Tesche, "Frontal theta activity in humans increases with memory load in a working memory task", *European Journal of Neuroscience*, vol. 15, no. 8, pp. 1395–1399, 2002. [Online]. Available: `https://doi.org/10.1046/j.1460-9568.2002.01975.x`.

[67] W. Klimesch, M. Doppelmayr, T. Pachinger, and B. Ripper, "Brain oscillations and human memory: EEG correlates in the upper alpha and theta band", *Neuroscience Letters*, vol. 238, no. 1–2, pp. 9–12, 1997. [Online]. Available: `https://doi.org/10.1016/S0304-3940`.

[68] J. Earle, P. Garciadergay, A. Manniello, and C. Dowd, "Mathematical cognitive style and arithmetic sign comprehension: A study of EEG alpha and theta activity", *International Journal of Psychophysiology*, vol. 21, pp. 1–13, 1996.

[69] M. Klados, K. Kanatsouli, I. Antoniou, F. Babiloni, V. Tsirka, P. Bamidis, and S. Micheloyannis, "A graph theoretical approach to study the Organization of the Cortical Networks during different mathematical tasks", *PLoS One*, vol. 8, no. 8, p. 71 800, 2013. [Online]. Available: `http://dx.doi.org/10.1371/journal.pone.0071800.`.

[70] V. Gorisek, A. Belic, C. Manouilidou, B. Koritnik, G. Repovs, J. Bon, J. Zibert, and J. Zidar, "The electrophysiological correlates of the working memory subcomponents: Evidence from high-density EEG and coherence analysis", *Neurol. Sci*, vol. 36, pp. 2199–2207, 2015.

[71] W. Klimesch, "Memory processes, brain oscillations and EEG synchronization", *Int. J. Psychophysiol*, vol. 24, pp. 61–100, 1996.

[72] B. Griesmayr, B. Berger, R. Stelzig-Schoeler, W. Aichhorn, J. Bergmann, and P. Sauseng, "EEG theta phase coupling during executive control of visual working memory investigated in individuals with schizophrenia and in healthy controls", *Cogn. Affect. Behav. Neurosci*, vol. 14, pp. 1340–1355, 2014.

[73] H. Mizuhara, L. Wang, K. Kobayashi, and Y. Yamaguchi, "Long-range EEG phase synchronization during an arithmetic task indexes a coherent cortical network simultaneously measured by fMRI", *NeuroImage*, vol. 27, pp. 553–563, 2005.

[74] A. Bowman, J. Griffis, K. Visscher, A. Dobbins, T. Gawne, M. DiFrancesco, and J. Szaflarski, "Alpha rhythm and the default mode network: An EEG-fMRI study (P6.021)", *Neurology*, vol. 84, no. 14, pp. 6–21, 2015.

[75] W. Klimesch, R. Fellinger, and R. Freunberger, "Alpha oscillations and early stages of visual encoding", *Front. Psychol*, vol. 2, p. 118, 2011.

[76] W. Klimesch, "Alpha-band oscillations, attention, and controlled access to stored information", *Trends Cogn. Sci*, vol. 16, pp. 606–617, 2012.

[77] Y. Ku, B. Hong, X. Gao, and S. Gao, "Spectra-temporal patterns underlying mental addition: An ERP and ERD/ERS study", *Neuroscience Letters*, vol. 472, no. 1, pp. 5–10, 2010. [Online]. Available: `https://doi.org/10.1016/j.neulet.2010.01.040`.

[78] A. Neubauer, A. Fink, R. Grabner, N. Christa, and K. Wolfgang, "Sensitivity of alpha band ERD to individual differences in cognition", *Progress in Brain Research*, vol. 159, pp. 167–178, 2006.

[79] T. Fernández, T. Harmony, M. Rodríguez, J. Bernal, J. Silva, A. Reyes, and E. Marosi, "EEG activation patterns during the performance of tasks involving different components of mental calculation", *Electroencephalogr. Clin. Neurophysiol*, vol. 94, no. 3, pp. 175–182. 1995. [Online]. Available: http://dx.doi.org/10.1016/0013-4694.

[80] T. Harmony, T. Fernández, J. Silva, J. Bernal, L. Díaz-Comas, A. Reyes, E. Marosi, M. Rodríguez, and M. Rodríguez, "EEG delta activity: An indicator of attention to internal processing during performance of mental tasks", *Int. J. Psychophysiol*, vol. 24, no. 1–2, pp. 161–171, 1996. [Online]. Available: http://dx.doi.org/10.1016/S0167-8760.

[81] P. Zarjam, J. Epps, F. Chen, and N. Lovell, "Estimating cognitive workload using wavelet entropy-based features during an arithmetic task", *Computers in Biology and Medicine*, vol. 43, no. 12, pp. 2186–2195, 2013. [Online]. Available: http://dx.doi.org/10.1016/j.compbiomed.2013.08.021..

[82] S. Dimitriadis, N. Laskaris, V. Tsirka, M. Vourkas, and S. Micheloyannis, "What does delta band tell us about cognitive processes: A mental calculation study", in, 2010.

[83] M. K. Islam, A. Rastegarnia, and Z. Yang, "Methods for artifact detection and removal from scalp EEG: A review", en, *Neurophysiologie Clinique/Clinical Neurophysiology*, vol. 46, no. 4-5, pp. 287–305, 2016, ISSN: 09877053. DOI: 10.1016/j.neucli.2016.07.002. [Online]. Available: http://linkinghub.elsevier.com/retrieve/pii/S098770531630199X (visited on 07/18/2018).

[84] P Berg and M Scherg, "Dipole modelling of eye activity and its application to the removal of eye artefacts from the EEG and MEG", en, *Clinical Physics and Physiological Measurement*, vol. 12, no. A, pp. 49–54, 1991, ISSN: 0143-0815. DOI: 10.1088/0143-0815/12/A/010. [Online]. Available: http://stacks.iop.org/0143-0815/12/i=A/a=010?key=crossref.f1e2b521dfc8adb24defe8ff16f07305 (visited on 07/18/2018).

[85] L. Pion-Tonachini, K. Kreutz-Delgado, and S. Makeig, "Iclabel: An automated electroencephalographic independent component classifier, dataset, and website", *NeuroImage*, vol. 198, pp. 181–197, 2019.

[86] I. Winkler, S. Haufe, and M. Tangermann, "Automatic classification of artifactual ica-components for artifact removal in eeg signals", *Behavioral and Brain Functions*, vol. 7, no. 1, p. 30, 2011.

[87] M. Jas, D. A. Engemann, Y. Bekhti, F. Raimondo, and A. Gramfort, "Autoreject: Automated artifact rejection for MEG and EEG data", *NeuroImage*, vol. 159, pp. 417–429, 2017.

[88] H. Nolan, R. Whelan, and R. B. Reilly, "FASTER: Fully automated statistical thresholding for EEG artifact rejection", *Journal of neuroscience methods*, vol. 192, no. 1, pp. 152–162, 2010.

[89] Q. Barthélemy, L. Mayaud, D. Ojeda, and M. Congedo, "The Riemannian potato field: A tool for online signal quality index of EEG", *IEEE Transactions on Neural Systems and Rehabilitation Engineering*, vol. 27, no. 2, pp. 244–255, 2019.

[90] T. Iuculano, A. Padmanabhan, and V. Menon, "Chapter 15 - Systems Neuroscience of Mathematical Cognition and Learning: Basic Organization and Neural Sources of Heterogeneity in Typical and Atypical Development", in *Heterogeneity of Function in Numerical Cognition*, A. Henik and W. Fias, Eds., Academic Press, 2018, pp. 287 –336, ISBN: 978-0-12-811529-9. DOI: 10.1016/B978-0-12-811529-9.00015-7. [Online]. Available: http://www.sciencedirect.com/science/article/pii/B9780128115299000157.

[91] S. E. Vogel, C. Goffin, J. Bohnenberger, K. Koschutnig, G. Reishofer, R. H. Grabner, and D. Ansari, "The left intraparietal sulcus adapts to symbolic number in both the visual and auditory modalities: Evidence from fMRI", *NeuroImage*, vol. 153, pp. 16–27, 2017.

[92] T. Allison, G. McCarthy, A. Nobre, A. Puce, and A. Belger, "Human extrastriate visual cortex and the perception of faces, words, numbers, and colors", *Cerebral cortex*, vol. 4, no. 5, pp. 544–554, 1994.

[93] A. Martin, "The representation of object concepts in the brain", *Annu. Rev. Psychol.*, vol. 58, pp. 25–45, 2007.

[94] J. Binder, D. Medler, C. Westbury, E. Liebenthal, and L. Buchanan, "Tuning of the human left fusiform gyrus to sublexical orthographic structure", *NeuroImage*, vol. 33, no. 2, pp. 739–748, 2006.

[95] R. Starrfelt and C. Gerlach, "The visual what for area: Words and pictures in the left fusiform gyrus", *Neuroimage*, vol. 35, no. 1, pp. 334–342, 2007.

[96] G. McCarthy, A. Puce, J. C. Gore, and T. Allison, "Face-specific processing in the human fusiform gyrus", *Journal of cognitive neuroscience*, vol. 9, no. 5, pp. 605–610, 1997.

[97] R. Grabner, D. Ansari, K. Koschutnig, G. Reishofer, F. Ebner, and C. Neuper, "To retrieve or to calculate? Left angular gyrus mediates the retrieval of arithmetic facts during problem solving", *Neuropsychologia*, vol. 47, pp. 604–608, 2009.

[98] A. Ischebeck, L. Zamarian, C. Siedentopf, F. Koppelstatter, T. Benke, S. Felber, and M. Delazer, "How specifically do we learn? Imaging the learning of multiplication and subtraction", *NeuroImage*, vol. 30, no. 4, pp. 1365–1375, 2006.

[99] T. Rickard, S. Romero, G. Basso, C. Wharton, S. Flitman, and J. Grafman, "The calculating brain: An fMRI study", *Neuropsychologia*, vol. 38, no. 3, pp. 325–335, 2000.

[100] D. Ansari, "Effects of development and enculturation on number representation in the brain", *Nature Reviews Neuroscience*, vol. 9, pp. 278–291, 2008.

[101] M. Andres, B. Pelgrims, N. Michaux, E. Olivier, and M. Pesenti, "Role of distinct parietal areas in arithmetic: An fMRI-guided TMS study", *NeuroImage*, vol. 54, no. 4, pp. 3048–3056, 2011.

[102] J. E. G. Hall, *Hall Textbook of Medical Physiology: Enhanced E-book*. Elsevier Health Sciences, 2010.

[103] S. Dehaene and L. Cohen, "Dissociable mechanisms of subitizing and counting: Neuropsychological evidence from simultanagnosic patients.", *Journal of Experimental Psychology: Human Perception and Performance*, vol. 20, no. 5, p. 958, 1994.

[104] M. Arsalidou and M. Taylor, "Is 2 + 2 = 4? Meta-analyses of brain areas needed for numbers and calculations", *NeuroImage*, vol. 54, pp. 2382–2393, 2011.

[105] J. C. Britton, K. L. Phan, S. F. Taylor, R. C. Welsh, K. C. Berridge, and I. Liberzon, "Neural correlates of social and nonsocial emotions: An fMRI study", *Neuroimage*, vol. 31, no. 1, pp. 397–409, 2006.

[106] A. J. Calder, J. Keane, F. Manes, N. Antoun, and A. W. Young, "Impaired recognition and experience of disgust following brain injury", *Nature neuroscience*, vol. 3, no. 11, p. 1077, 2000.

[107] M. L. Gorno-Tempini, S. Pradelli, M. Serafini, G. Pagnoni, P. Baraldi, C. Porro, R. Nicoletti, C. Umita, and P. Nichelli, "Explicit and incidental facial expression processing: An fMRI study", *Neuroimage*, vol. 14, no. 2, pp. 465–473, 2001.

[108] A. Heinzel, F. Bermpohl, R. Niese, A. Pfennig, A. Pascual-Leone, G. Schlaug, and G. Northoff, "How do we modulate our emotions? Parametric fMRI reveals cortical midline structures as regions specifically involved in the processing of emotional valences", *Cognitive Brain Research*, vol. 25, no. 1, pp. 348–358, 2005.

[109] M. P. Paulus and M. B. Stein, "An insular view of anxiety", *Biological psychiatry*, vol. 60, no. 4, pp. 383–387, 2006.

[110] S. A. Huettel, G. Güzeldere, and G. McCarthy, "Dissociating the neural mechanisms of visual attention in change detection using functional MRI", *Journal of Cognitive Neuroscience*, vol. 13, no. 7, pp. 1006–1018, 2001.

[111] R. Hester, C. Fassbender, and H. Garavan, "Individual differences in error processing: A review and reanalysis of three event-related fMRI studies using the GO/NOGO task", *Cerebral Cortex*, vol. 14, no. 9, pp. 986–994, 2004.

[112] L. Q. Uddin, A. Clare Kelly, B. B. Biswal, F Xavier Castellanos, and M. P. Milham, "Functional connectivity of default mode network components: Correlation, anticorrelation, and causality", *Human brain mapping*, vol. 30, no. 2, pp. 625–637, 2009.

[113] L. Q. Uddin and V. Menon, "The anterior insula in autism: Under-connected and under-examined", *Neuroscience & Biobehavioral Reviews*, vol. 33, no. 8, pp. 1198–1203, 2009.

[114] S. Cho, A. Metcalfe, C. Young, S. Ryali, D. Geary, and V. Menon, "Hippocampal-prefrontal engagement and dynamic causal interactions in the maturation of children's fact retrieval", *Journal of Cognitive Neuroscience*, vol. 24, no. 9, pp. 1849–1866, 2012.

[115] K. Supekar and V. Menon, "Developmental maturation of dynamic causal control signals in higher-order cognition: A neurocognitive network model", *PLoS Computational Biology*, vol. 8, no. 2, p. 1 002 374, 2012.

[116] K. Christoff and J. D. Gabrieli, "The frontopolar cortex and human cognition: Evidence for a rostrocaudal hierarchical organization within the human prefrontal cortex", *Psychobiology*, vol. 28, no. 2, pp. 168–186, 2000.

[117] J.-H. Song and Y. Jiang, "Visual working memory for simple and complex features: An fMRI study", *Neuroimage*, vol. 30, no. 3, pp. 963–972, 2006.

[118] C. Chang, S. Crottaz-Herbette, and V. Menon, "Temporal dynamics of basal ganglia response and connectivity during verbal working memory", *NeuroImage*, vol. 34, no. 3, pp. 1253–1269, 2007.

[119] M. Packard and B. Knowlton, "Learning and memory functions of the basal ganglia", *Annual Review of Neuroscience*, vol. 25, pp. 563–593, 2002.

[120] C. J. Stoodley and J. D. Schmahmann, "Functional topography in the human cerebellum: A meta-analysis of neuroimaging studies", *Neuroimage*, vol. 44, no. 2, pp. 489–501, 2009.

[121] C. V. Buhusi and W. H. Meck, "What makes us tick? Functional and neural mechanisms of interval timing", *Nature reviews neuroscience*, vol. 6, no. 10, p. 755, 2005.

[122] S. Dehaene, E. Spelke, P. Pinel, R. Stanescu, and S. Tsivkin, "Sources of mathematical thinking: Behavioral and brain-imaging evidence", *Science*, vol. 284, no. 5416, pp. 970–974, 1999.

[123] R. Grabner, C. Brunner, R. Leeb, C. Neuper, and G. Pfurtscheller, *Event-related*. 2007.

[124] D. Pinault, "The thalamic reticular nucleus: Structure, function and concept", *Brain research reviews*, vol. 46, no. 1, pp. 1–31, 2004.

[125] S. E. Nadeau, "The thalamus and working memory", *Journal of the International Neuropsychological Society*, vol. 14, no. 5, pp. 900–901, 2008.

[126] F. Marzinzik, M. Wahl, G.-H. Schneider, A. Kupsch, G. Curio, and F. Klostermann, "The human thalamus is crucially involved in executive control operations", *Journal of Cognitive Neuroscience*, vol. 20, no. 10, pp. 1903–1914, 2008.

[127] E. Curtis, M. Huebner, and J.-A. LeFevre, "The Relationship between Problem Size and Fixation Patterns During Addition, Subtraction, Multiplication, and Division", *Journal of Numerical Cognition*, vol. 2, no. 2, pp. 91–115, 2016. [Online]. Available: `https://doi.org/10.5964/jnc.v2i2.17`.

[128] J. D. Gabrieli, "Cognitive neuroscience of human memory", *Annual review of psychology*, vol. 49, no. 1, pp. 87–115, 1998.

[129] V. Lorenz, "Differences in eeg oscillations and response behavior between solving addition and multiplication problems", *KFU Graz*, pp. 1–94, 2019.

[130] J. W. Peirce, "Generating stimuli for neuroscience using PsychoPy", *Frontiers in neuroinformatics*, vol. 2, p. 10, 2009.

[131] L. Gabard-Durnam, A. Leal, C. Wilkinson, and A. Levin, "'The harvard automated processing pipeline for electroencephalography (HAPPE): Standardized processing software for developmental and high-artifact data,'" *Frontiers Neurosci*, vol. 12, p. 97, 2018.

[132] J. Onton, M. Westerfield, J. Townsend, and S. Makeig, "Imaging human EEG dynamics using independent component analysis", *Neuroscience & biobehavioral reviews*, vol. 30, no. 6, pp. 808–822, 2006.

[133] A. Delorme, T. Sejnowski, and S. Makeig, "Enhanced detection of artifacts in EEG data using higher-order statistics and independent component analysis", *Neuroimage*, vol. 34, no. 4, pp. 1443–1449, 2007.

[134] .

[135] A. Mognon, J. Jovicich, L. Bruzzone, and M. Buiatti, "ADJUST: An automatic EEG artifact detector based on the joint use of spatial and temporal features", *Psychophysiology*, vol. 48, pp. 229–240, 2011.

[136] W. Fias, V. Menon, and D. Szucs, "Multiple components of developmental dyscalculia", *Trends in Neuroscience and Education*, vol. 2, no. 2, pp. 43–47, 2013.

[137] N. Zbrodoff, "Than 2 + 3? Strength and interference as explanations of the problem-size effect. Memory &", *Cognition*, vol. 23, no. 6, pp. 689–700, 1995.